

INTEGRATION AND VALIDATION OF POWER HARDWARE-IN-THE-LOOP  
GENERATOR MODELS FOR DEPLOYMENT IN A DISTRIBUTED GENERATION

SOURCE TESTBED

By

Jacob L. Sanchez-Roddy

Presented to the Faculty of the Graduate School of  
The University of Texas at Arlington in Partial Fulfillment  
of the Requirements  
for the Degree of

DOCTOR OF PHILOSOPHY

THE UNIVERSITY OF TEXAS AT ARLINGTON

May 2019

Copyright © by Jacob L. Sanchez-Roddy 2019

All Rights Reserved



## Acknowledgements

This work would not have been possible without the financial support of the US Office of Naval Research (ONR) under grant numbers N00014-16-1-3001, N00014-17-1-2288, and N00014-14-1-0267. I am especially indebted to Dr. Wetz, Dr. Dillon, Dr. Lee, Dr. Turner, Dr. Davoudi, and Dr. Kenarangui for their guidance, support, professional and personal advice, and time to help me achieve my academic goals. Nobody has been more important to me in the pursuit of this education than the members of my family. I would like to thank my parents; Luis A Sanchez and Janise L Roddy whose love and guidance are with me in whatever I pursue. I would also like to thank the lifelong friends that I have made and have helped me achieve this over the years. Thank you, Charles, Brian, David, Clint, Isaac, Derek, Stephanie, Caroline, Alex, and Chris.

## Table of Contents

Acknowledgements .....	3
List of Figures.....	7
Abstract .....	14
Chapter 1: Introduction.....	16
Chapter 2: Hardware in the Loop Background .....	22
A. Controller Hardware in the Loop.....	22
B. Power Hardware in the Loop.....	22
C. Validity of Power Hardware in the Loop.....	23
D. Previous work with PHIL.....	27
Chapter 3: Induction Machine Background .....	33
Chapter 4: Synchronous Machine Background .....	39
Chapter 5: Single Shaft Turbine Background .....	45
Chapter 6: Hardware and PHIL Experimental Comparison .....	48
A. Experimental Setup .....	48
B. Motor-Generator Simulation .....	52
C. Motor-Generator with AC/DC Simulation.....	53
D. Hardware/PHIL Experimental Procedure.....	54
E. Hardware Vs Simulated System Comparison.....	54
F. Emulated AC Generation Source with Hardware AC/DC Converter .....	58

G.	Emulated DC Source Comparison to Hardware .....	63
H.	Emulated Motor-Generator Vs Hardware Conclusion.....	65
Chapter 7: Hardware and PHIL Small Scale System Integration Comparison .....		66
A.	Experimental Setup .....	66
B.	Induction Motor / Synchronous Generator Sources.....	67
C.	Experimental Procedure .....	70
D.	No buffering of the AC Source with Energy Storage Results.....	71
E.	Buffering of the AC Source with Energy Storage Results.....	76
F.	PHIL Motor-Generator Vs Hardware Small Scale System Integration Conclusion.....	79
Chapter 8: Emulated Diesel Generator Source for Power Quality Study.....		81
A.	Diesel Engine / Synchronous Generator Emulated Source .....	81
B.	Diesel Engine / Synchronous Generator Emulated Source Experimental Procedure .....	84
C.	No Buffering of the Diesel Engine / Synchronous Generator Source .....	84
D.	Diesel Engine / Synchronous Generator with Energy Storage Buffer.....	87
E.	PHIL Diesel Engine / Synchronous Generator System Integration Conclusion ...	90
Chapter 9: Conclusion.....		92
Appendix A.....		93
Appendix B.....		97
References.....		100



LIST OF FIGURES

FIGURE 1. VOLTAGE LEVELS DURING TRANSIENT EVENTS [6]..... 18

FIGURE 2. ROTOR SPEED DEVIATION DURING TRANSIENT LOADING [5]. ..... 18

FIGURE 3. MODEL OF LM2500 MARINE GAS TURBINE [7]. ..... 19

FIGURE 4. TOP LEVEL DIAGRAM OF A HESM ONTO A DC POINT OF COMMON COUPLING. .... 20

FIGURE 5. CONCEPTUAL BLOCK DIAGRAM OF CHIL. .... 22

FIGURE 6. CONCEPTUAL BLOCK DIAGRAM OF PHIL..... 23

FIGURE 7. DELAY THAT IS EXPERIENCED DURING A PHIL DEPLOYED GENERATION SOURCE [8]. ..... 24

FIGURE 8. PHIL DEPLOYED MODEL FEEDBACK DIAGRAM [8]..... 25

FIGURE 9. COMPARISON BETWEEN PHIL DEPLOYED MODEL AS HUT AND ORIGINAL CIRCUIT WITH STABLE CONDITIONS [8]. ..... 26

FIGURE 10. COMPARISON BETWEEN PHIL DEPLOYED MODEL AS HUT AND ORIGINAL CIRCUIT WITH UNSTABLE CONDITIONS [8]. ..... 26

FIGURE 11: PHIL EXPERIMENTAL SET UP FOR BATTERY EXPERIMENTATION [9]. ..... 28

FIGURE 12: RESULTS FROM ACCELERATION AND DECELERATION EXPERIMENT [9]. ..... 29

FIGURE 13: RESULTS OF HIL AND PHIL COMPARISON [9]. ..... 29

FIGURE 14. EXPERIMENTAL SET UP FOR POWER SYSTEM STABILIZATION ANALYSES [10]. ..... 30

FIGURE 15. FLORIDA STATE’S PHIL SETUP [11]. ..... 31

FIGURE 16. EXPERIMENTAL SETUPS USED FOR EVALUATING THE BRUSHLESS DC MOTOR CONTROLLER [9]. .....	32
FIGURE 17. A VISUAL REPRESENTATION OF AN INDUCTION MACHINE. NOTICE THAT THERE IS AN ANGLE DIFFERENCE BETWEEN THE STATOR AND ROTOR AXIS [10]. .....	34
FIGURE 18. EQUIVALENT CIRCUIT OF A INDUCTION MACHINE IN THE ROTARY REFERENCE FRAME [10]. .....	37
FIGURE 19. A TWO-POLE WYE CONNECTED SALIENT-POLE SYNCHRONOUS MACHINE [10]. .....	39
FIGURE 20. EQUIVALENT VOLTAGE AND FLUX LINKAGE CIRCUIT [10]. .....	44
FIGURE 21. A TOP-LEVEL UNDERSTANDING OF WHAT OCCURS IN A SINGLE SHAFT GAS TURBINE SYSTEM [11]. .....	45
FIGURE 22. LABVOLT 3 $\emptyset$ INDUCTION MOTOR (LEFT) AND 3 $\emptyset$ SYNCHRONOUS (RIGHT). .....	48
FIGURE 23. AMETEK CSW 5550 3 $\emptyset$ POWER SUPPLY THAT IS CAPABLE OF AC OR DC ANALOG CONTROL. .....	49
FIGURE 24. LABVOLT 8841-2 6 PULSE POWER THYRISTOR MODULE. ....	49
FIGURE 25. CONCEPTUAL DIAGRAM OF THE EXPERIMENTAL SETUPS. FURTHER COMPONENTS ARE ADDED INTO THE PHIL SIMULATION FOR COMPARISON PURPOSES .....	50
FIGURE 26. BLOCK DIAGRAM OF THE FULL HARDWARE TOPOLOGY. ....	51
FIGURE 27. DIAGRAM OF THE HIL EMULATED MOTOR-GENERATOR SOURCE HARDWARE TOPOLOGY. ....	51



FIGURE 28. DIAGRAM OF THE HIL EMULATED MOTOR-GENERATOR WITH RECTIFIER HARDWARE TOPOLOGY. ....	52
FIGURE 29. SIMULINK BLOCK DIAGRAM USED TO EMULATE THE LABVOLT MOTOR-GENERATOR SET IN REAL-TIME USING THE OPAL-RT REAL-TIME SIMULATOR. ....	53
FIGURE 30. SIMULINK BLOCK DIAGRAM USED TO EMULATE A MOTOR-GENERATOR WITH RECTIFIER IN REAL TIME USING OPAL-RT REAL-TIME SIMULATOR. ....	54
FIGURE 31. 3 $\theta$ VOLTAGE COMPARISON (HARDWARE ON THE LEFT AND MODELED ON THE RIGHT) BETWEEN SIMULATED AND PHYSICAL MOTOR-GENERATOR DURING TRANSIENT PROFILE. ....	55
FIGURE 32. 3 $\theta$ CURRENT COMPARISON (HARDWARE ON THE LEFT AND MODELED ON THE RIGHT) BETWEEN SIMULATED AND PHYSICAL MOTOR-GENERATOR DURING TRANSIENT PROFILE. ....	55
FIGURE 33. RECTIFIED VOLTAGE COMPARISON (HARDWARE ON THE LEFT AND MODELED ON THE RIGHT) BETWEEN SIMULATED AND PHYSICAL MOTOR-GENERATOR DURING TRANSIENT PROFILE. ....	56
FIGURE 34. RECTIFIER CURRENT COMPARISON (HARDWARE ON THE LEFT AND MODELED ON THE RIGHT) BETWEEN SIMULATED AND PHYSICAL MOTOR-GENERATOR DURING TRANSIENT PROFILE. ....	56
FIGURE 35. VOLTAGE HARMONIC COMPARISON BETWEEN SIMULATED AND HARDWARE SYSTEM. ....	57
FIGURE 36. CURRENT HARMONIC COMPARISON BETWEEN SIMULATED AND	

HARDWARE SYSTEM.....	57
FIGURE 37. 3 $\theta$ VOLTAGE COMPARISON (HARDWARE ON THE LEFT AND PHIL AC DEPLOYED MODEL ON THE RIGHT) BETWEEN SIMULATED AND PHYSICAL MOTOR-GENERATOR DURING TRANSIENT PROFILE. ....	59
FIGURE 38 3 $\theta$ CURRENT COMPARISON (HARDWARE ON THE LEFT AND PHIL AC DEPLOYED MODEL ON THE RIGHT) BETWEEN SIMULATED AND PHYSICAL MOTOR-GENERATOR DURING TRANSIENT PROFILE. ....	60
FIGURE 39. RECTIFIED VOLTAGE (HARDWARE ON THE LEFT AND PHIL AC DEPLOYED MODEL ON THE RIGHT) BETWEEN SIMULATED AND PHYSICAL MOTOR-GENERATOR DURING TRANSIENT PROFILE. ....	61
FIGURE 40. RECTIFIER CURRENT (HARDWARE ON THE LEFT AND PHIL AC DEPLOYED MODEL ON THE RIGHT) BETWEEN SIMULATED AND PHYSICAL MOTOR-GENERATOR DURING TRANSIENT PROFILE. ....	61
FIGURE 41. VOLTAGE HARMONIC COMPARISON BETWEEN PHIL DEPLOYED MOTOR-GENERATOR AND HARDWARE SYSTEM.....	62
FIGURE 42. CURRENT HARMONIC COMPARISON BETWEEN SIMULATED AND HARDWARE SYSTEM.....	62
FIGURE 43. RECTIFIED VOLTAGE (HARDWARE ON THE LEFT AND PHIL DC DEPLOYED MODEL ON THE RIGHT) BETWEEN SIMULATED AND PHYSICAL MOTOR-GENERATOR DURING TRANSIENT PROFILE. ....	64
FIGURE 44. RECTIFIER CURRENT (HARDWARE ON THE LEFT AND PHIL DC DEPLOYED MODEL ON THE RIGHT) BETWEEN SIMULATED AND PHYSICAL MOTOR-GENERATOR DURING TRANSIENT PROFILE. ....	65

FIGURE 45. CONCEPTUAL BLOCK DIAGRAM OF THE EXPERIMENTAL SETUP...	67
FIGURE 46. LABVOLT 3 $\phi$ MOTOR-GENERATOR SET.....	67
FIGURE 47. BLOCK DIAGRAM OF THE HARDWARE TOPOLOGY DEPLOYING A HARDWARE MOTOR-GENERATOR SET.....	68
FIGURE 48. BLOCK DIAGRAM OF THE HARDWARE TOPOLOGY DEPLOYING A HIL EMULATED AC GENERATOR.....	69
FIGURE 49. EXPERIMENTAL SETUP OF MANY COMPONENTS OF THE POWER SYSTEM BEING STUDIED.....	69
FIGURE 50. SIMULINK BLOCK DIAGRAM USED TO EMULATE A MOTOR- GENERATOR SET IN REAL-TIME USING THE OPAL-RT REAL-TIME SIMULATOR.	70
FIGURE 51. CURRENT DRAWN BY THE PROGRAMMABLE LOAD DURING EACH RESPECTIVE EXPERIMENT PERFORMED IN WHICH NO HESM WAS USED TO BUFFER THE AC SOURCE. ....	72
FIGURE 52. RECTIFIED CURRENT SUPPLIED BY THE AC SOURCE DURING EACH RESPECTIVE EXPERIMENT PERFORMED IN WHICH NO HESM WAS USED TO BUFFER THE AC SOURCE. ....	72
FIGURE 53. THE PCC DC BUS VOLTAGE SHOWING DEVIATION WHEN THE HESM IS NOT USED TO BUFFER THE AC SOURCE.....	73
FIGURE 54. PHASE VOLTAGE DROOPS OBSERVED WHEN THE AC SOURCE IS USED TO SUPPLY THE FULL TRANSIENT LOAD CURRENT.....	74
FIGURE 55. HIL SOURCE AND MOTOR-GENERATOR PHASE VOLTAGES ARE WITHIN 10.0% ERROR DESPITE HARMONIC DISTORTION IN THE MOTOR- GENERATOR. ....	74

FIGURE 56. LINE CURRENTS OF EACH RESPECTIVE AC SOURCE DURING A 1 SECOND REST PERIOD IN EXPERIMENTS WHERE NO BUFFERING SUPPLY IS USED. .... 75

FIGURE 57. LINE CURRENTS OF EACH RESPECTIVE AC SOURCE DURING A 5 SECOND LOAD PERIOD IN EXPERIMENTS WHERE NO BUFFERING SUPPLY IS USED. .... 75

FIGURE 58. CURRENT DRAWN BY THE PROGRAMMABLE LOAD DURING EACH RESPECTIVE EXPERIMENT PERFORMED WHEN THE HESM WAS USED TO BUFFER THE AC SOURCE. .... 77

FIGURE 59. RECTIFIED CURRENT SUPPLIED BY THE AC SOURCE DURING EACH RESPECTIVE EXPERIMENT PERFORMED WHEN THE HESM WAS USED TO BUFFER THE AC SOURCE. .... 77

FIGURE 60. THE PCC DC BUS VOLTAGE SHOWING MUCH REDUCED DEVIATION WHEN THE HESM IS USED TO BUFFER THE AC SOURCE. .... 78

FIGURE 61. PHASE VOLTAGE DROOPS OBSERVED WHEN THE HESM IS USED TO BUFFER THE AC SOURCE. .... 78

FIGURE 62. HIL SOURCE AND MOTOR-GENERATOR PHASE VOLTAGES ARE WITHIN 10.0% ERROR DESPITE HARMONIC DISTORTION IN THE MOTOR-GENERATOR WHEN BUFFERED BY HESM. .... 79

FIGURE 63. LINE CURRENTS OF EACH RESPECTIVE AC SOURCE DURING A 5 SECOND LOAD PERIOD IN EXPERIMENTS WHERE THE BUFFERING SUPPLY IS USED ..... 79

FIGURE 64. BLOCK DIAGRAM OF THE HARDWARE TOPOLOGY DEPLOYING A HIL

EMULATED AC GENERATOR AND AN AC/DC POWER SUPPLY FOR RECTIFICATION.....	81
FIGURE 65. DEPLOYED MODEL ON OPAL-RT HIL SYSTEM. ....	82
FIGURE 66. SM_MACHINE SIMULINK MODEL. ....	83
FIGURE 67. SM_USER MONITORS THE EXTERNAL MEASUREMENT SIGNALS, DYNAMIC LOAD, MACHINE PARAMETERS, AND STATOR VOLTAGES.....	83
FIGURE 68. (A) ROTOR SPEED DURING HIL GENERATOR DEPLOYED DURING EXPERIMENT. (B) ROTOR SPEED DURING THE LOAD PROFILE.....	85
FIGURE 69. (A) POWER SOURCED DURING HIL GENERATOR DEPLOYED DURING EXPERIMENT. (B) POWER SOURCED DURING THE LOAD PROFILE.....	86
FIGURE 70. (A) FOURIER TRANSFORM OF STATOR VOLTAGES DURING HIL GENERATOR DEPLOYED DURING EXPERIMENT. (B) FOURIER TRANSFORM OF STATOR VOLTAGE DURING LOAD PROFILE.....	87
FIGURE 71. (A) ROTOR SPEED DURING HIL GENERATOR DEPLOYED DURING EXPERIMENT. (B) ROTOR SPEED DURING THE LOAD PROFILE.....	89
FIGURE 72. (A) POWER SOURCED DURING HIL GENERATOR DEPLOYED DURING EXPERIMENT. (B) POWER SOURCED DURING LOAD PROFILE.....	89
FIGURE 73. (A) FOURIER TRANSFORM OF STATOR VOLTAGES DURING HIL GENERATOR DEPLOYED DURING EXPERIMENT. (B) FOURIER TRANSFORM OF STATOR VOLTAGES DURING LOAD PROFILE. ....	90

## Abstract

# INTEGRATION AND VALIDATION OF POWER HARDWARE-IN-THE-LOOP GENERATOR MODELS FOR DEPLOYMENT IN A DISTRIBUTED GENERATION SOURCE TESTBED

Jacob L. Sanchez-Roddy, PhD

The University of Texas at Arlington, 2019

SUPERVISING PROFESSOR: DAVID WETZ, PHD

Hardware in the Loop (HIL) is an established technology that allows for rapid prototyping of controls and verification of how physical devices respond for valid simulated systems. This involves deploying a model of a system onto a Field Programmable Gate Array (FPGA) that can take in external inputs and outputs the state variables present in the system. An example of this could involve the control of the roll, pitch, and yaw of a plane. A simulated plane could output the current state variables of the plane to an external controller which will respond with control signals to the simulated system to stabilize. This is a valuable way of evaluating controllers without the physical system present. Another method of HIL systems is known as Power Hardware in the Loop (PHIL). PHIL is typically used when a simulated system is emulated as a physical device (typically an amplifier) that either sinks or sources current into a physical energy storage device. One aspect of PHIL that has had little exploration is the process of deploying a model of a generation source to be emulated in a physical test bed for hardware validation. This would involve

emulating the generation source through a physical power supply that can accurately respond to the PHIL model. This type of operation would be of great interest for microgrids. Microgrids are becoming more popular as a backup system if it were to become isolated from the main grid. If this were to occur, an AC generation source could become the only source of power given the correct conditions. It is known that transient events can cause poor power quality that could cause damage to critical loads within the microgrid. Traditional generation sources consist of gas turbine sets coupled to a synchronous machine to supply the AC voltage needed to power devices present in the isolated microgrid. With possible repetitive transient events lowering the power quality of the generation source, a valid model of the generation source could be deployed as a PHIL model for hardware validation without the physical hardware being present. The repetitive transient events that will be studied are 1 to 30 seconds which are considered “short” transient events [6]. The models presented here were built using the SimPowerSystem toolbox within MATLAB/Simulink. The real time FPGA simulator for deploying the generation source model will be OPAL-RT which is capable of simulating system with an update time of  $5\mu\text{s}$ . This allows the simulation to be updated in  $5\mu\text{s}$  increments allowing the dynamics of the generation source to be taken into account and control the external power supply to emulate the modeled generation source with the real time updated stator voltages within the PHIL model.

## CHAPTER 1: INTRODUCTION

Traditionally, power distribution systems have consisted of large power plants that supply power to large portions of the population at a time. Last reported in 2017, there are 8,652 power plants that generate over 1MW of power in the United States as [1]. These power 127.59 million households in the United States [2]. With the ratio of generation sources to households to power being so high, a push toward more local sized distributed generation systems have become of interest in recent years. One challenge that faces these local sized microgrids are power outages that require a black start in order to bring the grid back online. If a blackout were to occur and a black start is needed, the generation source capable of restoring power to the grid would first be brought up with no load attached. After the generation source is brought up, a breaker would have to be closed even though there is no power within the grid. When the breakers close, this would be considered a very high transient event [3].

A microgrid is a network that combines a variety of different generation sources such as fossil fuel generators, solar panels, fuel cells, flywheels, wind turbines, and batteries. These are controlled intelligently in order to supply the energy needed for any load connected. Microgrids allow for different generation sources to communicate and share the desired energy requirements in an optimal way. One aspect of microgrids is that they can operate independently from the main grid. Microgrids connect to the main grid through a point of common coupling that maintains the same voltage and frequency levels. This is to either put excess power into the main grid or accept power from the main grid if needed. In the scenario that a microgrid got disconnected from the main grid during a high-power need, this would cause a transient event to occur on the fuel-based



generator. The fuel-based generator would experience the highest transient event within the microgrid due to the high energy density of fuel compared to all other sources within the system. Given the right circumstances, the fuel-based generation source could be the only online source. If this were to occur, this would be a high varying and possibly random power is demanded depending on the loads that are connected and disconnected from the microgrid.

With microgrid type architecture becoming more popular, the study of a variety of different load profiles is something that would need to be experimentally evaluated for different generation sources. A major problem if a microgrid's fuel-based generator were to become the only source of power, the power quality of the generator would suffer greatly.

Power quality refers to the quality of the voltage waveform during operation. When referring to quality, there is an acceptable range for commercial devices. When reference to the voltage magnitude, the power quality standard according to Pacific Power for 120V to 600V AC systems ranges from 92% to 105% of the nominal voltage level [4]. The frequency deviation, according to Pacific Power, for steady state operation is considered to be worst case  $\pm 0.100$  Hz for normal operation,  $\pm 0.150$  Hz for sudden changes, and  $\pm 0.750$  Hz for major breakup scenarios [4]. With constrains like these and the possibility of a smaller generator within a microgrid being the only power source, the random power demands that could occur could cause the voltage to sag or rise to unacceptable levels or cause the frequency to deviate outside the acceptable levels. When a transient event occurs with a fuel-based generation source, the rotor speed drops which causes a decrease in electrical frequency. During this time, more fuel is input into the system to

recover the rotor speed to the nominal value. When the transient event ends, more fuel is being input into the system to account for the previous transient event. When this occurs, the rotor speed overshoots and causes an increase in electrical frequency. These shifts in frequency and amplitude could damage equipment, cause the voltage to collapse, or stall the engine when used as a motor application [5]. Examples of these events are shown below in Figure 1 and Figure 2.

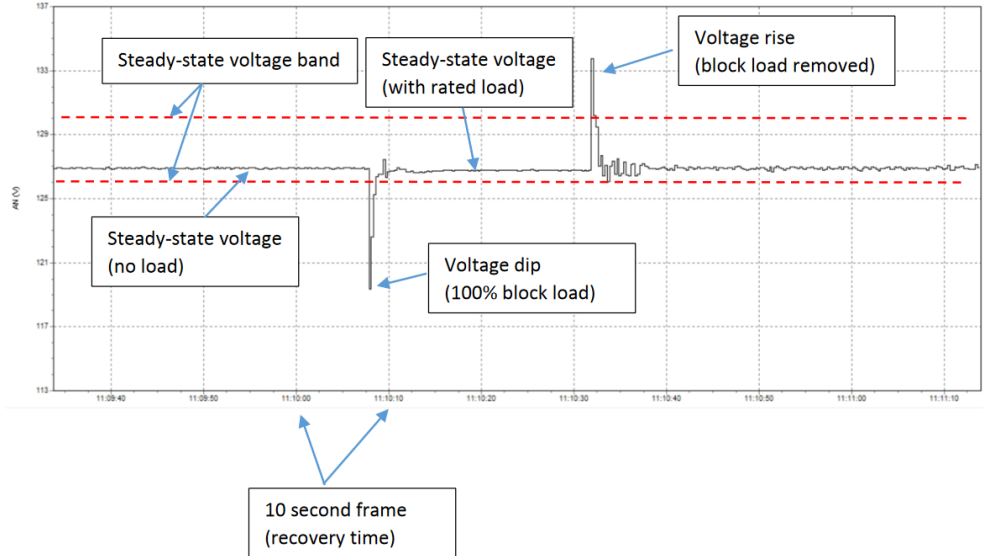


Figure 1. Voltage levels during transient events [6].

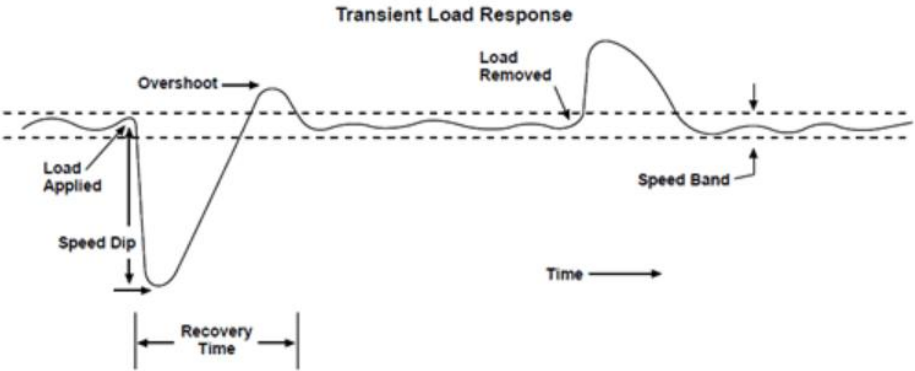


Figure 2. Rotor speed deviation during transient loading [5].

To experimentally evaluate the power quality of AC generation sources, the physical

generation source is needed for integration into a built test bed to evaluate the performance. For example, a model of a LM2500 Marine Gas Turbine is shown below in Figure 3. To apply this to a generation source, a synchronous machine would be coupled to the shaft to make the system into a Gas Turbine Generator Set (GTGS). To experimentally evaluate a generation source such as the LM2500, the source would first have to be obtained and a test bed built around the parameters and size of the GTGS. Obtaining a generation source such as the LM2500 would be incredibly difficult and building a test bed around it would be incredibly expensive and impractical. The size of the LM2500 is a volume of 146m<sup>3</sup> and has a base weight of 90,000 kg which again makes it incredibly impractical and costly to build a testbed in order to experimentally evaluate the power quality during repetitive short transient events [7].

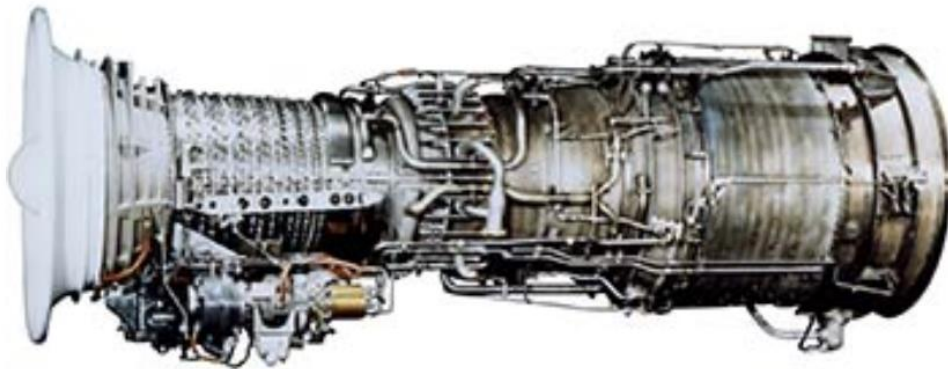


Figure 3. Model of LM2500 Marine Gas Turbine [7].

With the need for power quality to be improved during possible transient events, a Hybrid Energy Storage Module (HESM) could be introduced into the system to buffer the AC generator during these transient events. A HESM operates by sinking or sourcing energy depending on the current requirements of the load connected. If a load is suddenly taken off the grid causing a large drop in power demand, instead of a transient event

occurring on the AC generation source, this difference in power would be redirected into the HESM in order to keep the generation source consistently loaded. Likewise, if a large increase in power demand occurs, instead of a transient event causing the generator to supply all the extra energy required, the HESM would make up for the increase power load which keeps the generation source base loaded. A top-level diagram of an AC source with a HESM for mitigating transient events is shown below in Figure 4.

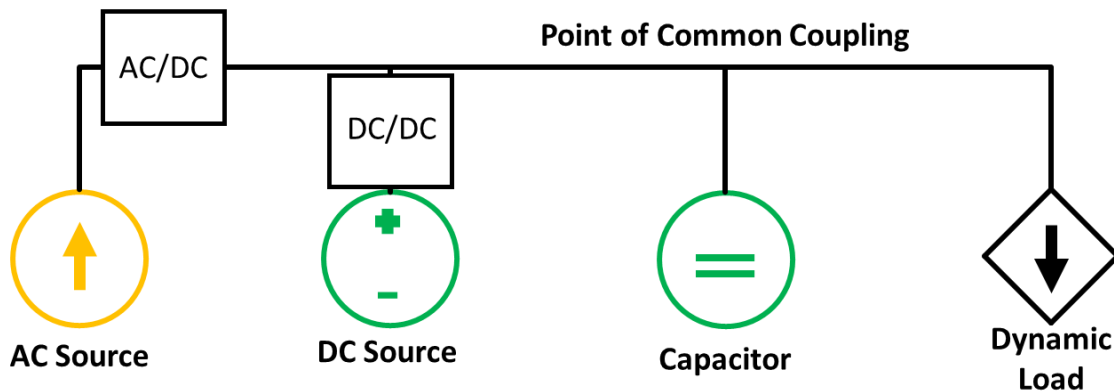


Figure 4. Top level diagram of a HESM onto a DC point of common coupling.

The LM2500 would be considered the AC source in the system described above. The regulation of this generation source would be through power electronics to regulate the DC voltage onto the point of common coupling between the distributed sources. The DC source could be represented as electrochemical batteries that either sink or source current based on the power demands of the load. The capacitor is considered the DC link between the load and generators.

Previous work performed at the PPEL at the University of Texas at Arlington (UTA) has shown the effectiveness of HESM's in buffering transient loading on a rotating machine in order to improve power quality. A gasoline engine driven single-phase generator was used as the rotating machine and a DC power supply was used as a rectifier. The work

performed to date has been incredibly valuable in demonstrating HESM viability. However, the ability to experiment and demonstrate the HESM viability with different generation sources is unknown due to the limitations of acquiring the generation source needed for experimentation. While it would be ideal to acquire and conduct experiments on a variety of generation sources, this is not practical and alternative evaluation methods are needed.

To experiment with a variety of different generation sources, an established technology called Hardware in the Loop (HIL) capable of running a simulation in real time and can receive external inputs measurements and output state variables of a simulated generation source is proposed to be a viable method of evaluating the power quality within a built testbed without the physical generation source being needed. Emulating a generation source in this fashion could be considered a new way of using Power Hardware in the Loop (PHIL). With this technique, with a valid generator model, the dynamics and power quality can be experimentally evaluated and studied without the physical generation source needed. The coupling point within a microgrid will be assumed to be a DC voltage. Therefore, for all the experiments performed in this validation, an AC/DC converter was used for the load connection. The profiles studied are considered short transient events that range between 1 and 30 second time frame [5].

## CHAPTER 2: HARDWARE IN THE LOOP BACKGROUND

HIL is a technique that allows simulated systems to be deployed onto an FPGA and allows external signals to manipulate the simulated system. There are two methods of using this technology which are known as Controller Hardware in the Loop (CHIL) and Power Hardware in the Loop (PHIL).

### A. Controller Hardware in the Loop.

CHIL is where a simulated system, for example a microgrid, is deployed onto the FPGA. The outputs of the system are node voltages and line currents which are received from the real time simulation into an external controller. The controller, which is fed the node voltages and line currents, controls the simulated system as if the actual system was physically present for experimentation. A simple block diagram of CHIL is shown below in Figure 5.

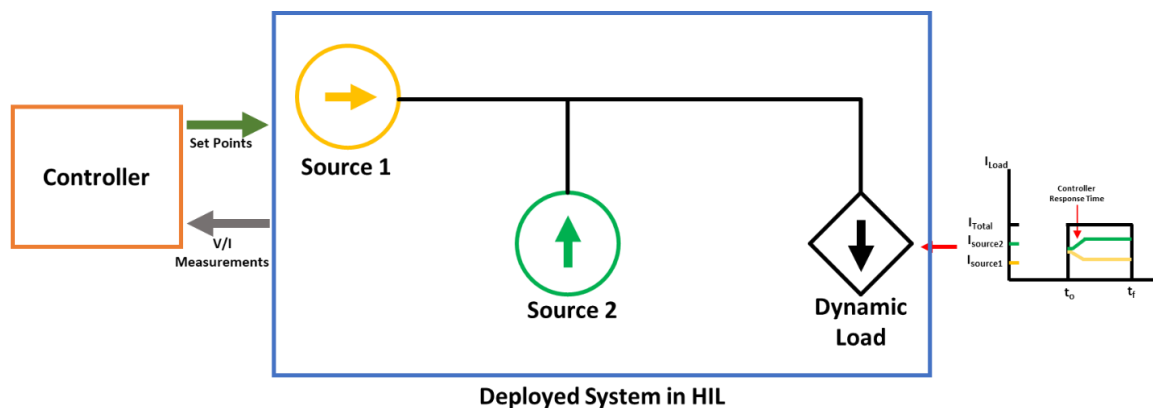


Figure 5. Conceptual Block Diagram of CHIL.

### B. Power Hardware in the Loop

PHIL is typically used when a simulated system is emulated as a physical device, typically an amplifier, and either sinks or sources current into a physical energy storage device to evaluate the performance. One aspect of PHIL that has little exploration is

replacing a physical generation source with a PHIL deployed model for hardware validation. This allows one to experimentally evaluate a generation source not presently owned by implementing the PHIL model into a physical testbed or physical setup. A simple block diagram of PHIL is shown below in Figure 6.

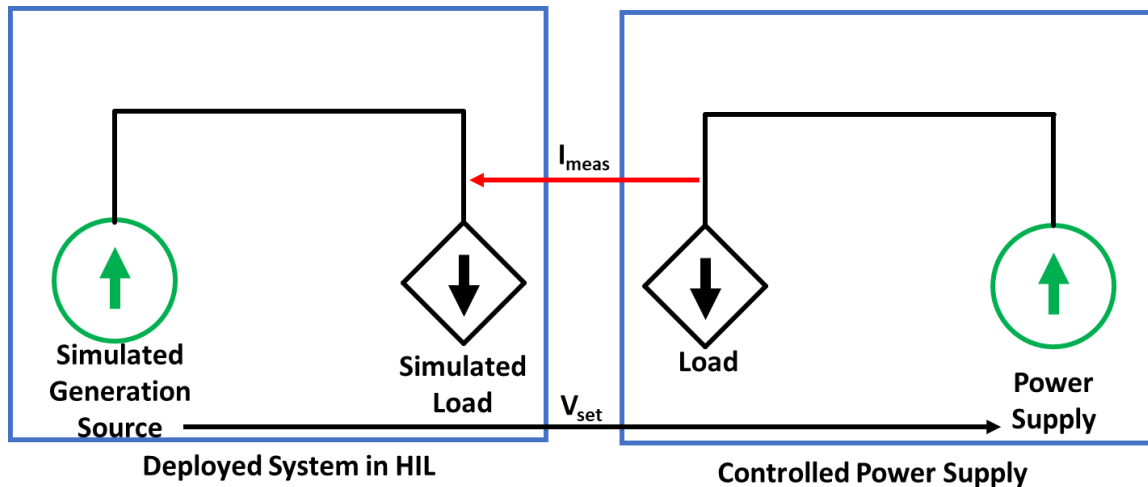


Figure 6. Conceptual block diagram of PHIL.

To understand the above figure, the simulated generation source's voltage is sent to the power supply to emulate the simulation. With this generation source emulated as an external power supply, when a load is attached to this power supply, the current drawn from the power supply is received as an analog input and loads the generation source within simulation. This loading effect in simulation will affect the simulated generation source which will change the  $V_{set}$  point for the controlled power supply. This cycle will repeat updating the set point of the controlled power supply as the generation source is loaded in real time. This allows us to emulate the generation source in real time and study the power quality.

### C. Validity of Power Hardware in the Loop

PHIL has some draw backs for being a simulated generation source as there are some

delays due to the analog to digital converter (A/D) and Digital to Analog (D/A) converters needed to receive external signals and output the simulation state variables. Figure 7 shows a flow chart of what processes are occurring to cause delays in the real time simulation [8].



Figure 7. Delay that is experienced during a PHIL deployed generation source [8].

Previous evaluations of PHIL systems show how accurate a simulated PHIL deployed model is to a hardware equivalent circuit [8]. For this validation, the author constructed a series RL circuit using a variable autotransformer as an ideal sinusoidal voltage source connected to a series RL circuit. This circuit was then simulated as a virtual circuit and deployed onto an external amplifier. The block diagram of signal transfers is shown in Figure 8. For clarification, the virtual circuit is a deployed model of the sinusoidal voltage source where the A/D( $T_V$ ) and D/A( $T_I$ ) converters are the interface between the simulation and the hardware under test (HuT).  $T_{HuT}$  is the measurement response time of the hardware under test (HuT) before the A/D converter.



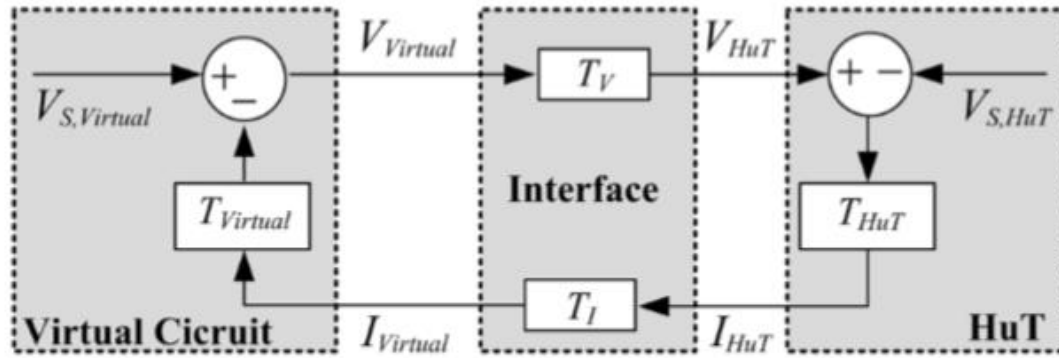


Figure 8. PHIL deployed model feedback diagram 100[8].

From the above figure starting from the left input, the PHIL model sets a voltage set point that is then transferred to the external power supply to be amplified to emulate the voltage source in simulation. The feedback is the current draw from the external power supply that is received through the analog(A/D) inputs to load the PHIL deployed model.

Below, the results from [8] show that there is a very small error between the original circuit and HuT. This small error in delay and amplitude is expected as to the complex nature of the FPGA and update time of the simulation itself. Although the step time of the authors simulation is not specified, the simplicity of the circuit leads to the assumption that the simulation time step is on the order of 100ns. The results below show a stable system where there is very little difference between the original circuit and HuT. Figure 9 and Figure 10 shows a comparison of a stable and unstable system which again, shows that there is very little difference between the original circuit and PHIL deployed model.

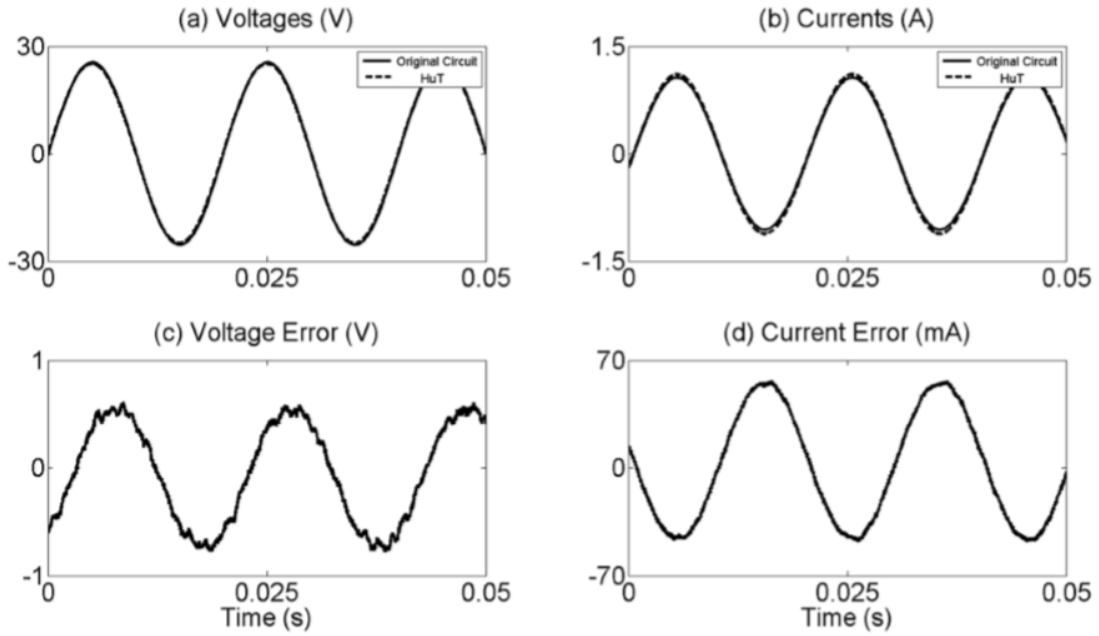


Figure 9. Comparison between PHIL deployed model as HuT and original circuit with stable conditions [8].

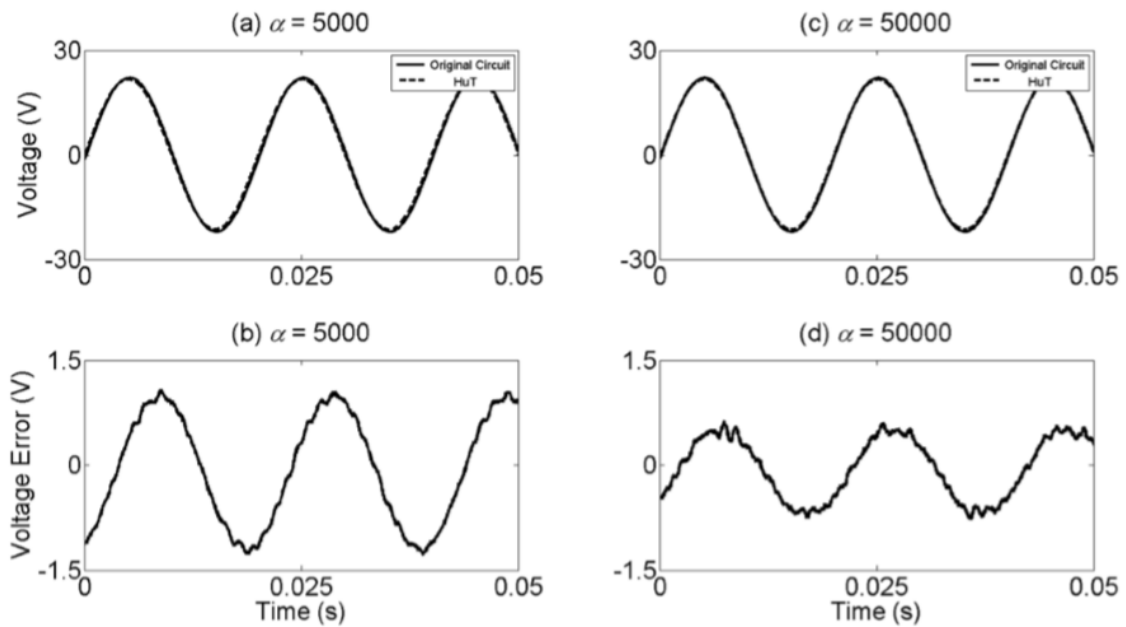


Figure 10. Comparison between PHIL deployed model as HuT and original Circuit with unstable conditions [8].

In these previous experiments, it has been shown that validating the accuracy of PHIL

deployed models for simple circuits, the next logical step is to experiment with more complex systems. The real time simulation system used for these simulations is Opal-RT's real time simulator OP5670.

#### D. Previous work with PHIL

Previous work involving PHIL focuses on the validations of inverter controls for scenarios such as electric vehicles [9], power system stabilization [10], PV converters [11], and motor drive controls [12]. Little focus has been on the hardware validation of generation PHIL models when implemented into a physical testbed. For a quick top-level understanding of the work that has previously been done, a modeled system was deployed into a HIL emulator for real controllers to be evaluated. The HIL deployed model would send the current state variables to the physical controller and would respond as if the physical system was present.

In [9], A PHIL model of an electric vehicle is used to experimentally evaluate the batteries proposed to be used in the electric vehicle. Below in Figure 11, the PHIL experimental set up is shown for evaluating their battery choice.

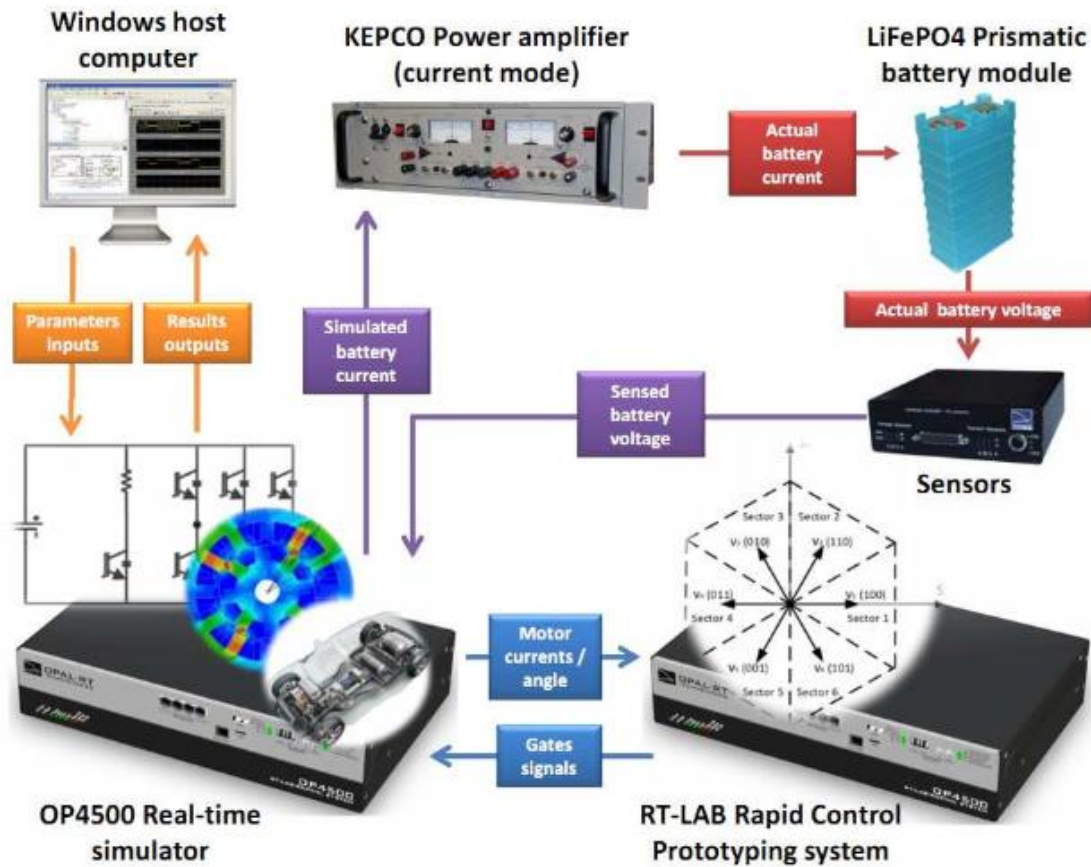


Figure 11: PHIL experimental set up for battery experimentation [9].

For the above experimental set up, the electric vehicle is modeled and deployed onto the OP4500 Real-time simulator. The parameters of the electric vehicle are sent via the Windows host computer. This real time simulator outputs the current draw from the simulation to a power amplifier that draws current from the physical battery. The battery voltage is monitored and sent into the OP4500 to update the voltage set point of the simulated battery. The control of the electric car is performed by a RT-LAB Rapid Control Prototyping system that sends the gate signals based on the motor currents/angles [9]. The information being sent to the control system is based on the scenario the user inputs from the host PC. The results of a simulated case where the vehicle accelerates and decelerates to evaluate the battery's performance during this operation.

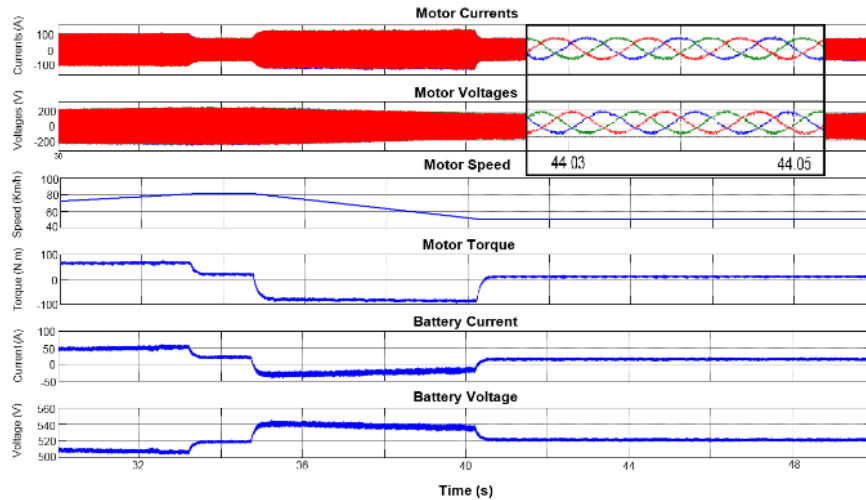


Figure 12: Results from acceleration and deceleration experiment [9].

One other aspect studied is the comparison between an HIL and PHIL experiment. For one experiment, a simulated battery is used as opposed to the hardware battery obtained. This was done to show the validity of PHIL because the parameters that dictate the battery voltage vary with state of charge and current draw where the HIL model has hard coded parameters [9]. The results of this comparison are shown below in Figure 13.

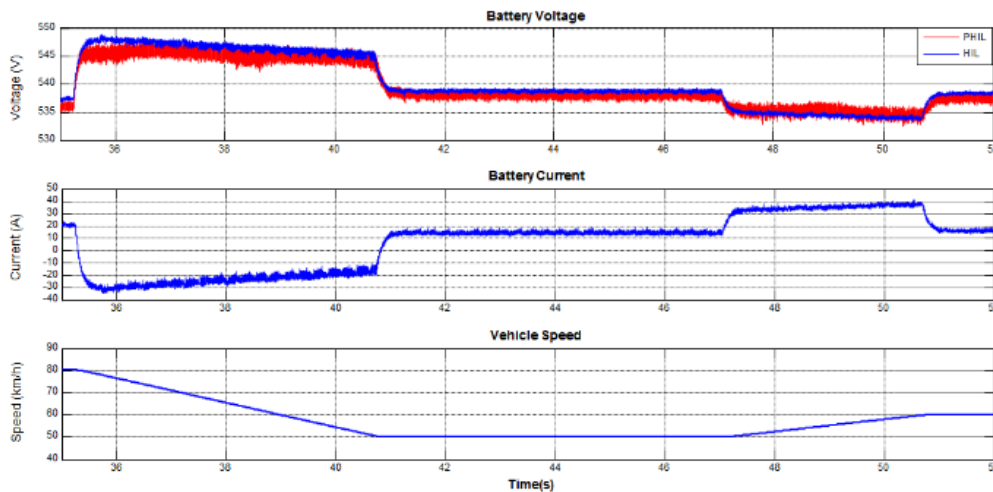


Figure 13: Results of HIL and PHIL comparison [9].

Another focus for PHIL is with power system stability analysis [10]. In this experiment, A PHIL model of a distribution grid with ~10k nodes is modeled. The hardware setup consists of three power amplifiers capable of ~90kW connected to three different converters that, when engaged by the power amplifier, feed current measurements into the PHIL model to mimic a distribution node within the simulated system [10]. A diagram of the experimental set up is shown in Figure 14.

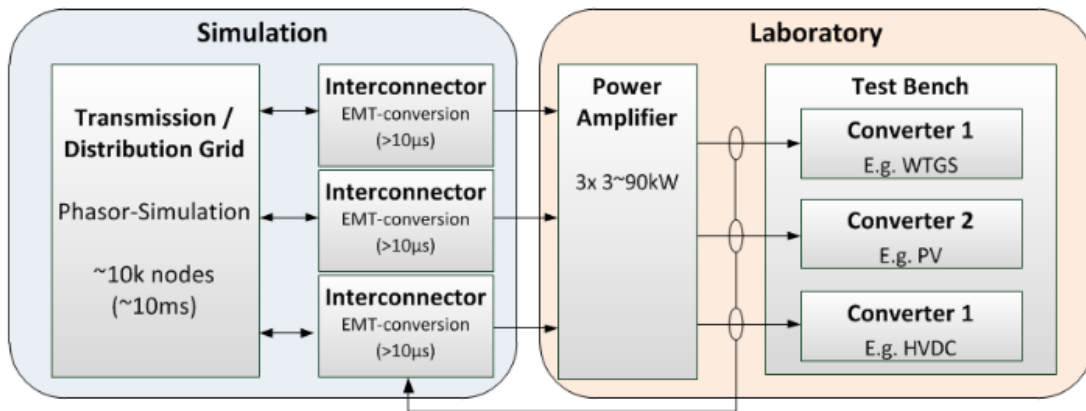


Figure 14. Experimental set up for power system stabilization analyses [10].

The conclusion for this work was that PHIL can support advanced testing of large interconnected power systems for stability analysis. This allows for innovative methods to be evaluated within a lab-based testing as opposed to purely simulation-based testing.

Florida State University is using PHIL as the base for anti-islanding testing for PV converters [11]. Figure 15 shows is the experimental PHIL setup.

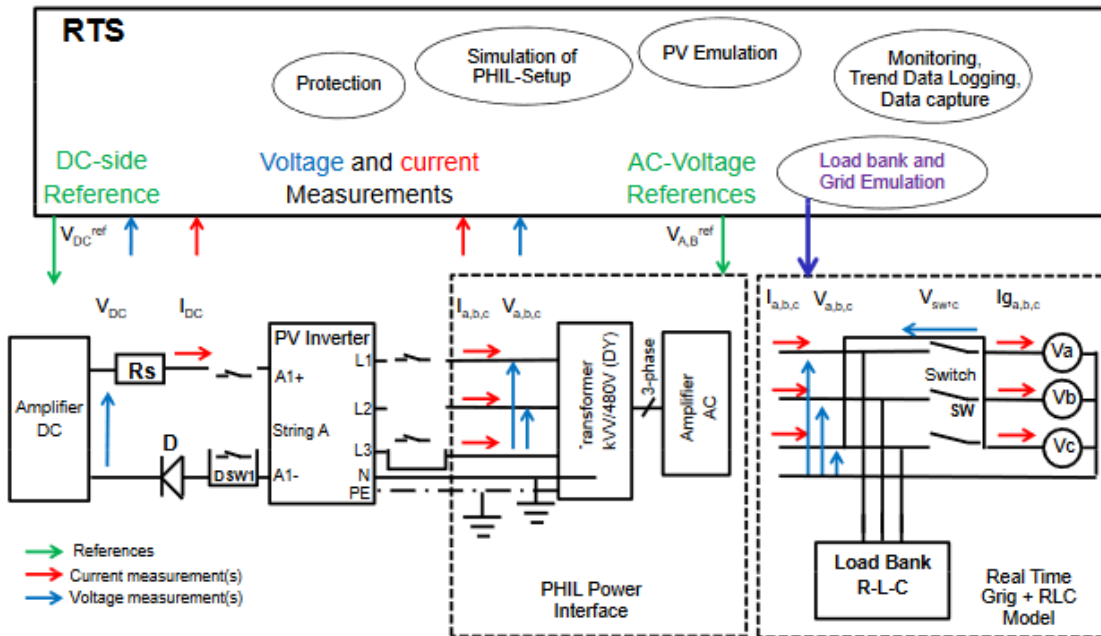


Figure 15. Florida State’s PHIL setup [11].

For the purpose of this experiment, the RLC load bank seen above was incorporated into the real time model and compared to the condition where the RLC load bank was part of the physical setup. Florida State concluded that the RLC load bank being incorporated into the PHIL simulation was a valid replacement to having the hardware equivalent physically owned. When the RLC load bank was incorporated, the load bank vs PHIL experiments show comparable responses implying that the integration of the RLC load bank into the PHIL model is a valid way of proceeding with the experimentation [11].

The final example using PHIL is a case study by Plastic Omnium where a 30 BLDC motor sensorless controller with trapezoidal back EMF needed to be evaluated at low power levels in steady state [12]. Figure 16 shows the setup used during this study.

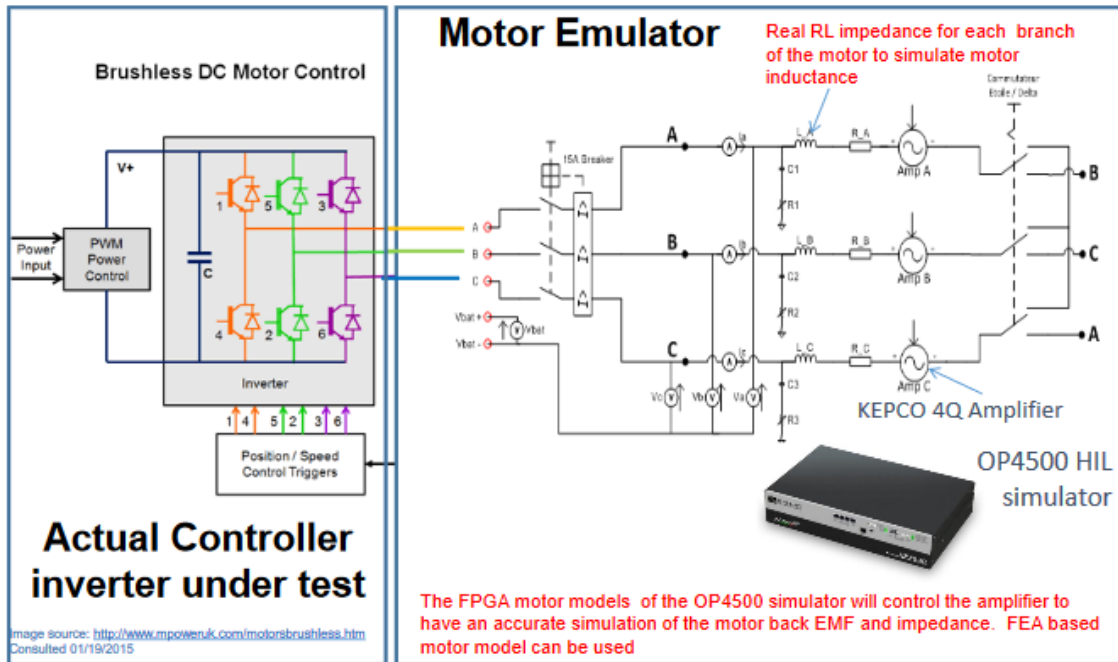


Figure 16. Experimental setups used for evaluating the brushless DC motor controller [12].

For this experimental setup, a brushless DC motor was emulated using the OP4500 and controlled 3 KEPCO 4Q amplifiers for power draw from the controller. Information needed for the control system was from the emulated system to the controller under test to send the trigger signals to the inverter. The inverter sources current to the emulated motor for evaluation.

From the literature shown above, no study has been done on hardware validation of generation sources within physical test beds using PHIL deployed models. This is the focus of the research presented here. Next, the logical step to understand the complexity of the generation sources that will be modeled and evaluated without the physical generation source having to be acquired.



### CHAPTER 3: INDUCTION MACHINE BACKGROUND

Induction machines are the means of converting electrical power to mechanical power [13]. An understanding of induction machines is essential to understand the complexity of the generation source that is modeled later for a proof of concept that PHIL is a valid method to experimentally evaluate generation sources not available, but a valid PHIL deployed model is present. For the purposes of this paper, a 3 $\theta$  symmetrical induction machine with sinusoidal distributed stator and rotor windings will be assumed. The voltage equations of an induction machine are as follows [13].

$$V_{abcs} = r_s i_{abcs} + p \lambda_{abcs} \quad (1)$$

$$V_{abc4} = r_r i_{abc4} + p \lambda_{abc4} \quad (2)$$

Where  $s$  denotes parameters associated with the stator circuit and  $r$  denotes parameters with the rotor. It should be noted that  $r_r$  and  $r_s$  are diagonal matrices each with equal values as shown below [13].

$$r_x = \begin{bmatrix} r_x & 0 & 0 \\ 0 & r_x & 0 \\ 0 & 0 & r_x \end{bmatrix} \quad (3)$$

$\lambda$  is the flux linkage and is expressed as

$$\begin{bmatrix} \lambda_{abcs} \\ \lambda_{abc4} \end{bmatrix} = \begin{bmatrix} L_s & L_{sr} \\ (L_{sr})^T & L_r \end{bmatrix} \begin{bmatrix} i_{abcs} \\ i_{abc4} \end{bmatrix} \quad (4)$$

and the winding inductances ( $L_s, L_r, L_{sr}$ ) are shown below.

$$L_s = \begin{bmatrix} L_{ls} + L_{ms} & -\frac{1}{2}L_{ms} & -\frac{1}{2}L_{ms} \\ -\frac{1}{2}L_{ms} & L_{ls} + L_{ms} & -\frac{1}{2}L_{ms} \\ -\frac{1}{2}L_{ms} & -\frac{1}{2}L_{ms} & L_{ls} + L_{ms} \end{bmatrix} \quad (5)$$

$$L_r = \begin{bmatrix} L_{lr} + L_{mr} & -\frac{1}{2}L_{mr} & -\frac{1}{2}L_{mr} \\ -\frac{1}{2}L_{mr} & L_{lr} + L_{mr} & -\frac{1}{2}L_{mr} \\ -\frac{1}{2}L_{mr} & -\frac{1}{2}L_{mr} & L_{lr} + L_{mr} \end{bmatrix} \quad (6)$$

$$L_{sr} = \begin{bmatrix} \cos\theta_r & \cos(\theta_r + \frac{2\pi}{3}) & \cos(\theta_r - \frac{2\pi}{3}) \\ \cos(\theta_r - \frac{2\pi}{3}) & \cos\theta_r & \cos(\theta_r + \frac{2\pi}{3}) \\ \cos(\theta_r + \frac{2\pi}{3}) & \cos(\theta_r - \frac{2\pi}{3}) & \cos\theta_r \end{bmatrix} \quad (7)$$

Where the inductance equations  $L_{ls}$  and  $L_{ms}$  are the leakage magnetization inductances of the stator windings.  $L_{lr}$  and  $L_{mr}$  are the leakage magnetization inductances of the rotor.  $L_{sr}$  is the amplitude of the mutual inductances between the stator and rotor windings [13]. A visual representation of an induction machine is shown below.

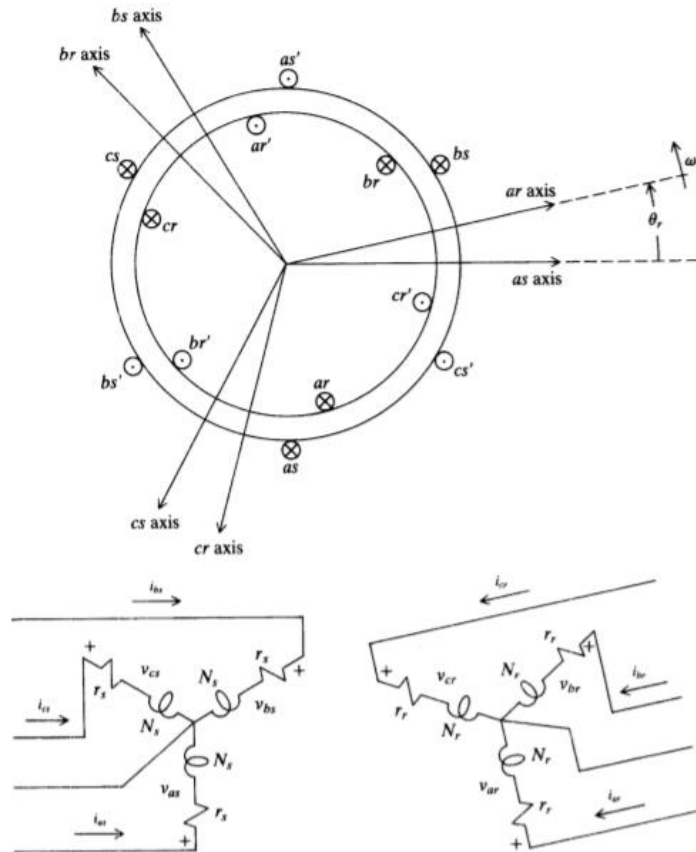


Figure 17. A visual representation of an induction machine. Notice that there is an angle difference between the stator and rotor axis [13].

The above equations are considered in the synchronous reference frame. To make the analysis and modeling simpler, a transformation to the rotary reference frame needs to be applied. The equation for this transformation is shown below.

$$K_r = \frac{2}{3} \begin{bmatrix} \cos(\theta - \theta_r) & \cos(\theta - \theta_r - \frac{2\pi}{3}) & \cos(\theta - \theta_r + \frac{2\pi}{3}) \\ \sin(\theta - \theta_r) & \sin(\theta - \theta_r - \frac{2\pi}{3}) & \sin(\theta - \theta_r + \frac{2\pi}{3}) \\ \frac{1}{2} & \frac{1}{2} & \frac{1}{2} \end{bmatrix} \quad (8)$$

Where

$$I_{dq0s} = KI_{abcs} \quad (9)$$

$$V_{dq0s} = KV_{abcs} \quad (10)$$

The voltage equations in the rotary reference frame is shown below.

$$V_{qd0s} = r_s i_{dq0s} + \omega \lambda_{ds} + \frac{d}{dt} \lambda_{dq0s} \quad (11)$$

$$V_{qd0r} = r'_r i'_{qd0s} + (\omega - \omega_r) \lambda'_{dqr} + \frac{d}{dt} \lambda'_{qd0r} \quad (12)$$

Where

$$(\lambda_{dqs})^T = [\lambda_{ds} \quad -\lambda_{qs} \quad 0] \quad (13)$$

$$(\lambda'_{dqr})^T = [\lambda'_{dr} \quad -\lambda'_{qr} \quad 0] \quad (14)$$

Next, the flux linkages equations are determined, this is done by substituting the equations expressed in the synchronous reference frame

$$\begin{bmatrix} \lambda_{qd0s} \\ \lambda'_{qd0r} \end{bmatrix} = \begin{bmatrix} K_S L_S (K_S)^{-1} & K_S L'_{Sr} (K_r)^{-1} \\ K_r (L'_{Sr})^T (K_S)^{-1} & K_r L'_r (K_r)^{-1} \end{bmatrix} \begin{bmatrix} i_{qd0s} \\ i'_{qd0r} \end{bmatrix} \quad (15)$$

Where

$$K_S L_S (K_S)^{-1} = \begin{bmatrix} L_{ls} + L_M & 0 & 0 \\ 0 & L_{ls} + L_M & 0 \\ 0 & 0 & L_{ls} \end{bmatrix} \quad (16)$$

$$K_r L'_r (K_r)^{-1} = \begin{bmatrix} L'_{lr} + L_M & 0 & 0 \\ 0 & L'_{lr} + L_M & 0 \\ 0 & 0 & L'_{lr} \end{bmatrix} \quad (17)$$

and can be shown that

$$K_s L'_{sr} (K_r)^{-1} = K_r (L'_{sr})^T (K_s)^{-1} = \begin{bmatrix} L_M & 0 & 0 \\ 0 & L_M & 0 \\ 0 & 0 & 0 \end{bmatrix} \quad (18)$$

This allows the voltage equations to be written in an expanded form.

$$v_{qs} = r_s i_{qs} + \omega \lambda_{ds} + \frac{d}{dt} \lambda_{qs} \quad (19)$$

$$v_{ds} = r_s i_{ds} + \omega \lambda_{qs} + \frac{d}{dt} \lambda_{ds} \quad (20)$$

$$v_{0s} = r_s i_{0s} + \frac{d}{dt} \lambda_{0s} \quad (21)$$

$$v'_{qr} = r_r i_{rs} + (\omega - \omega_r) \lambda'_{dr} + \frac{d}{dt} \lambda_{qr} \quad (22)$$

$$v'_{dr} = r'_r i'_{dr} + (\omega - \omega_r) \lambda'_{qr} + \frac{d}{dt} \lambda'_{dr} \quad (23)$$

$$v'_{0r} = r'_r i'_{0r} + \frac{d}{dt} \lambda'_{0r} \quad (24)$$

and the flux linkage equations to be written as follows.

$$\lambda_{qs} = L_{ls} i_{qs} + L_M (i_{qs} + i'_{qr}) \quad (25)$$

$$\lambda_{ds} = L_{ls} i_{ds} + L_M (i_{ds} + i'_{dr}) \quad (26)$$

$$\lambda_{0s} = L_{ls} i_{0s} \quad (27)$$

$$\lambda'_{qr} = L'_{lr} i'_{qr} + L_M (i_{qs} + i'_{qr}) \quad (28)$$

$$\lambda'_{dr} = L'_{lr} i'_{dr} + L_M (i_{ds} + i'_{dr}) \quad (29)$$

$$\lambda'_{0r} = L'_{lr} i'_{0r} \quad (30)$$

The above voltage and flux linkage equations allow us to draw an equivalent circuit shown below in Figure 18.

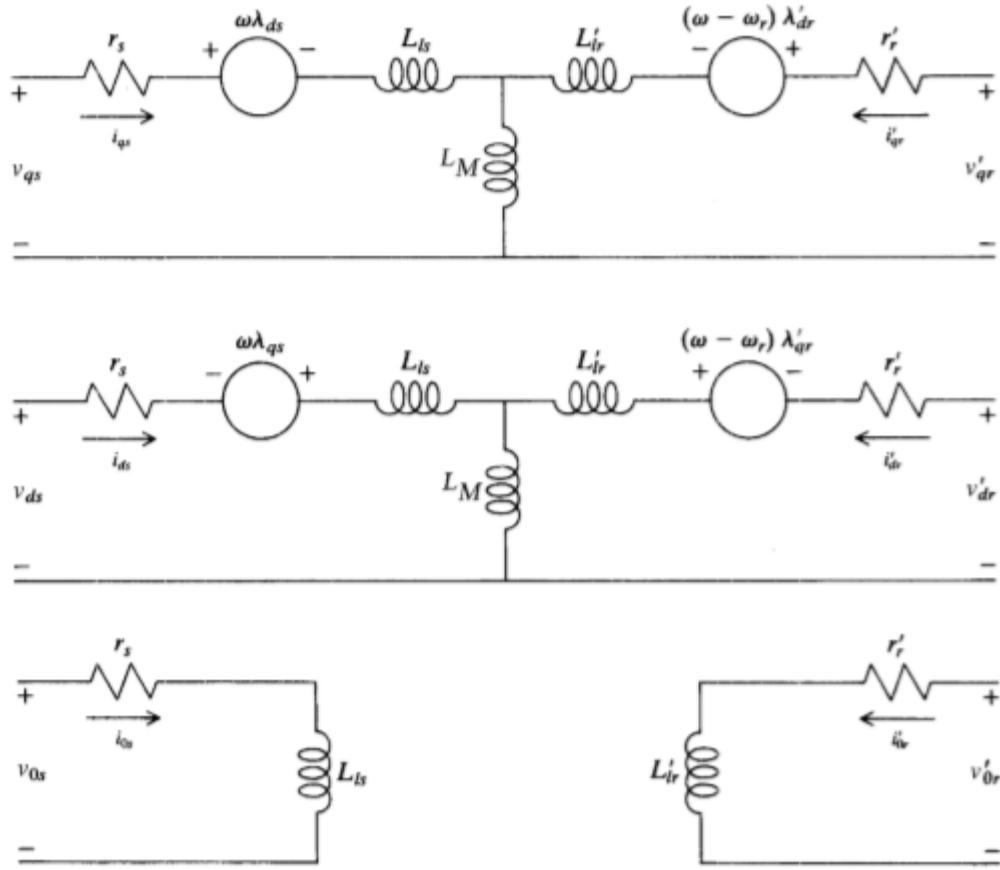


Figure 18. Equivalent circuit of an induction machine in the rotary reference frame [13].

The equation for the electromagnetic torque is shown below.

$$T_e = \frac{3}{2} \left( \frac{P}{2} \right) \lambda_{ds} i_{qs} - \lambda_{qs} i_{ds} \quad (31)$$

and the relationship between electromagnetic torque and rotor speed is

$$T_e = J \left( \frac{2}{P} \right) \frac{d}{dt} \omega_r + T_L \quad (32)$$

Where J is the inertia of the rotor, P is the number of poles the rotating machine has.  $T_L$  is the torque load on the induction machine.

An induction machine is a very complex system which will be modeled for the experimental validation of a PHIL model vs the physical hardware. This understanding of

the number of state variables and state transitions occurring during operation shows the complexity of the modeled system when deployed as a replacement to the physical machine.

These equations are a necessity because this is the model used for asynchronous machine in the MATLAB/Simulink library. For the experiment discussed later in the hardware/PHIL comparison, an induction machines rotor is coupled to a synchronous machine generator to produce a 208 3 $\theta$  voltage signal. The synchronous machine analysis will be explained in the next section.

## CHAPTER 4: SYNCHRONOUS MACHINE BACKGROUND

Synchronous machines are used for nearly all electric power generation throughout the world [13]. Just as induction machines are the prime means of converting electrical energy to mechanical energy, synchronous machines are the prime means of converting mechanical energy to electrical energy. For synchronous machines, the stator windings are physically placed  $120^\circ$  apart and the rotor of a synchronous machine is equipped with a field winding. These field windings are magnetically unsymmetrical in order to achieve the transformation into the rotor reference frame. This is how the MATLAB/Simulink toolbox models synchronous machines. A two pole  $3\theta$  wye connected synchronous machine is shown below in Figure 19.

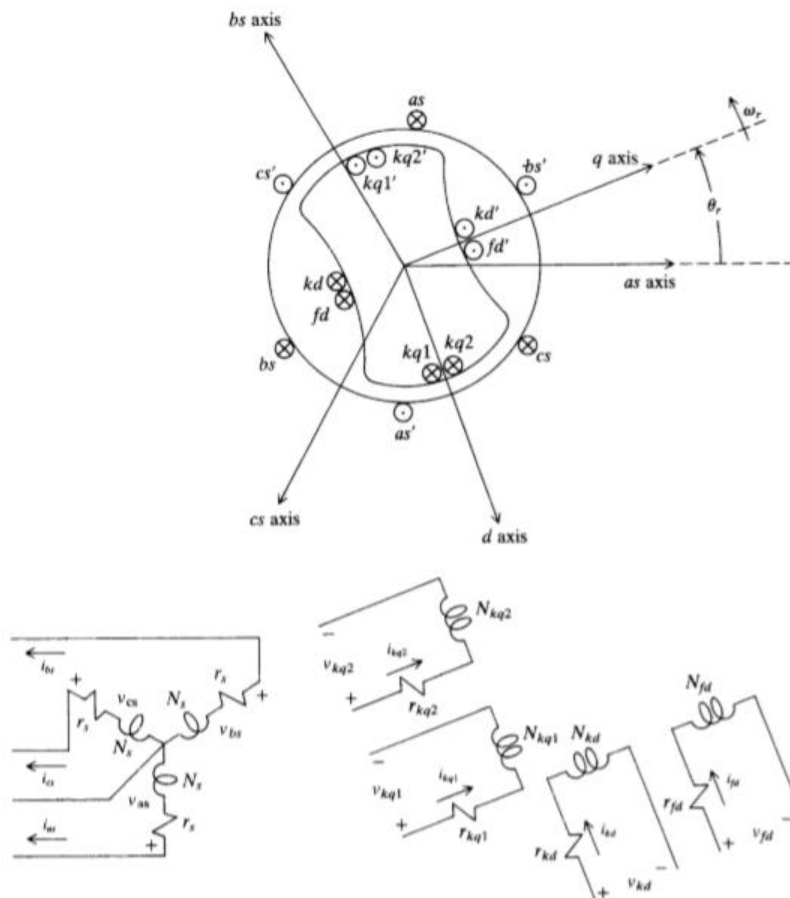


Figure 19. a two-pole wye connected salient-pole synchronous machine [13].

First, the machine variable equations will be shown and then transformed into the rotary reference because this is how the MATLAB/Simulink toolbox simulates the synchronous machine. The voltage equations are shown below

$$v_{abcs} = -r_s i_{abcs} + \frac{d}{dt} \lambda_{abcs} \quad (33)$$

$$v_{qdr} = r_r i_{qdr} + \frac{d}{dt} \lambda_{qdr} \quad (34)$$

Where,

$$r_s = \begin{bmatrix} r_s & 0 & 0 \\ 0 & r_s & 0 \\ 0 & 0 & r_s \end{bmatrix} \quad (35)$$

$$r_r = \begin{bmatrix} r_{kq1} & 0 & 0 & 0 \\ 0 & r_{kq2} & 0 & 0 \\ 0 & 0 & r_{fd} & 0 \\ 0 & 0 & 0 & r_{kd} \end{bmatrix} \quad (36)$$

and the flux linkage equations are

$$\begin{bmatrix} \lambda_{abcs} \\ \lambda_{qdr} \end{bmatrix} = \begin{bmatrix} L_s & L_{sr} \\ (L_{sr})^T & L_r \end{bmatrix} \begin{bmatrix} -i_{abcs} \\ i_{qdr} \end{bmatrix} \quad (37)$$

Where the inductances  $L_s$ ,  $L_{sr}$ , and  $L_r$  are

$$L_s = \begin{bmatrix} L_{ls} + L_A - L_B \cos 2\theta_r & -\frac{1}{2}L_A - L_B \cos 2(\theta_r - \frac{\pi}{3}) & -\frac{1}{2}L_A - L_B \cos 2(\theta_r + \frac{\pi}{3}) \\ -\frac{1}{2}L_A - L_B \cos 2(\theta_r - \frac{\pi}{3}) & L_{ls} + L_A - L_B \cos 2(\theta_r - \frac{2\pi}{3}) & -\frac{1}{2}L_A - L_B \cos 2(\theta_r + \pi) \\ -\frac{1}{2}L_A - L_B \cos 2(\theta_r + \frac{\pi}{3}) & -\frac{1}{2}L_A - L_B \cos 2(\theta_r + \pi) & L_{ls} + L_A - L_B \cos 2(\theta_r + \frac{2\pi}{3}) \end{bmatrix} \quad (38)$$

$$L_{sr} = \begin{bmatrix} L_{skq1} \cos \theta_r & L_{skq2} \cos \theta_r & L_{sfd} \sin \theta_r & L_{skd} \sin \theta_r \\ L_{skq1} \cos(\theta_r - \frac{2\pi}{3}) & L_{skq2} \cos(\theta_r - \frac{2\pi}{3}) & L_{sfd} \sin(\theta_r - \frac{2\pi}{3}) & L_{skd} \sin(\theta_r - \frac{2\pi}{3}) \\ L_{skq1} \cos(\theta_r + \frac{2\pi}{3}) & L_{skq2} \cos(\theta_r + \frac{2\pi}{3}) & L_{sfd} \sin(\theta_r + \frac{2\pi}{3}) & L_{skd} \sin(\theta_r + \frac{2\pi}{3}) \end{bmatrix} \quad (39)$$

$$L_r = \begin{bmatrix} L_{lkq1} + L_{mkq1} & L_{kq1kq2} & 0 & 0 \\ L_{kq1kq2} & L_{lkq2} + L_{mkq2} & 0 & 0 \\ 0 & 0 & L_{lfd} + L_{mfd} & L_{fdqk} \\ 0 & 0 & L_{fdkd} & L_{lkd} + L_{mkd} \end{bmatrix} \quad (40)$$

and the magnetizing inductance is defined as



$$L_{mq} = \frac{3}{2}(L_A - L_B) \quad (41)$$

$$L_{md} = \frac{3}{2}(L_A + L_B) \quad (42)$$

Now the flux linkages may be written as

$$\begin{bmatrix} \lambda_{abc} \\ \lambda'_{qdr} \end{bmatrix} = \begin{bmatrix} L_s & L'_{sr} \\ (L'_{sr})^T & L'_r \end{bmatrix} \begin{bmatrix} -i_{abc} \\ i'_{qdr} \end{bmatrix} \quad (43)$$

Where  $L_s$ ,  $L'_{sr}$ , and  $L'_r$  are

$$L'_{sr} = \begin{bmatrix} L_{mq} \cos \theta_r & L_{mq} \cos \theta_r & L_{md} \sin \theta_r & L_{md} \sin \theta_r \\ L_{mq} \cos(\theta_r - \frac{2\pi}{3}) & L_{mq} \cos(\theta_r - \frac{2\pi}{3}) & L_{md} \sin(\theta_r - \frac{2\pi}{3}) & L_{md} \sin(\theta_r - \frac{2\pi}{3}) \\ L_{mq} \cos(\theta_r + \frac{2\pi}{3}) & L_{mq} \cos(\theta_r + \frac{2\pi}{3}) & L_{md} \sin(\theta_r + \frac{2\pi}{3}) & L_{md} \sin(\theta_r + \frac{2\pi}{3}) \end{bmatrix} \quad (44)$$

$$L'_r = \begin{bmatrix} L'_{lkq1} + L_{mq} & L_{mq} & 0 & 0 \\ L_{mq} & L'_{lkq2} + L_{mq} & 0 & 0 \\ 0 & 0 & L'_{lfd} + L_{md} & L_{md} \\ 0 & 0 & L_{md} & L'_{lkd} + L_{md} \end{bmatrix} \quad (45)$$

and the voltage equations expressed in terms of machine variables referred to the stator windings are

$$\begin{bmatrix} v_{abc} \\ v'_{qdr} \end{bmatrix} = \begin{bmatrix} r_s + \frac{d}{dt} L_s & \frac{d}{dt} L'_{sr} \\ \frac{2}{3} (L'_{sr})^T & r'_r + \frac{d}{dt} L'_r \end{bmatrix} \begin{bmatrix} -i_{abc} \\ i'_{qdr} \end{bmatrix} \quad (46)$$

Now using equation 6 to transform into the rotary reference frame, the voltage equation can be written as

$$V_{qd0s} = -r_s i_{dq0s} + \omega \lambda_{dq0s} + \frac{d}{dt} \lambda_{dq0s} \quad (47)$$

Where

$$(\lambda_{dq0s})^T = [\lambda_{ds} \quad -\lambda_{qs} \quad 0] \quad (48)$$

and since the rotor equations were expressed in the rotor reference frame, the equations stay as

$$v_{qdr}^{r'} = r'_r i_{qdr}^{r'} + \frac{d}{dt} \lambda_{qdr}^{r'} \quad (49)$$

Where the superscript 'r' denotes the rotor reference frame.

Since we are assuming a linear magnetic system, the flux linkage equations are

$$\begin{bmatrix} \lambda_{qd0s} \\ \lambda_{qdr}^{r'} \end{bmatrix} = \begin{bmatrix} K_S L_S (K_S)^{-1} & K_S L'_{sr} \\ \frac{2}{3} (L'_{sr})^T (K_S)^{-1} & L'_r \end{bmatrix} \begin{bmatrix} -i_{qd0s} \\ i_{qdr}^{r'} \end{bmatrix} \quad (50)$$

and it can be shown that the term  $K_S L'_{sr}$  is

$$K_S L'_{sr} = \begin{bmatrix} L_{mq} \cos(\theta - \theta_r) & L_{mq} \cos(\theta - \theta_r) & -L_{md} \sin(\theta - \theta_r) & -L_{md} \sin(\theta - \theta_r) \\ L_{mq} \sin(\theta - \theta_r) & L_{mq} \sin(\theta - \theta_r) & L_{md} \cos(\theta - \theta_r) & -L_{md} \cos(\theta - \theta_r) \\ 0 & 0 & 0 & 0 \end{bmatrix} \quad (51)$$

Now, we can rewrite the voltage equations in the rotary reference frame. The voltage equations for the stator and rotor are

$$v_{qd0s}^r = -r'_s i_{qd0s}^r - \omega_r \lambda_{dqs}^r + \frac{d}{dt} \lambda_{qd0s}^r \quad (52)$$

$$v_{qdr}^{r'} = r'_r i_{qdr}^{r'} + \frac{d}{dt} \lambda_{qdr}^{r'} \quad (53)$$

Where

$$(\lambda_{qds}^r)^T = [\lambda_{ds}^r \quad -\lambda_{qs}^r \quad 0] \quad (54)$$

and setting  $\theta = \theta_r$ ,  $K_S$  becomes  $K_S^r$  and the flux linkage equations become

$$\begin{bmatrix} \lambda_{qd0s}^r \\ \lambda_{qdr}^{r'} \end{bmatrix} = \begin{bmatrix} K_S^r L_S (K_S^r)^{-1} & K_S^r L'_{sr} \\ \frac{2}{3} (L'_{sr})^T (K_S^r)^{-1} & L'_r \end{bmatrix} \begin{bmatrix} -i_{qd0s}^r \\ i_{qdr}^{r'} \end{bmatrix} \quad (55)$$

To denote that all variables are now in the rotary reference frame. Now,  $K_S^r L_S (K_S^r)^{-1}$ ,

$K_S^r L'_{sr}$ , and  $\frac{2}{3} (L'_{sr})^T (K_S^r)^{-1}$  become

$$K_S^r L_S (K_S^r)^{-1} = \begin{bmatrix} L_{ls} + L_{mq} & 0 & 0 \\ 0 & L_{ls} + L_{md} & 0 \\ 0 & 0 & L_{ls} \end{bmatrix} \quad (56)$$

$$K_S^r L'_{sr} = \begin{bmatrix} L_{mq} & L_{mq} & 0 & 0 \\ 0 & 0 & L_{md} & L_{md} \\ 0 & 0 & 0 & 0 \end{bmatrix} \quad (57)$$

$$\frac{2}{3}(L'_{sr})^T(K_s^r)^{-1} = \begin{bmatrix} L_{mq} & 0 & 0 \\ L_{mq} & 0 & 0 \\ 0 & L_{md} & 0 \\ 0 & L_{md} & 0 \end{bmatrix} \quad (58)$$

and now, we can write the voltage equations in the rotor reference frame

$$v_{qs}^r = -r_s i_{qs}^r + \omega_r \lambda_{ds}^r + \frac{d}{dt} \lambda_{qs}^r \quad (59)$$

$$v_{ds}^r = -r_s i_{ds}^r - \omega_r \lambda_{qs}^r + \frac{d}{dt} \lambda_{ds}^r \quad (60)$$

$$v_{0s} = -r_s i_{0s} + \frac{d}{dt} \lambda_{0s} \quad (61)$$

$$v_{kq1}^{r'} = r'_{kq1} i_{kq1}^{r'} + \frac{d}{dt} \lambda_{kq1}^{r'} \quad (62)$$

$$v_{kq2}^{r'} = r'_{kq2} i_{kq2}^{r'} + \frac{d}{dt} \lambda_{kq2}^{r'} \quad (63)$$

$$v_{fd}^{r'} = r'_{fd} i_{fd}^{r'} + \frac{d}{dt} \lambda_{fd}^{r'} \quad (64)$$

$$v_{kd}^{r'} = r'_{kd} i_{kd}^{r'} + \frac{d}{dt} \lambda_{kd}^{r'} \quad (65)$$

and the flux linkage equations are

$$\lambda_{qs}^r = -L_{ls} i_{qs}^r + L_{mq} (-i_{qs}^r + i_{kq1}^{r'} + i_{kq2}^{r'}) \quad (66)$$

$$\lambda_{ds}^r = -L_{ls} i_{ds}^r + L_{md} (-i_{ds}^r + i_{fd}^{r'} + i_{kd}^{r'}) \quad (67)$$

$$\lambda_{0s} = -L_{ls} i_{0s} \quad (68)$$

$$\lambda_{kq1}^{r'} = L'_{lkq1} i_{kq1}^{r'} + L_{mq} (-i_{qs}^r + i_{kq1}^{r'} + i_{kq2}^{r'}) \quad (69)$$

$$\lambda_{kq2}^{r'} = L'_{lkq2} i_{kq2}^{r'} + L_{mq} (-i_{qs}^r + i_{kq1}^{r'} + i_{kq2}^{r'}) \quad (70)$$

$$\lambda_{fd}^{r'} = L'_{lfd} i_{fd}^{r'} + L_{md} (-i_{ds}^r + i_{fd}^{r'} + i_{kd}^{r'}) \quad (71)$$

$$\lambda_{kd}^{r'} = L'_{lkd} i_{kd}^{r'} + L_{md} (-i_{ds}^r + i_{fd}^{r'} + i_{kd}^{r'}) \quad (72)$$

and with the above voltage and flux linkage equations, the equivalent circuit is shown in Figure 20.

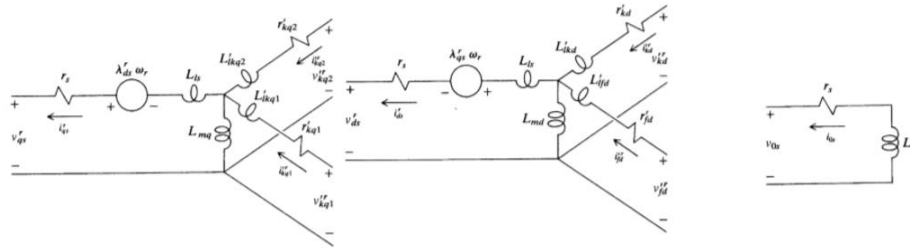


Figure 20. Equivalent voltage and flux linkage circuit [13].

The equation for the electromagnetic torque is shown below.

$$T_e = \frac{3}{2} \left( \frac{P}{2} \right) \lambda_{ds}^r i_{qs}^r - \lambda_{qs}^r i_{ds}^r \quad (73)$$

and the relationship between electromagnetic torque and rotor speed is

$$T_e = -J \left( \frac{2}{P} \right) \frac{d^2}{dt^2} \delta + T_L \quad (74)$$

Where

$$\delta = \theta_r - \theta_{ev} \quad (75)$$

and  $\omega_r = \frac{d}{dt} \theta_r$  completes the relationship between rotor speed and torque.

J is the inertia of the rotor, P is the number of poles the rotating machine has, and  $T_L$  is the torque load on the synchronous machine [13].

A synchronous machine is a very complex system which will be modeled for the experimental validation of a PHIL model vs the physical hardware. This understanding of the number of state variables and state transitions occurring during operation shows the complexity of the modeled system when deployed as a replacement to the physical machine

These equations are a necessity in understanding because this is the model used for synchronous machine in the MATLAB/Simulink library. For the experiment discussed later in the hardware/PHIL comparison, an induction machines rotor is coupled to a synchronous machine generator to produce a 208 3ϕ voltage signal.

## CHAPTER 5: SINGLE SHAFT TURBINE BACKGROUND

To experimentally evaluate a fuel-based generation source, an understanding of the complexity for fuel based turbine generation sources is needed. A single shaft gas turbine engine will be simulated and coupled to a synchronous machine to produce the 30 generation source. The basic principles of a gas turbine generator consist of a gas volume entering a chamber which increases the volume and is output at a higher pressure. A top-level diagram of this is shown below in Figure 21.

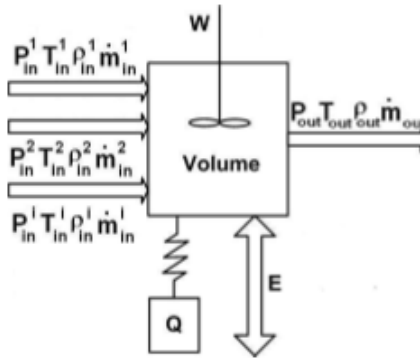


Figure 21. A top-level understanding of what occurs in a single shaft gas turbine system [14].

The above figure includes the heat transfer to adjacent metal structures(Q), losses in the components (E), and mechanical work (W) interactions within the system.

The model of the dynamic behavior of each engine component is

$$\frac{dP_{out}}{dt} = \left( \frac{\partial P_{out}}{\partial t} \right)_v + \sum_j \frac{\partial P_{out}}{\partial \zeta_j} \frac{\partial \zeta_j}{\partial t} \quad (76)$$

$$\frac{dT_{out}}{dt} = \left( \frac{\partial T_{out}}{\partial t} \right)_v + \sum_l \frac{\partial T_{out}}{\partial \varepsilon_l} \frac{\partial \varepsilon_l}{\partial t} \quad (77)$$

Where  $\zeta$  and  $\varepsilon$  are the internal thermodynamic state and mechanical variables used to model irreversible or dissipative processes [14]. Gas dynamics are mathematically modelled by a set of differential equations used to describe accumulation of gas energy

and mass within major volumes of the engine [14].

Conservation balance of total mass:

$$\frac{\partial m}{\partial t} = \sum_l \dot{m}_{in}^i - \dot{m}_{out} \quad (78)$$

and the conservation balance derived from the ideal gas equation

$$\frac{\partial P_{out}}{\partial t} = \frac{RT_{out}}{V} (\sum_l \dot{m}_{in}^i - \dot{m}_{out}) + \frac{P_{out}}{T_{out}} \frac{\partial T_{out}}{\partial t} \quad (79)$$

and the conservation balance of energy

$$\frac{\partial T_{out}}{\partial t} = \frac{1}{C_v \rho V} \left[ \left( \frac{\sum_l \dot{m}_{in}^i c_{in}^i T_{in}^i - \dot{m}_{out} C_p T_{out}}{-C_v T_{out} (\sum_l \dot{m}_{in}^i - \dot{m}_{out})} + q \right) \right] \quad (80)$$

Where  $C_p$  and  $C_v$  are specific heats, and  $q$  is heat flow.

The energy transfer rate between the surroundings and the gas  $q$  is defined as

$$q = h A_s (T_{gas} - T_m) \quad (81)$$

Where  $h$  is defined as

$$h = \left( \frac{T_{gas}}{T_{dgas}} \right)^x \left( \frac{\dot{m}_{gas}}{\dot{m}_{dgas}} \right)^y \frac{k}{L} \quad (82)$$

Where  $k$  is the thermal conductivity,  $L$  is a characteristic length and  $A_s$  is the surface area of exposed metal [14].

This accounts for the heat transfer losses associated with the surrounding meta.

Next, the compressor is modeled as an ideal component with input and output volume.

The temperature difference between input and output is

$$T_{outcomp} = T_{incomp} \pi_{comp}^{\frac{\gamma-1}{\gamma_{air} n_{comp}}} \quad (83)$$

Where  $\gamma$  is the specific heat ration that varies with temperature.

Next, the turbine is modelled via state map that is based on the turbine pressure ratio

$$\left( \pi_t = \frac{P_{int}}{P_{outt}} \right) \text{ and turbine corrected speed } (\bar{n}_t = \frac{n_t}{\sqrt{T_{int}}})$$

The turbine corrected mass flow map is

$$\frac{\dot{m}_t \sqrt{T_{int}}}{P_{int}} = tfmap(\pi_t, \bar{n}_t) \quad (84)$$

The tfmap allows for a response to transient conditions.

The combustion system is modelled with the following equation

$$\frac{\partial T_{outcomp}}{\partial t} = \frac{1}{C_v \rho V_{comb}} \left[ \begin{array}{l} \dot{m}_{air} C_{p,air} T_{air} + \dot{m}_{fuel} C_{p,fuel} T_{fuel} \\ -\dot{m}_{outcomp} C_{p,gas} T_{outcomb} + H_{fuel} \sigma_{comb} \dot{m}_{fuel} \\ +q - C_v T_{outcomb} (\dot{m}_{air} + \dot{m}_{fuel} - \dot{m}_{gas}) \end{array} \right] \quad (85)$$

Where  $H_{fuel}$  is the lower calorific value of fuel and  $\sigma_{comb}$  is the variable combustor efficiency.

The complexity of fuel-based generation sources that are modeled within the MATLAB/Simulink environment have been shown for a single shaft turbine generator. These processes are vastly different compared to an induction/ synchronous machine pair which will be evaluated in the next section. After this has been evaluated, a fuel-based generator is modeled and deployed as a PHIL model for power quality study during a short transient event. The processes explained here show how much detail and dynamics are occurring when a fuel-based generation source is used.

A. Experimental Setup

The first step of validation for a PHIL deployed generation source is to compare a PHIL deployed model of a motor-generator set vs the physical hardware during the transient event of interest.

The motor-generator pair was procured from Festo Didactic, shown in Figure 22. The motor is a LabVolt series 8505 3 $\theta$  wound-rotor induction motor. The generator is a LabVolt series 8507 3 $\theta$  synchronous generator. Paired together, they allow for a maximum power output of around 1.5 kVA. Both are rated for a stator voltage of 208 VAC at 60 Hz.



Figure 22. LabVolt 3 $\theta$  induction motor (left) and 3 $\theta$  synchronous (right).

The power supply controlled by the OPAL-RT HIL system is a California Instruments CSW 5550 by Ametek, shown in Figure 23. The CSW 5550 is a high slew-rate, 5 V/ $\mu$ s, 3 $\theta$  power supply that can be controlled using analog reference signals input to the supply. These analog inputs allow the power supply to emulate the individual phase voltages of a real-world generator.





Figure 23. Ametek CSW 5550 **30** power supply that is capable of AC or DC analog control.

The AC/DC converter is a 6-pulse power thyristor procured from Festo Didactic, shown in Figure 24. This module is a LabVolt series 8841-2 Power Thyristor that is controlled by 6 0-5 V pulse signals. This module is controlled by OPAL-RT and set to a known firing angle for a more accurate comparison between the three experimental scenarios.



Figure 24. LabVolt 8841-2 6 pulse power thyristor module.

In Figure 25, a conceptual block diagram of the three different topologies that will be evaluated for comparison is shown. Starting from the left, the AC source, either in hardware or emulated by the OPAL-RT is rectified to a DC voltage without any output filter to compare the output ripple between the three scenarios. The AC/DC rectifier is an SCR based 6-pulse rectifier that outputs  $\sim 280\text{VDC}$  that is then connected to a load for

power quality study when transient events occur. The inclusion of the AC/DC converter into the PHIL model further shows the capability of PHIL deployed model's ability to accurately represent the hardware during this short transient event study. Having a DC output as opposed to an AC output simplifies the feedback into the PHIL model to a single DC voltage and current measurement. The simplified feedback and simplified output could be more desirable allowing for a more accurate representation of the modeled system.

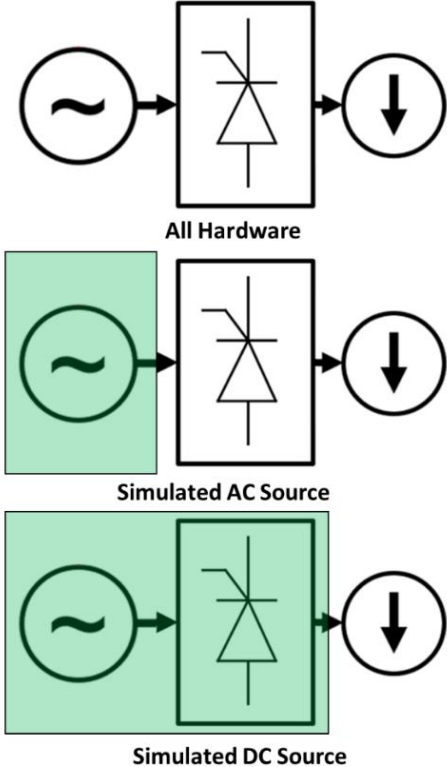


Figure 25. Conceptual diagram of the experimental setups. Further components are added into the PHIL simulation for comparison purposes

Figure 26 depicts a more detailed diagram of the experimental setup which depicts the 30 motor-generator set and the AC/DC converter is connected to a programmable load for comparison and validation.

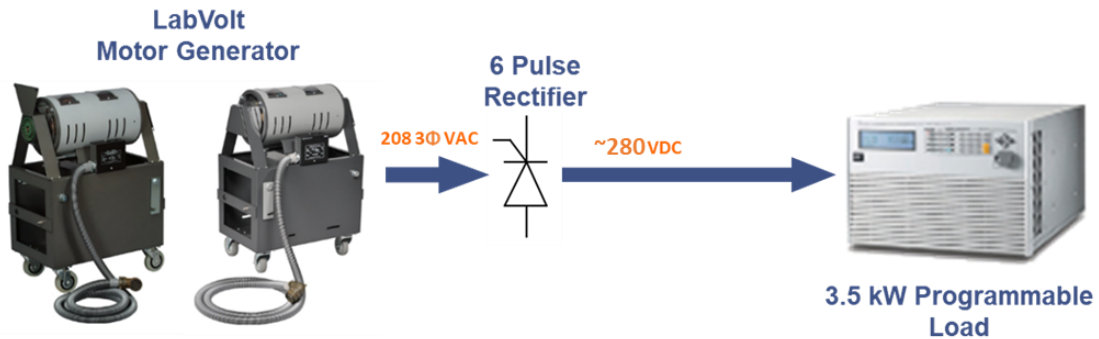


Figure 26. Block diagram of the full hardware topology.

Figure 27 depicts the same setup, except the motor-generator has been replaced with the 3Φ power supply being controlled by the OPAL-RT real-time simulator. The red arrow represents the analog control being applied to the power supply, and the green arrow represents the feedback signals used by OPAL-RT to update the model.

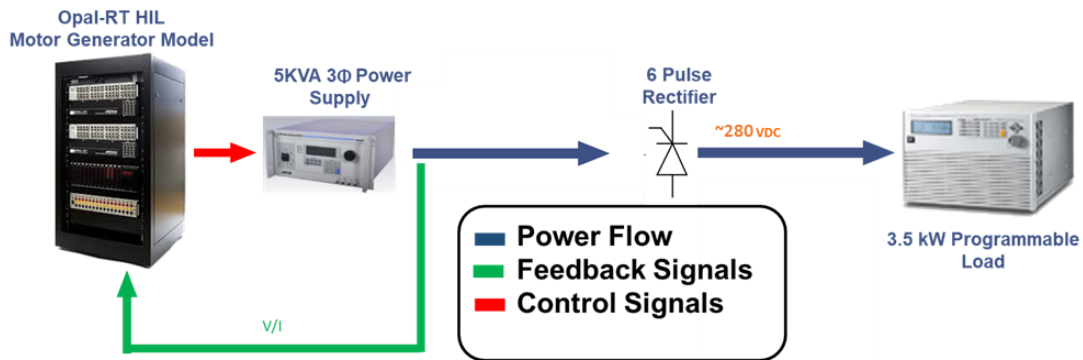


Figure 27. Diagram of the PHIL emulated motor-generator source hardware topology.

Figure 28 depicts the same set up as shown in figure 27 but the AC/DC converter has been integrated into the PHIL model to see if improvements are made with the simplified feedback and simplified output.

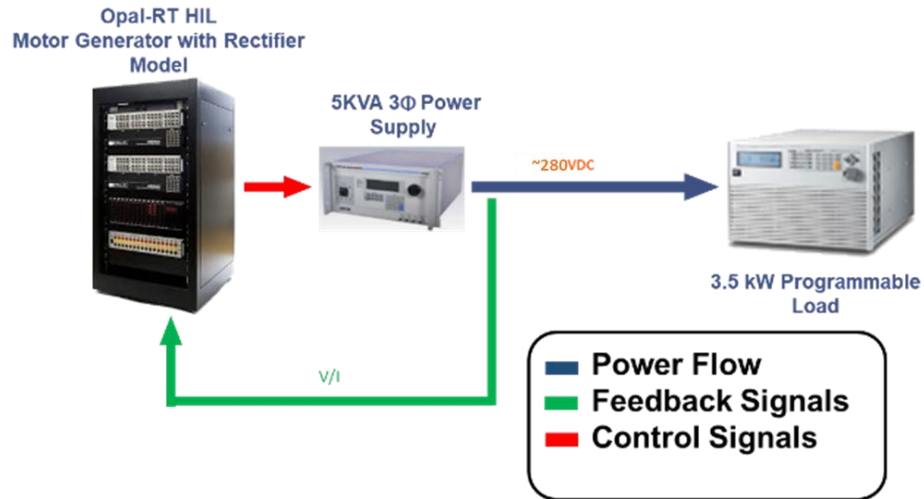


Figure 28. Diagram of the HIL emulated motor-generator with rectifier hardware topology.

With these three different scenarios, a detailed comparison of performance and accuracy will be shown between the hardware and PHIL deployed models. First, the full system will be modelled and compared to the accuracy of the hardware system. Next, the PHIL model will be deployed as an AC or DC source as shown above in Figure 25.

### B. Motor-Generator Simulation

The PHIL deployable model of the LabVolt motor-generator set was developed using existing blocks in the Simscape Power Systems toolbox. Once the motor-generator PHIL model is running, the generator's stator voltages are output to a high slew-rate 3Φ Ametek CSW5550 power supply. During the experiments, the line currents of the power supply are measured and fed back into the OPAL-RT. Based on these measurements, the stator voltages and generator frequency are adjusted in the model. On the next time step, adjustments are made to the OPAL-RT's analog outputs, which in turn alter the 3Φ voltages of the power supply. This process repeats for the duration of the test and allows for the emulation of the physical motor-generator set. The LabVolt motor-generator model

is shown below in Figure 29.

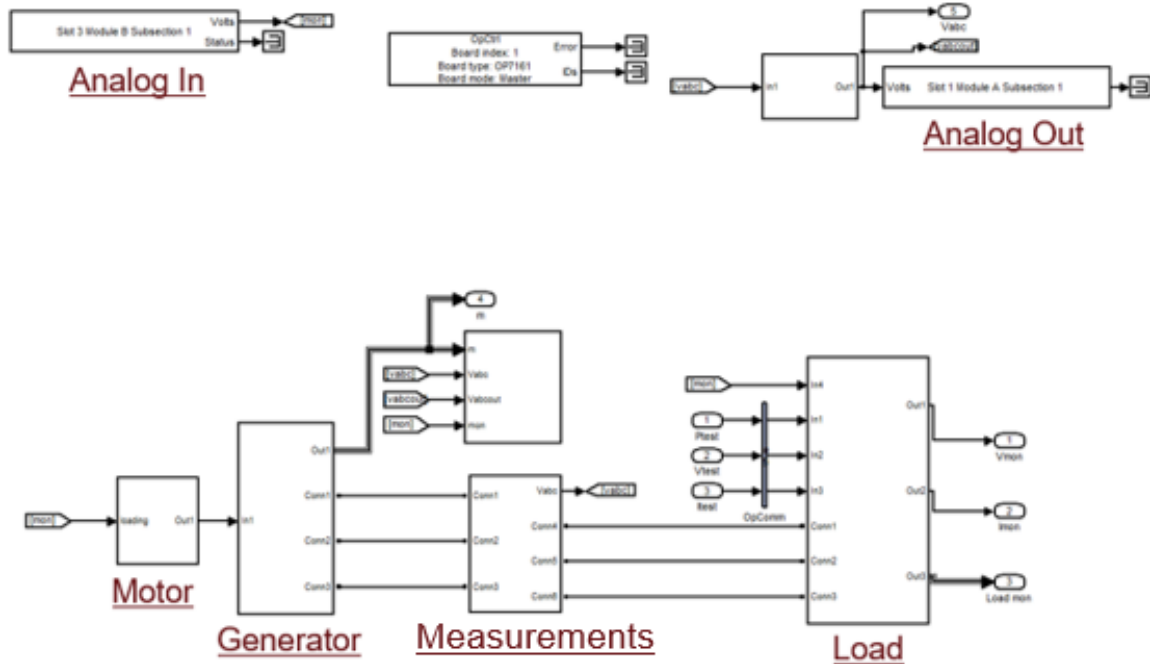


Figure 29. Simulink block diagram used to emulate the LabVolt motor-generator set in real-time using the OPAL-RT real-time simulator.

### C. Motor-Generator with AC/DC Simulation

The next step in this process is to include the AC/DC converter into the deployed PHIL simulation for comparison. The setup for this experiment is shown above in Figure 28. This simulation, shown below in Figure 30, contains all the hardware components before the load. The output of this simulation is a rectified DC voltage that is sent to the high slew rate Ametek CSW5550 which is capable of AC or DC applications. With a rectified DC voltage, the emulated generation source can be directly connected to a DC transient load.

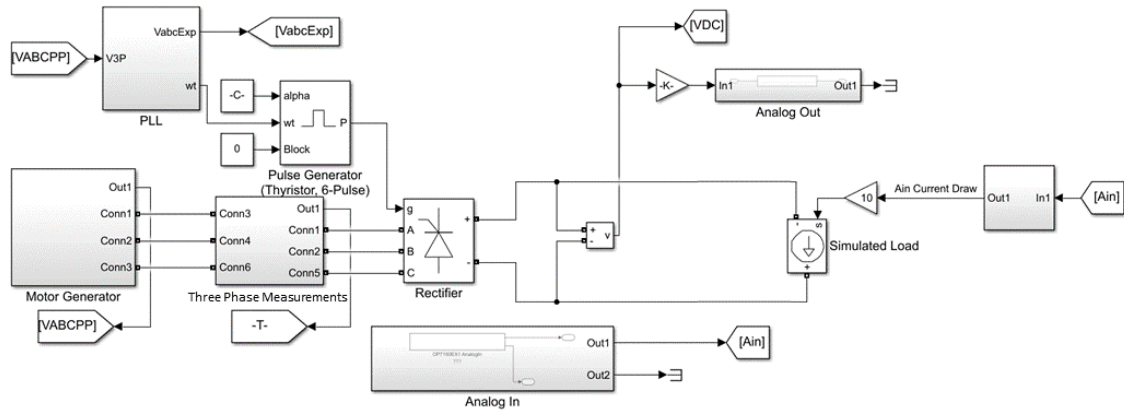


Figure 30. Simulink block diagram used to emulate a motor-generator with the AC/DC converter in OPAL-RT.

#### D. Hardware/PHIL Experimental Procedure

All results shown were setup to have a constant resistance profile to emulate a short transient condition that could be seen in a microgrid system. This profile consists of 5 seconds of discharging at 80Ω followed by 5 second of 10kΩ to simulate a repetitive transient condition. This 5 on 5 off profile is repeated 5 times to gather information on how the transient load conditions affect the power quality of the system and compare the 3 scenarios for validation of the PHIL model.

#### E. Hardware Vs Simulated System Comparison

This section shows a side by side comparison of the simulated system for comparison prior to being deployed as a PHIL model. Below in Figure 31 to Figure 36 shows how comparable the physical and simulated systems are. The error between the two systems are within 1%.

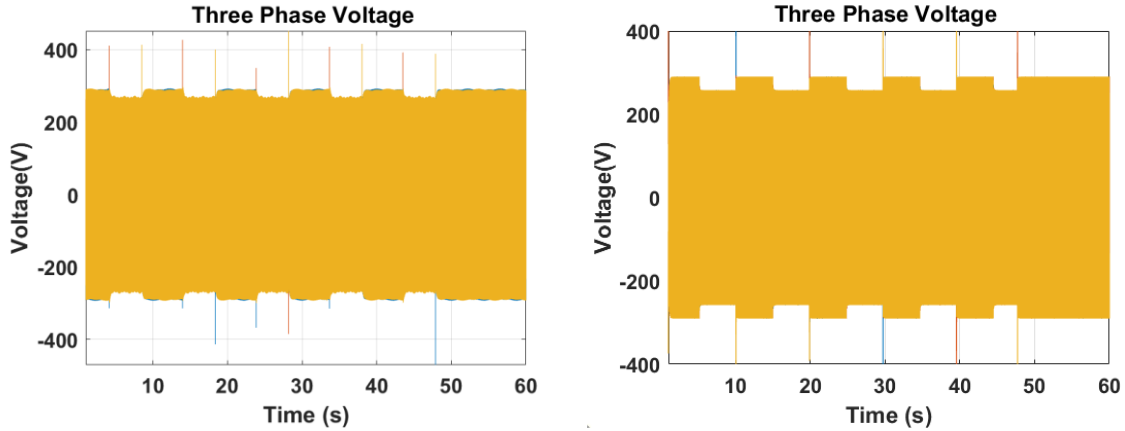


Figure 31. 3 $\theta$  voltage comparison (hardware on the left and modeled on the right) between simulated and physical motor-generator during the transient profile.

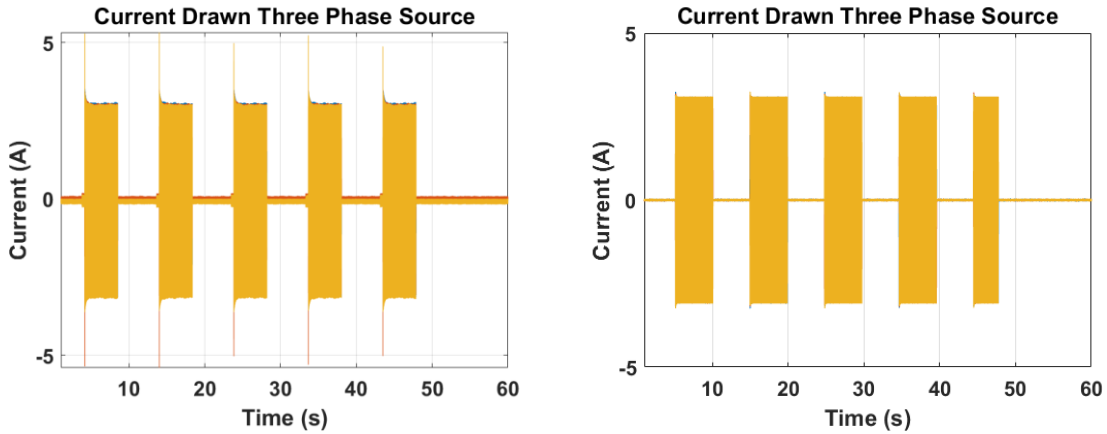


Figure 32. 3 $\theta$  current comparison (hardware on the left and modeled on the right) between simulated and physical motor-generator during the transient profile.

As shown in Figure 31 and Figure 32, the voltage droop and current draw out of the system is comparable between the simulated and physical hardware. The measured voltage droop between the two systems is  $\sim 30$  V during the short transient event. The difference between the simulated and physical voltage droop is  $\sim 2$  V during the transient events. This is within a 1% error between the simulated and physical measurements. The current draw shown in Figure 32 is  $\sim 3.05$  A during the transient event for the hardware system and  $\sim 3.1$  A for the simulated system. Again, these comparable results are within

a 1% error. Next, the rectified voltage and current will be compared to accurately quantify the error between the physical and simulated system.

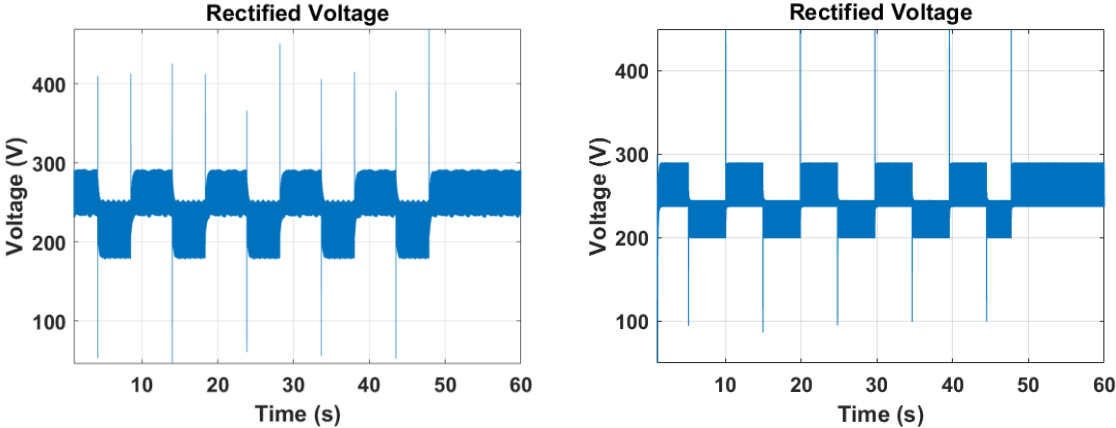


Figure 33. Rectified voltage comparison (hardware on the left and modeled on the right) between simulated and physical motor-generator during the transient profile.

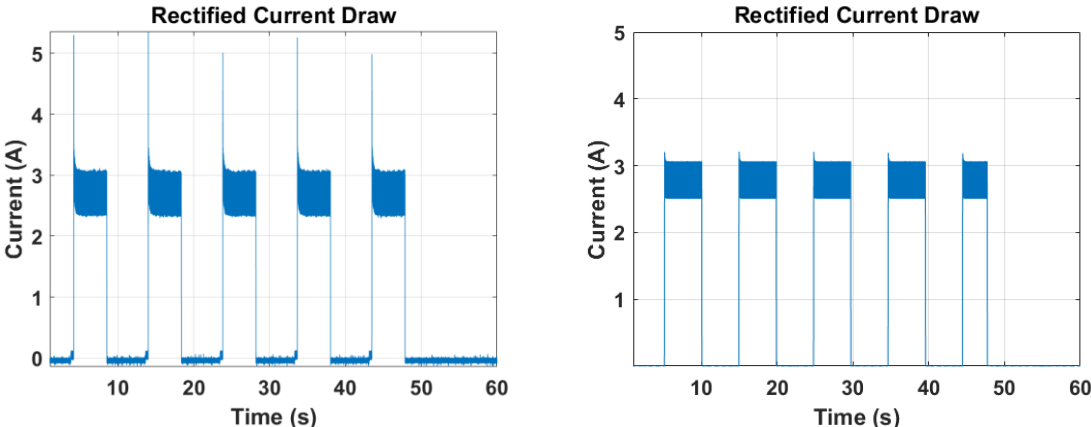


Figure 34. Rectifier current comparison (hardware on the left and modeled on the right) between simulated and physical motor-generator during the transient profile.

As shown in Figure 33 and Figure 34, the voltage droop and current draw out of the system is comparable between the simulated and physical hardware. The measured voltage ranges between a maximum of 245 V and a minimum of 190 V during the short transient event. This is reflected within the simulated system with the voltage ripple ranging between 247 V and 200 V during the short transient event. The error between the



simulated and hardware voltage waveforms are within 1%. The current draw shown in Figure 34 ranges between maximum of 3 A and a minimum of 2.4 A during the transient event for the hardware system. This is reflected within the simulated system where the maximum current draw ranges from a maximum of 3.1 A to a minimum of 2.5 A during the short transient event. These results are within a 1.0% error. With this portion of the simulated system being accurately modeled within 1.0% error, the final aspect to compare is the voltage and current harmonics. The results of the voltage and current harmonics are shown below in Figure 35 and Figure 36.

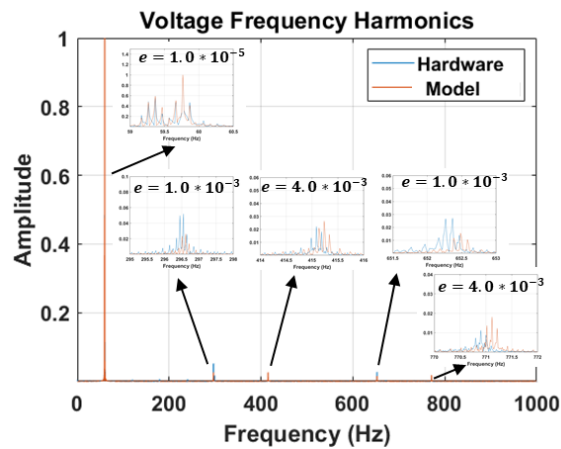


Figure 35. Voltage harmonic comparison between simulated and hardware system.

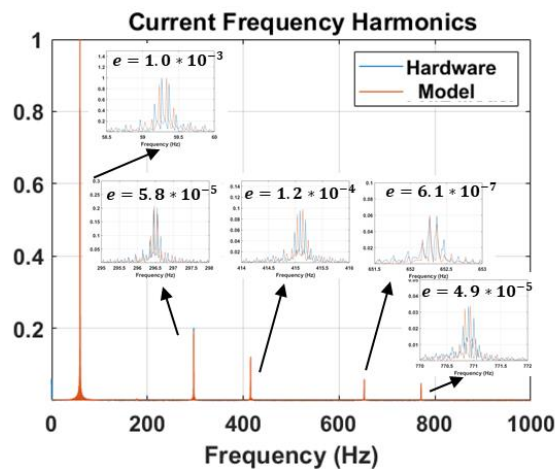


Figure 36. Current harmonic comparison between simulated and hardware system.

As shown in Figure 35 and Figure 36, the error between the physical hardware and

simulated system are highly accurate. Comparing the voltage harmonics, the highest error measured between the fundamental and shown harmonics is at the 5<sup>th</sup> harmonic and the measured error between amplitude and frequency is 0.1% and 0.5%, respectively. Comparing the current harmonics, the highest error measured between the fundamental and shown harmonics is seen at the 7<sup>th</sup> harmonic with a measured error between amplitude and frequency is 0.01% and 0.05%. With this portion of the simulated system being accurately modeled within 0.1% error, the simulated system is now capable of being deployed as a PHIL model. The next section is comparing the physical and emulated AC source, the second scenario shown in Figure 25, to verify that a deployable model of the a physical motor-generator set is replaceable with a PHIL model.

#### F. Emulated AC Generation Source with Hardware AC/DC Converter

This section shows a side by side comparison of the AC PHIL deployed model and hardware. Below in Figure 37 to Figure 42 shows how comparable the physical and simulated systems are. The error between the two systems are within 10%. This highlights the challenges when deploying PHIL models of generation sources. The added delays on feedback, control signals sent to the external power supply, high transient nature of the feedback needed to be slowed down within simulation to insure stability, and other minor nuances that become more pronounced due to the interactions with the physical system.

The first major limitation of this system is when transient events occur. As seen within the simulated system, when the load is applied in a transient nature, the solver can keep the system stable due to the iterative nature of the simulation. This is not the case when deployed as a PHIL model because the solver is unable to iterate the solution due to the

real time aspect of the simulation.

The next limitation of the deployed system is the excitation system of the physical vs simulated source. For the physical system, the stator voltage was controlled with an excitation voltage from an external power supply where the field current was higher to produce the stator voltage. This higher current would allow less droop when loaded and cannot be fully emulated within the Simulink environment. This limitation is not as pronounced as the transient nature of the feedback but does play a role when deploying an AC generation source within a physical testbed.

With these limitations, the error between the physical and PHIL motor-generator set is still comparable to within an error of 10%. This shows that the deploying of generation sources with a static excitation voltage is not a desirable method when deploying PHIL models.

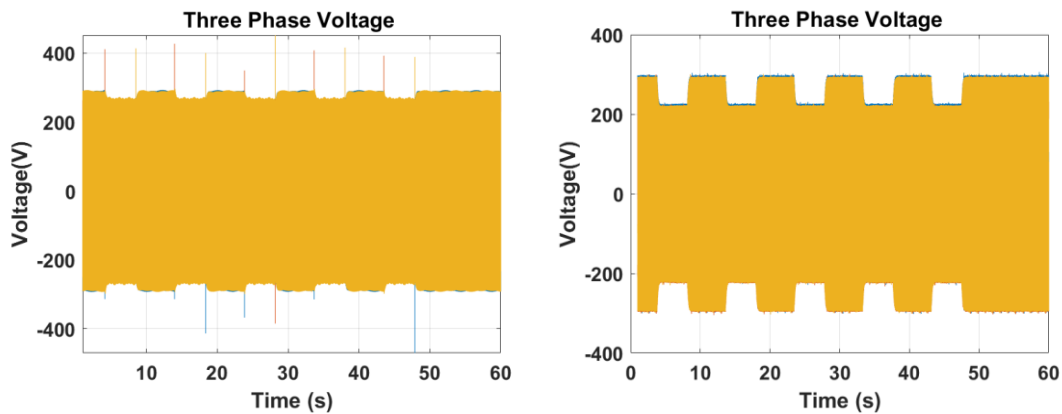


Figure 37. 3 $\theta$  voltage comparison (hardware on the left and PHIL AC deployed model on the right) between simulated and physical motor-generator during the transient profile.

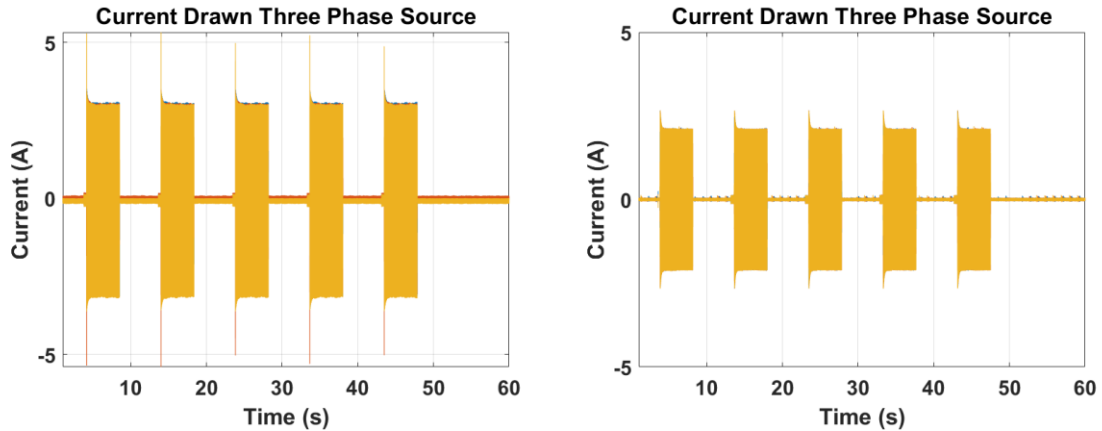


Figure 38. 3 $\theta$  current comparison (hardware on the left and PHIL AC deployed model on the right) between simulated and physical motor-generator during the transient profile.

As shown in Figure 37 and Figure 38, the voltage droop and current draw out of the system is comparable within 10% between the simulated and physical hardware. The difference between the simulated and physical voltage droop is  $\sim 20$  V during the transient events. This is within a 10% error between the PHIL model and physical measurements. The current draw shown in Figure 32 is  $\sim 3.05$  A during the transient event for the hardware system and  $\sim 2.8$  A for the simulated system. Again, these are not as exact as the simulated system but are still within 10% error. Next, the rectified voltage and current will be compared to accurately quantify the error between the physical and simulated system.

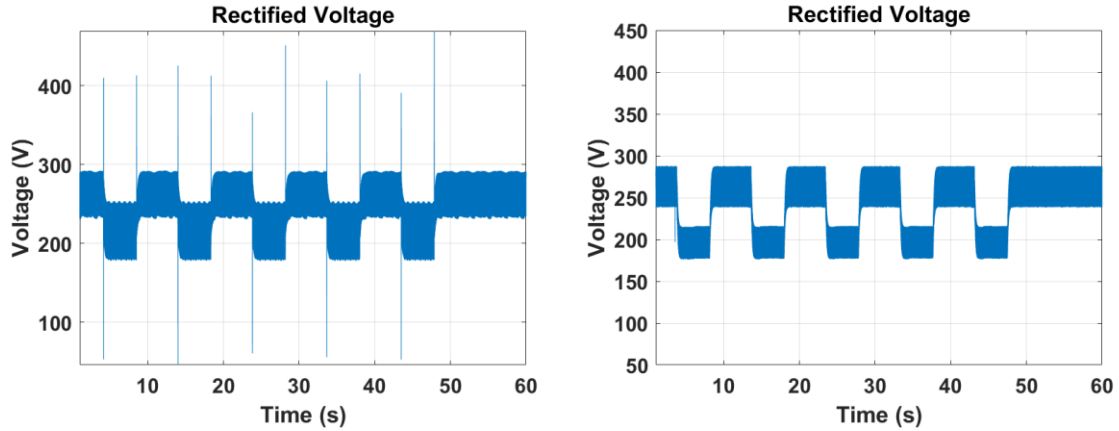


Figure 39. Rectified voltage (hardware on the left and PHIL AC deployed model on the right) between simulated and physical motor-generator during the transient profile.

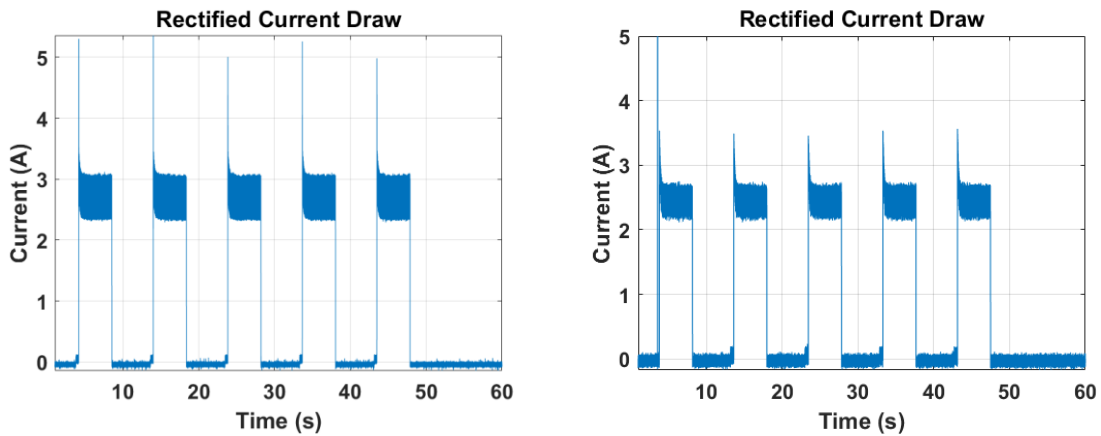


Figure 40. Rectifier current (hardware on the left and PHIL AC deployed model on the right) between simulated and physical motor-generator during the transient profile.

As shown in Figure 39 and Figure 40 , the voltage droop and current draw out of the system is within 10% just as the previous results in the AC voltage comparison. The limitations discussed earlier cause the AC voltage to droop lower which in turn causes a lower current draw due to Ohms Law. This corresponds to a ripple voltage of a maximum of 220 V and minimum of 180V during the short transient event. This is within the 10% error of the physical system. The current draw shown in Figure 40 ranges between maximum of 2.8 A and a minimum of 2.4 A during the transient event for the hardware

system. These comparable results are within a 10.0% error. It was expected that the deployed PHIL model of the motor-generator would not be as accurate as the simulated system which was verified within this set of experiments. The final aspect needed to be compared is the harmonic component of the voltage and current waveforms. The results of the voltage and current harmonics are shown below in Figure 41 and Figure 42.

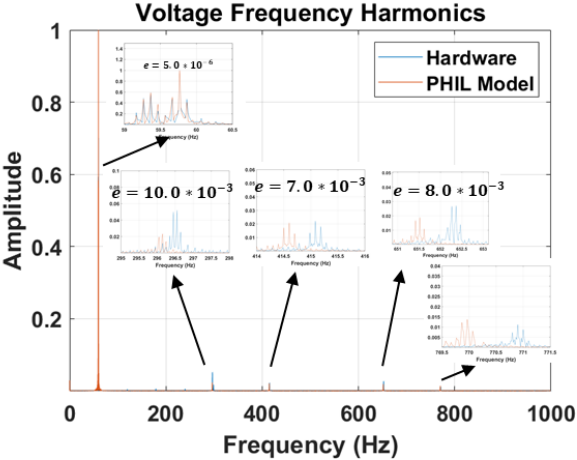


Figure 41. Voltage harmonic comparison between PHIL deployed motor-generator and hardware system.

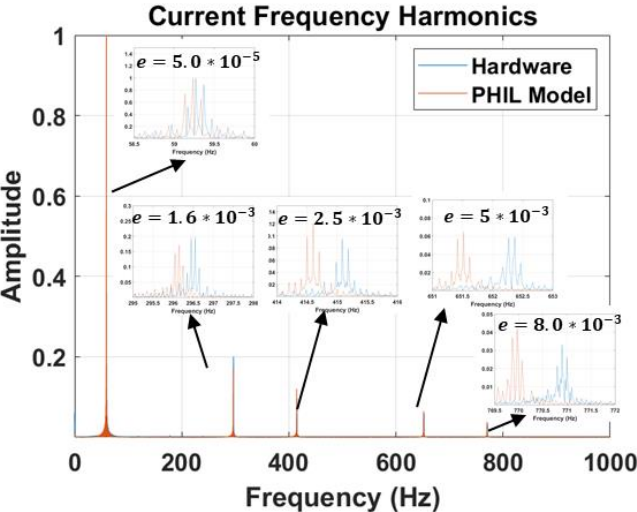


Figure 42. Current harmonic comparison between simulated and hardware system.

As shown in Figure 41 and Figure 42, the error between the physical hardware and PHIL deployed motor-generator system are highly accurate for the fundamental

frequencies for both voltage and current. For both voltage and current harmonics, the error when comparing harmonic amplitude as well as harmonic frequency go up by 2.0%. The cumulative error of the harmonic components of the voltage go to 10.0% between the hardware and PHIL deployed model. The cumulative error of the harmonic components for current go to 10.0% between the hardware and PHIL deployed model. As mentioned earlier, these errors are expected due to the number of multiple feedbacks, delays of the system, and limitations of Simulink's ability to properly model nuances that are present within a physical system. Although the harmonic content is not exact, the fundamental frequency components are within a 1.0% error of the physical system indicating that this PHIL motor-generator model is capable of power quality study within the frequency domain. The measured shift in the fundamental frequency ranges from 58.5 Hz to 60 Hz during the transient profile. This is considered poor power quality due to the range of the fundamental frequency only being acceptable within  $\pm 0.15$  Hz for these short transient events. The next section is comparing the physical and emulated DC source, the third scenario shown in Figure 25, to explore if the simplified feedback and simplified output allow for a more accurate representation of the generation source.

#### G. Emulated DC Source Comparison to Hardware

This section shows a side by side comparison of the simulated system for comparison prior to being deployed as a PHIL model. Below in Figure 43 and Figure 44 shows how comparable the physical and DC PHIL deployed model is. The error between the two systems are within 5.0%. This was a surprising result when compared to the previous experiment. The improvement in accuracy is due to the simplicity of the feedback into the PHIL model. Instead of having the 3 $\theta$  current fed back to load the PHIL motor-generator,

the DC current is fed back into the simulation to load the DC bus with the actual current that is being drawn by the DC load. When the 3 $\theta$  AC load was applied, the voltage and current measurements could be unstable for a single sample on one of the phases that would compound itself as the PHIL model updates over the course of the transient profile.

This simplified DC feedback and DC output implies that PHIL generation sources, when being deployed onto a DC bus, give more accurate and comparable results as opposed to when an AC PHIL model is deployed.

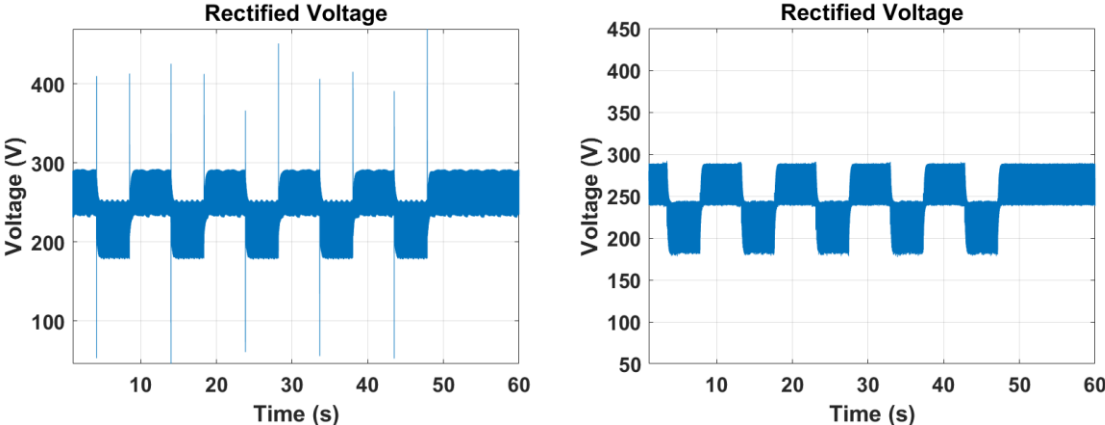


Figure 43. Rectified voltage (hardware on the left and PHIL DC deployed model on the right) between simulated and physical motor-generator during transient profile.

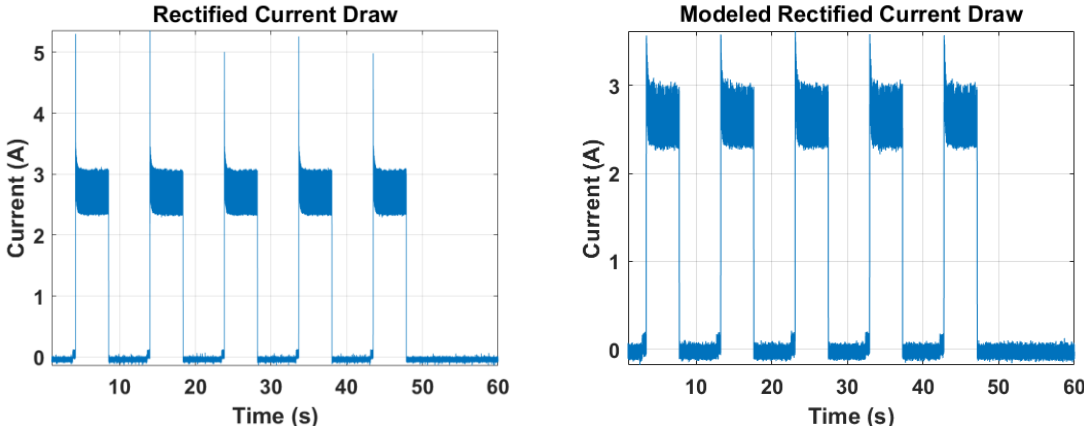




Figure 44. Rectifier current (hardware on the left and PHIL DC deployed model on the right) between simulated and physical motor-generator during transient profile.

As shown in Figure 43 and Figure 44, the voltage droop and current draw DC PHIL model is much more comparable than the previous AC deployed model. The error between the DC voltage ripple ranges from a maximum 245 V to a minimum of 180 V which is within 5% of the physical system. The error between the DC current ripple ranges from a maximum of 3.0 A and a minimum of 2.35 A. This ripple is within 5% of the physical system.

#### H. Emulated Motor-Generator Vs Hardware Conclusion

In this set of experiments, a physical motor-generator set was procured and accurately modeled for deployment as a PHIL system within a physical test bed. During this set of experiments, a possible repetitive short transient event that could occur within an isolated microgrid was used to experiment with the validity of deploying a PHIL model to replace a physical motor-generator set. The results presented in this section show that a physical generation source can be emulated within 10.0% error of the physical motor-generator set. This shows that PHIL deployed models are viable replacements for physical generation sources for the purposes of power quality study during short transient events. The next step in the process of evaluating if a deployed motor-generator PHIL model is comparable to the physical motor-generator when integrated into a low power hardware system. The next chapter will focus on the integration and comparison of the motor-generator PHIL model and physical motor-generator when incorporated into a known physical system.

A. Experimental Setup

In this section, the modeled motor-generator set acquired from LabVolt was deployed as a PHIL model for validation on a system integration level. The first is an induction motor/synchronous generator set that UTA possesses. Experiments were performed using the actual hardware as well as the emulated model for system integration and power quality study. Figure 45 shows a conceptual block diagram of the hardware/PHIL setup being used. Starting from the left, a 208 VAC source, implemented using either hardware or through HIL emulation is fed into an AC/DC rectifier. The 3 $\theta$  waveform is rectified to roughly 30 VDC using a 3 $\theta$  multi-pulse rectifier. The rectified DC voltage is regulated using a DC/DC converter whose output is connected to a DC bus that serves as PCC with the HESM. To reiterate what a HESM is, A HESM operates by sinking or sourcing energy depending on the current requirements of the load connected. If a load is suddenly taken off the grid causing a large drop in power demand, instead of a transient event occurring on the AC generation source, the power would be redirected into the HESM in order to keep the generation source consistently loaded. Likewise, if a large increase in power demand occurs, instead of a transient event causing the generator to supply all the extra energy required, the HESM would make up for the increase power load which keeps the generation source base loaded. This was shown in Figure 4. The PCC is loaded using a DC programmable load, which in this case is utilized in a constant current mode. The HESM contains the energy dense batteries and power dense ultracapacitors that are utilized to buffer the AC generation source. A more detailed block diagram of a HESM is shown below in Figure 45.

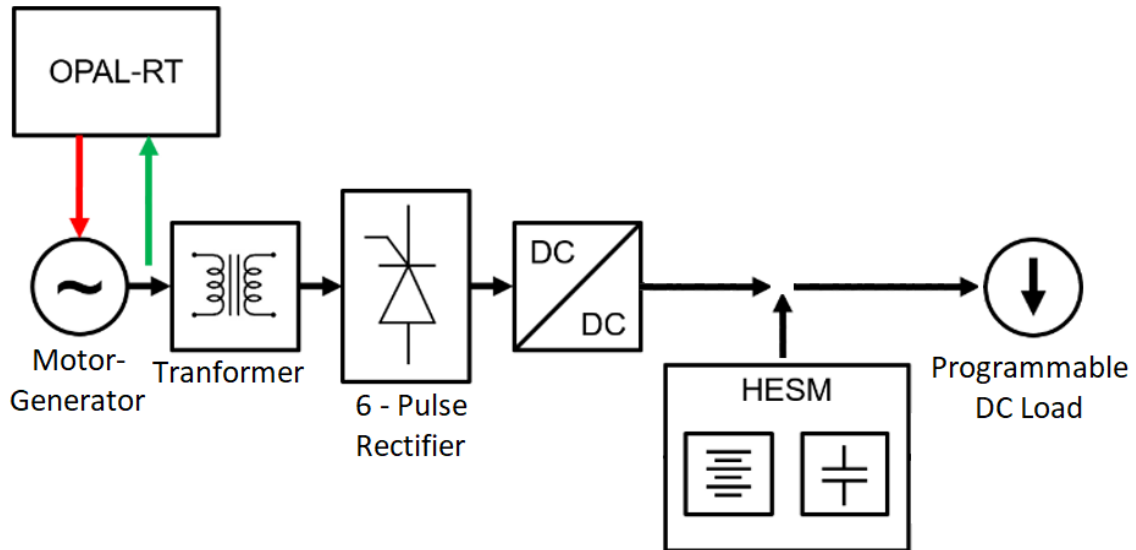


Figure 45. Conceptual block diagram of the experimental setup.

### B. Induction Motor / Synchronous Generator Sources

The first source evaluated was an induction motor/synchronous generator set, manufactured by Festo Didactic and sold by LabVolt that is possessed by UTA. The motor is a LabVolt series 8505 3 $\theta$  wound-rotor induction motor and the generator are a LabVolt series 8507 3 $\theta$  synchronous generator. Paired together, they allow for a maximum power output of around 1.5 kVA. Both are rated for a stator voltage of 208 VAC at 60 Hz. The motor-generator set is shown below in Figure 46.



Figure 46. LabVolt 3 $\theta$  motor-generator set.

The two experimental setups deployed in this series of experiments are shown in Figure 47 and Figure 48. In Figure 47, the hardware motor-generator feeds into a 10 to 1 stepdown transformer, rectified by a 6-pulse AC/DC converter, then bucked down by a controlled DC/DC converter onto the PCC. In Figure 48, the PHIL model controls the Ametek CSW 5550 when feeds into the 10 to 1 stepdown transformer, rectified by a 6-pulse AC/DC converter, then bucked down by a controlled DC/DC converter onto the PCC. To reiterate, the California Instruments CSW 5550 is used to amplify the OPAL-RT's simulated output. The CSW 5550 is a high slew-rate, 5 V/ $\mu$ s, 3 $\theta$  power supply that can be controlled using analog reference signals input to the supply. These analog inputs allow the power supply to emulate the individual phase voltages of a real-world generator. The HESM is tied onto the PCC and actively controlled using its own real-time controller. The Chroma programmable load is used to load the DC bus with a transient profile, which will be shown later in the results section. A photograph of the entire experimental setup is shown in Figure 49.

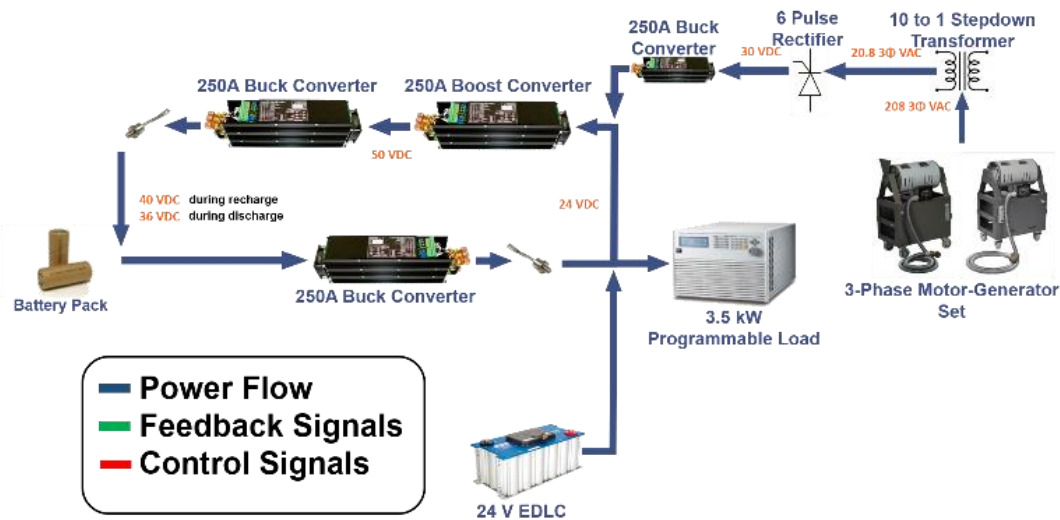


Figure 47. Block diagram of the hardware topology deploying a hardware motor-generator set.

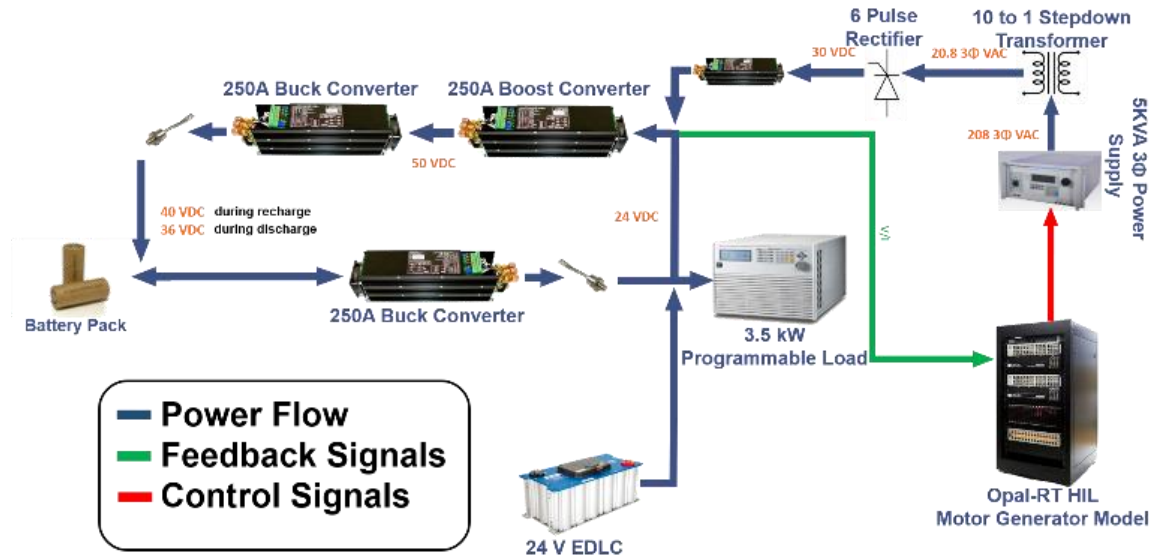


Figure 48. Block diagram of the hardware topology deploying a HIL emulated AC generator.

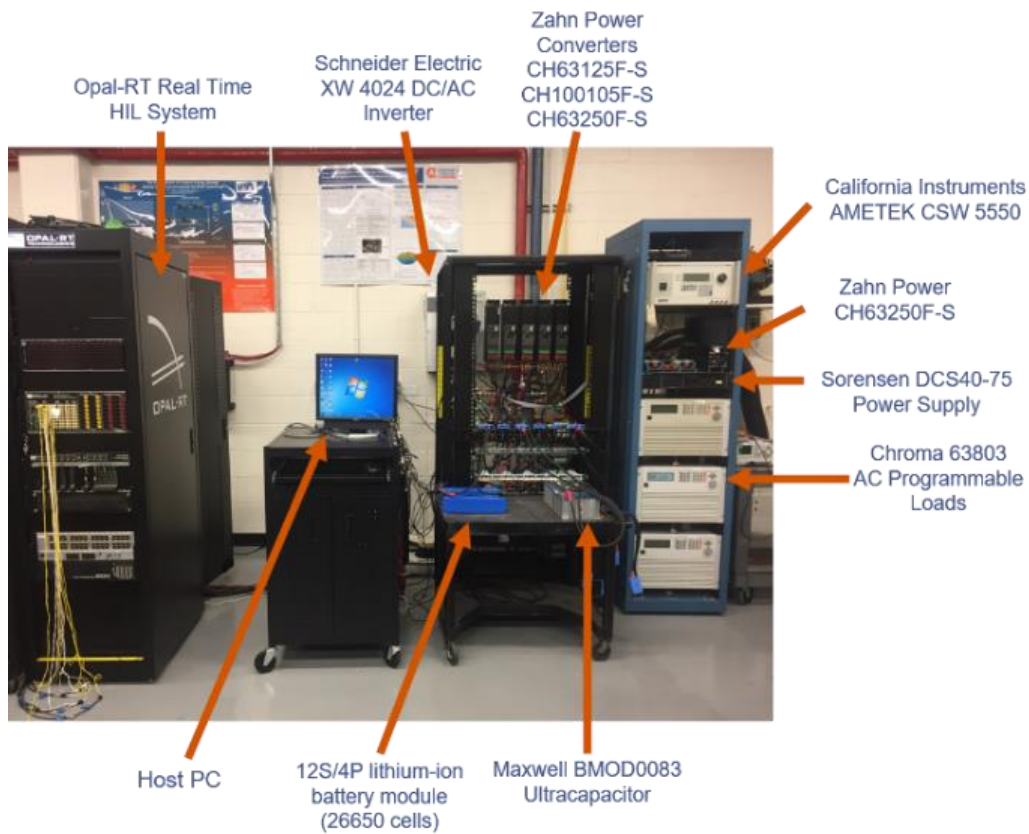


Figure 49. Experimental setup of many components of the power system being studied.

From the previous section, the PHIL model has been shown to be representative of the LabVolt motor-generator set. When running, Opal-RT outputs three, 0V – 10V analog signals, each of which linearly represents the output of one respective phase of the synchronous generator. The three analog signals are output to the Ametek power supply shown in the experimental setup schematics above. The loaded line currents of the power supply are measured and fed back into the OPAL-RT to load the PHIL model. To review the PHIL process, the stator voltages and generator frequency are adjusted in the model at each time step, adjustments are made to the OPAL-RT's analog outputs, which in turn alter the 3 $\theta$  voltages of the power supply. This process repeats for the duration of the experiment allowing for the emulation of the physical motor-generator set. The PHIL deployed model is shown below in Figure 50.

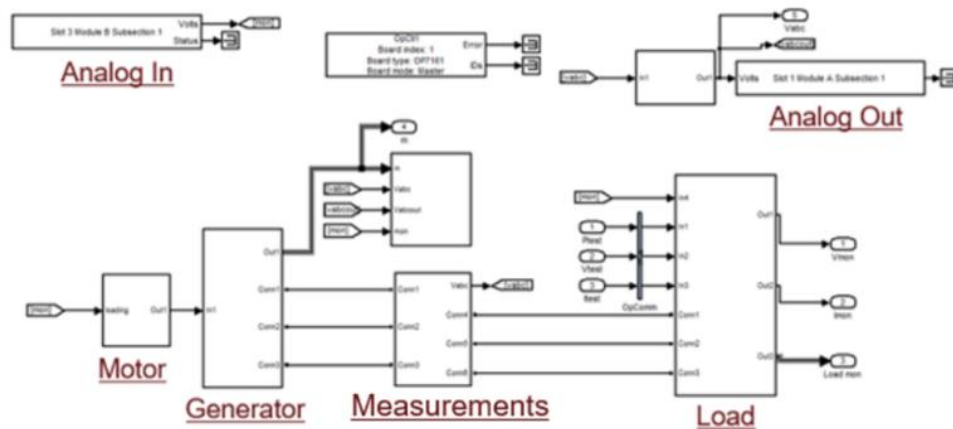


Figure 50. Simulink block diagram used to emulate a motor-generator set in real-time using the OPAL-RT real-time simulator.

### C. Experimental Procedure

In all the results presented here, the programmable load was setup to draw a constant current (CC) from the PCC in a transient manner. The profile turns the load on for 5

seconds, drawing 31 A CC, and then turns it off for 1 second before repeating four more times for a total of five 5 on 1 off transient events. Assuming 31 A and roughly 24 V, the load was drawing roughly 750 W when on. In each series of experiments performed, two identical experiments were performed. One experiment involved the physical motor-generator set and the other involved the PHIL deployed model to study the power quality of the generator. It should be noted that the experiments presented were repeated many times each and the results shown are representative of all experiments.

#### D. No buffering of the AC Source with Energy Storage Results

In this experiment, a comparison between the physical motor-generator and the PHIL generator model was evaluated without the HESM providing any buffering. In other words, the transient load is supplied entirely by the motor-generator or PHIL model depending on the experiment. Figure 51 shows the load current being drawn by the programmable load. In all the plot legends, 'MG' refers to the data collected when the physical motor-generator was used as the source and 'HIL' refers to data collected when the PHIL model was deployed. The current sourced by each AC source in its respective experiment is plotted in Figure 52. This transient loading results almost 5 V of droop on the PCC DC bus as seen in Figure 53. The difference between the motor-generator and PHIL model are within 0.1% during the rest phase of the transient profile and within 1% error during the on phase of the transient profile. These results show that the PHIL deployed model is accurate to the physical motor-generator when deployed within the physical testbed. These figures also show the inefficiency resulting from short transient loading without the HESM active, as well as poor power quality on the DC bus.

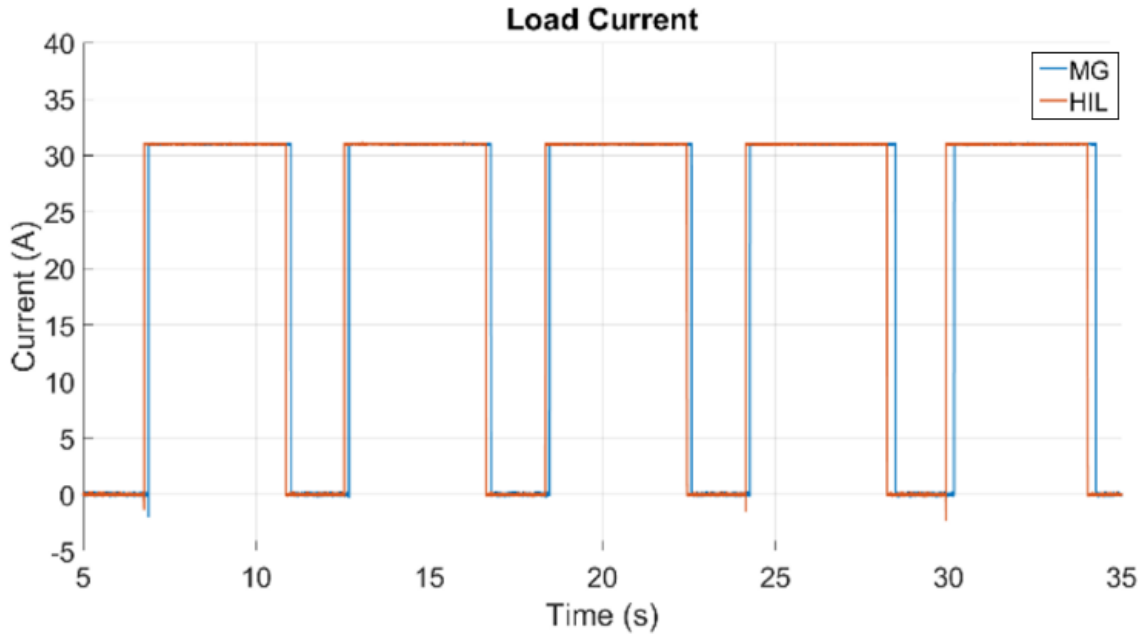


Figure 51. Current drawn by the programmable load during each respective experiment performed in which no HESM was used to buffer the AC source.

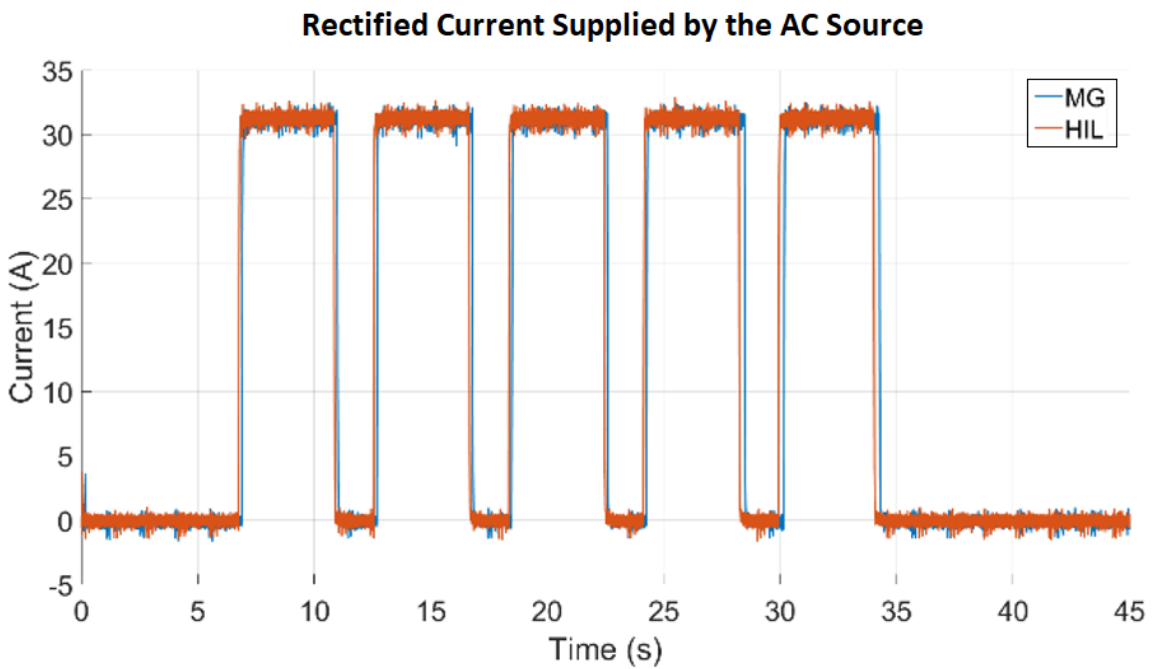


Figure 52. Rectified current supplied by the AC source during each respective experiment performed in which no HESM was used to buffer the AC source.



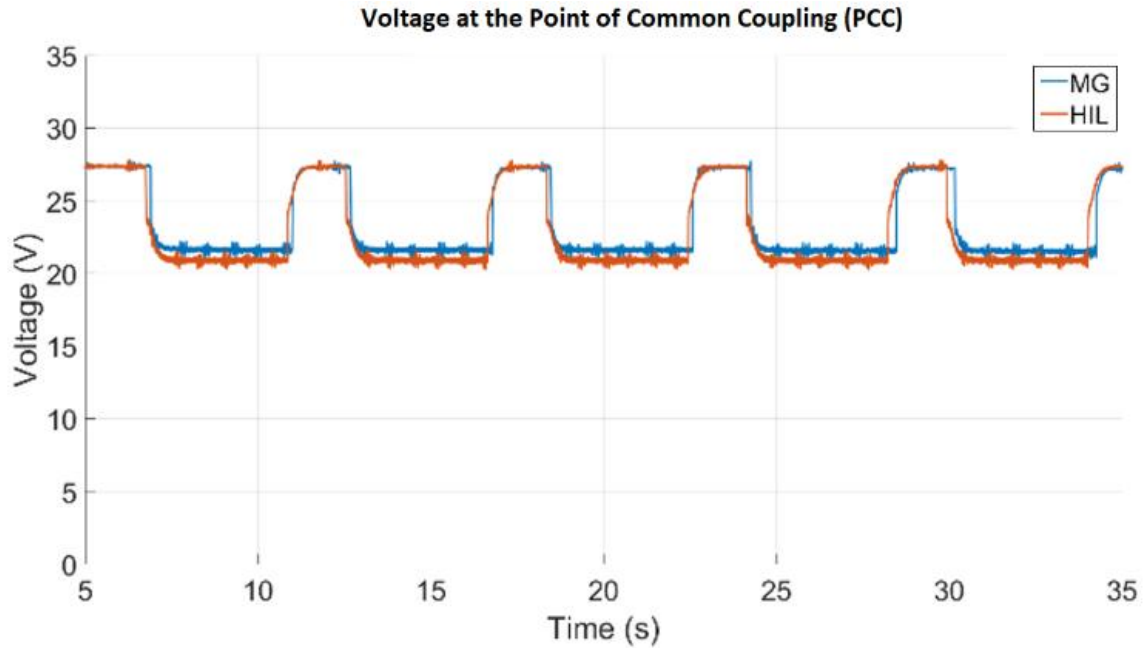


Figure 53. The PCC DC bus voltage showing deviation when the HESM is not used to buffer the AC source.

The AC voltages measured on Phase B of each source during its respective experiment are shown in Figure 54. Though the two voltage waveforms have slightly different magnitudes but are still within 10% of the physical motor-generator. A closer inspection, shown in Figure 54, shows that the variation in magnitude is largely due to harmonic distortion while the fundamental component of the phase voltages are what was expected from the previous section.

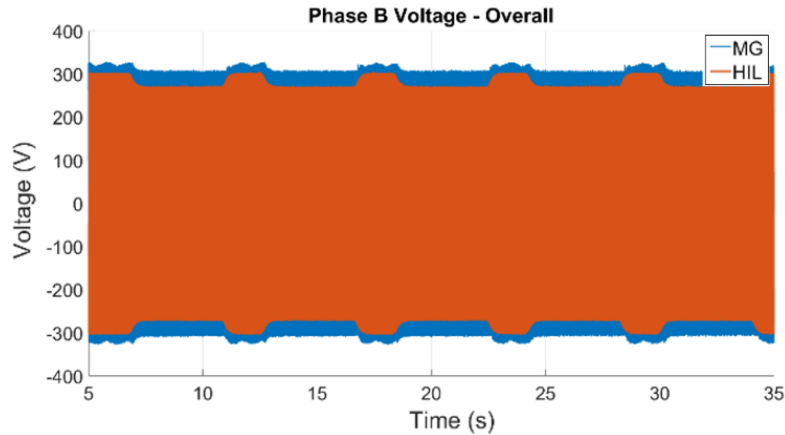


Figure 54. Phase voltage droops observed when the AC source is used to supply the full transient load current.

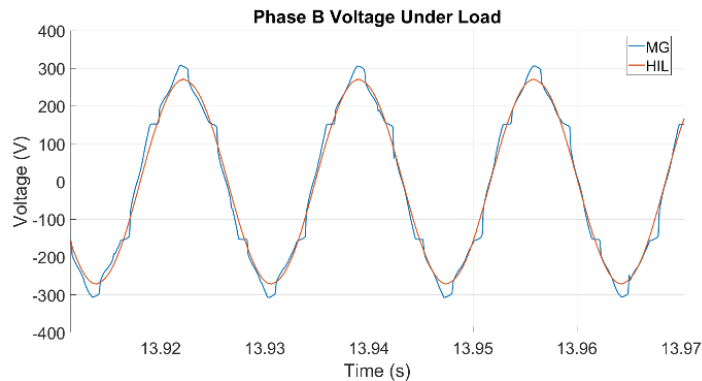


Figure 55. HIL source and motor-generator phase voltages are within 10.0% error despite harmonic distortion in the motor-generator.

Since the current waveforms change dramatically depending on the loading condition, the line current under no load is presented in Figure 56 and the line current under full load is presented in Figure 57. Despite the difference in loading conditions, the emulated source matches the results obtained from physical motor-generator within a maximum of 10.0% during the no load period and 12.0% during the loading period. These variations are caused by harmonic distortion indicating that the harmonic levels are lower but are still comparable to the physical motor-generator results. These results provide two

valuable insights. First, they further validate earlier results obtained that show how utilization of an AC source alone to supply transient loads results in a degradation in both AC and DC power quality. Second, they suggest that the HIL is a valid limited substitute for AC generation sources that are not physically available for experimentation.

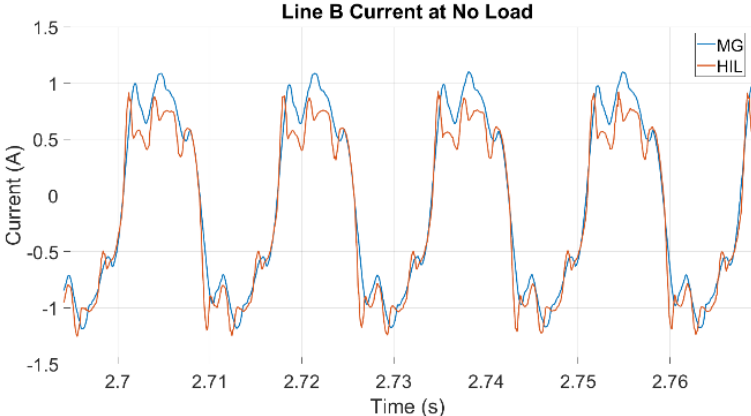


Figure 56. Line currents of each respective AC source during a 1 second rest period in experiments where no buffering supply is used.

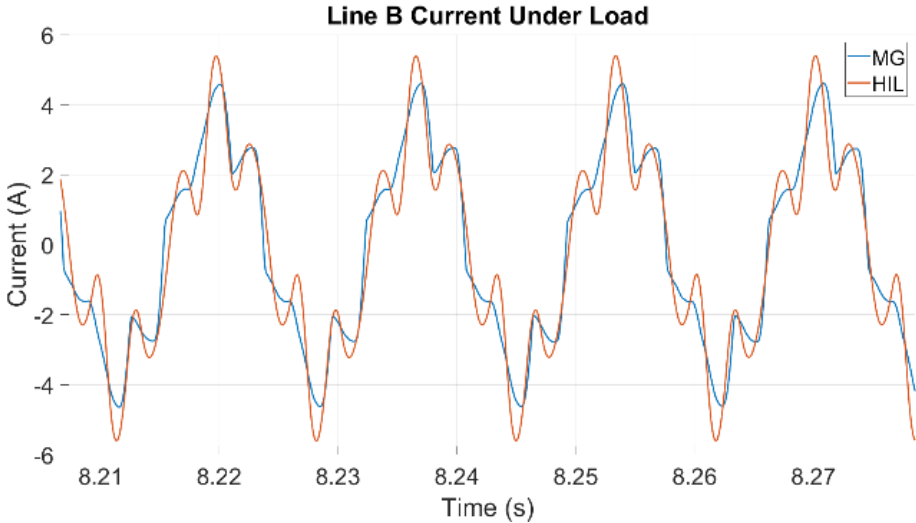


Figure 57. Line currents of each respective AC source during a 5 second load period in experiments where no buffering supply is used.

Next, the intelligent controller will be enabled to buffer the generation sourced during the off period to improve the power quality of the generation source. During this next experiment, it is expected that the power quality of the generation source will improve when buffered by the HESM system. With the PHIL model showing comparable results within 10% of the physical system, the same comparable results are expected with the next set of experiments.

#### E. Buffering of the AC Source with Energy Storage Results

In this experiment, a comparison between the physical motor-generator and the PHIL generator model was evaluated with the HESM actively buffering the generation source. Figure 58 shows the same load profile being operated on the programmable load as that performed as in the previous series of experiments. Because the HESM is buffering the AC source, it is constantly loaded, supplying a nearly constant current to the PCC as shown in Figure 59. The HESM's batteries and capacitors provide a portion of the load current while it a load is applied and continue to load the AC source when the load is off by charging the batteries. This improves the stability of the PCC DC voltage bus considerably, shown in Figure 60, where deviations less than 1 V are observed during the full transient profile. This is within a 5% error on the DC bus and shows that even though the bus is being actively controlled, the PHIL deployed model is not a perfect representation but is comparable within a 5% error.

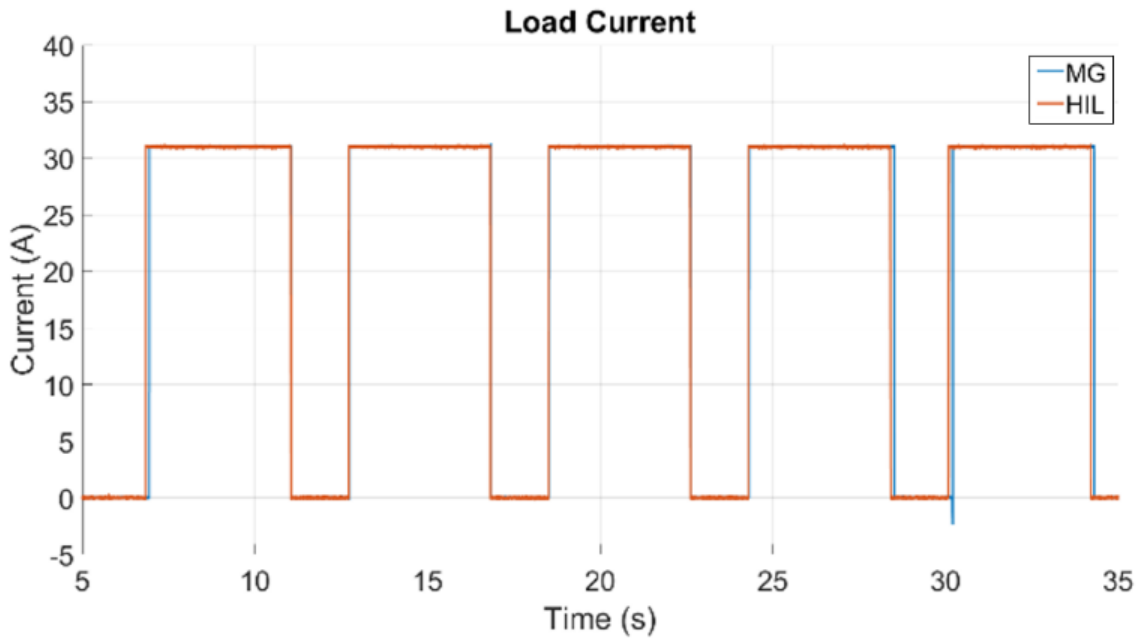


Figure 58. Current drawn by the programmable load during each respective experiment performed when the HESM was used to buffer the AC source.

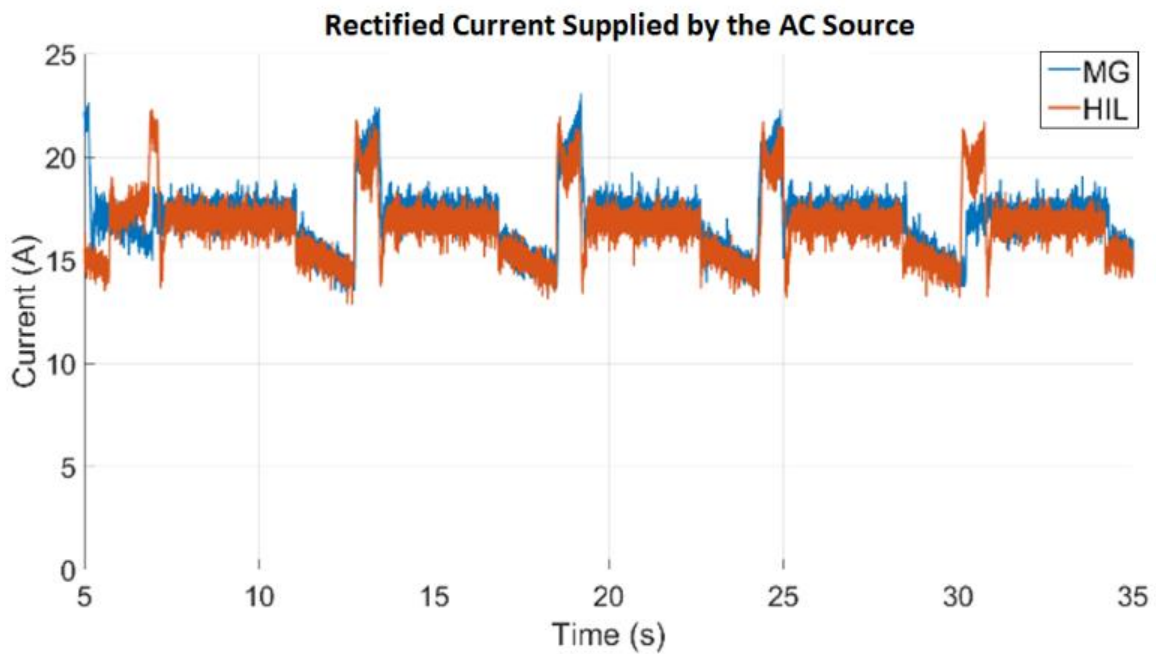


Figure 59. Rectified current supplied by the AC source during each respective experiment performed when the HESM was used to buffer the AC source.

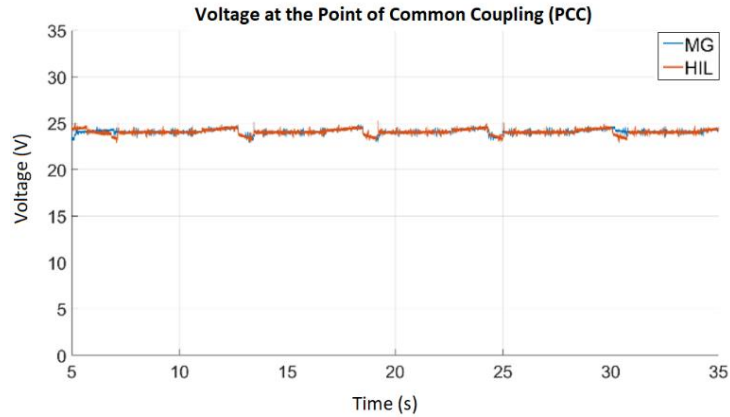


Figure 60. The PCC DC bus voltage showing much reduced deviation when the HESM is used to buffer the AC source.

As shown in Figure 59, the current sourced by the generator is consistent during the full transient profile. This causes the stator voltage to be consistent during the transient profile. As was observed in Figure 61 and Figure 62, there is harmonic distortion but it is reduced due to the consistent loading of the generator. The error between the PHIL and physical motor-generator stator voltages is 10.0% during the transient profile. Figure 63 present line current when the HESM is utilized during the transient profile. The line current harmonics in the emulated source are very similar to the physical motor-generator.

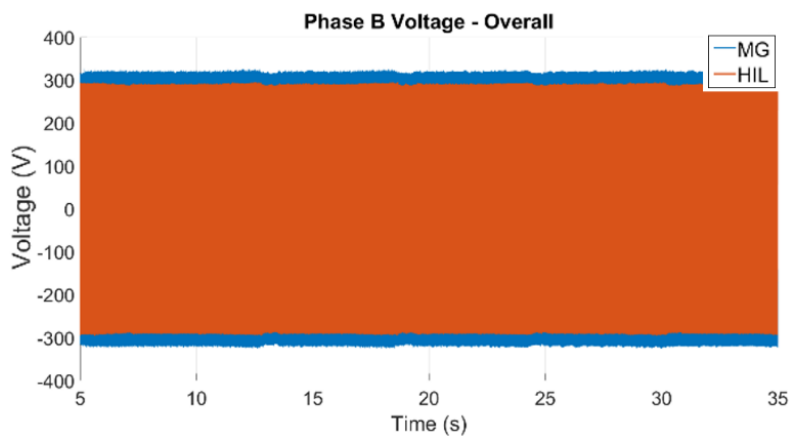


Figure 61. Phase voltage droops observed when the HESM is used to buffer the AC source.

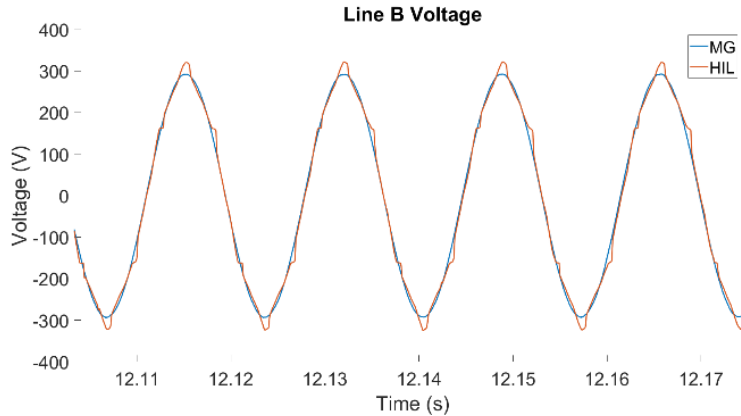


Figure 62. HIL source and motor-generator phase voltages are within 10.0% error despite harmonic distortion in the motor-generator when buffered by HESM.

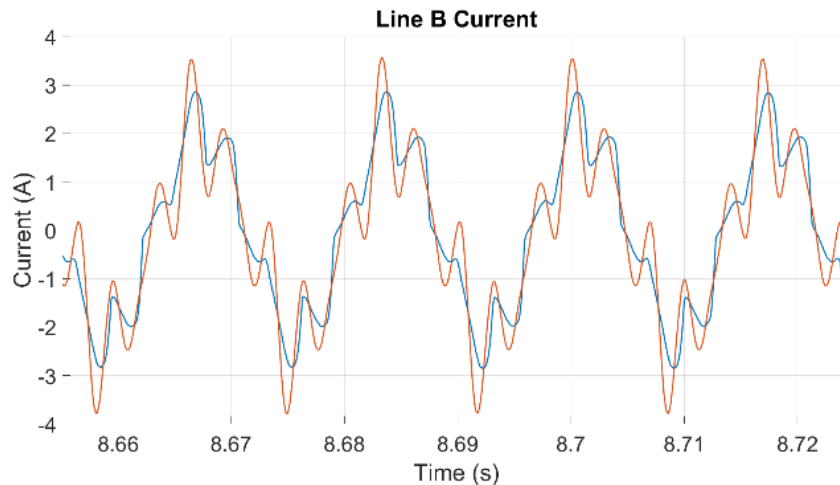


Figure 63. Line currents of each respective AC source during a 5 second load period in experiments where the buffering supply is used

#### F. PHIL Motor-Generator Vs Hardware Small Scale System Integration Conclusion

In this set of experiments, a physical motor-generator set was procured and accurately modeled for deployment as a PHIL model within a built actively controlled HESM to experimentally evaluate the system integration of PHIL deployed models. During this set of experiments, a possible repetitive short transient event was used to evaluate a comparison between a PHIL deployed model of a known motor-generator set when

buffered and not buffered with an actively controlled HESM. This repetitive transient profile could occur within an isolated microgrid and was shown that the physical motor-generator could be replaced with a PHIL model. The error seen between the PHIL and hardware motor-generator when buffered and not buffered by the HESM was within 10.0%. Again, this shows that PHIL deployed models are viable replacements for physical generation sources for the purposes of power quality study during short transient events. The final step in the process of evaluating if a deployed PHIL models are viable replacements is to demonstrate the capability by incorporating a fuel-based generation source not physically owned within a small scale test bed for power quality study. The next chapter will focus on the integration of a PHIL deployed fuel-based generation source into a known HESM test bed to demonstrate the capability of power quality analysis and improvements.



## CHAPTER 8: EMULATED DIESEL GENERATOR SOURCE FOR POWER QUALITY STUDY

### A. Diesel Engine / Synchronous Generator Emulated Source

In this section, a simulated 4160 VAC synchronous generator that is spun using a diesel engine is deployed as a PHIL model. This generation source is not physically owned for hardware validation but is representative of a 3 MVA diesel generator. This is to show that modeled generation sources not physically owned are capable of being evaluated when a PHIL model is available. The schematic, shown in Figure 64, is similar to Figure 48 with two main differences. The first is that a 3kW AC/DC power supply is used as a rectifier in place of the step-down transformer and 6-pulse rectifier. The second is that the DC bus is inverted to a 120 VAC and the programmable load is run in an AC constant Resistance mode.

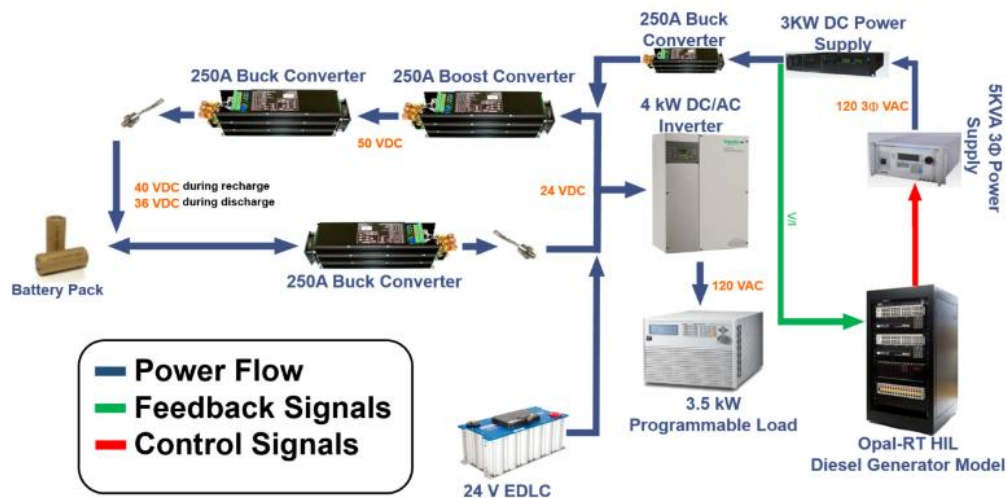


Figure 64. Block diagram of the hardware topology deploying a PHIL emulated AC generator and a DC power supply as the AC/DC converter.

The Simulink model being deployed in Opal-RT is shown below. The generator model

is contained within the block labeled SM\_Machine while the SC\_User block contains all the parameter monitoring sub-blocks.

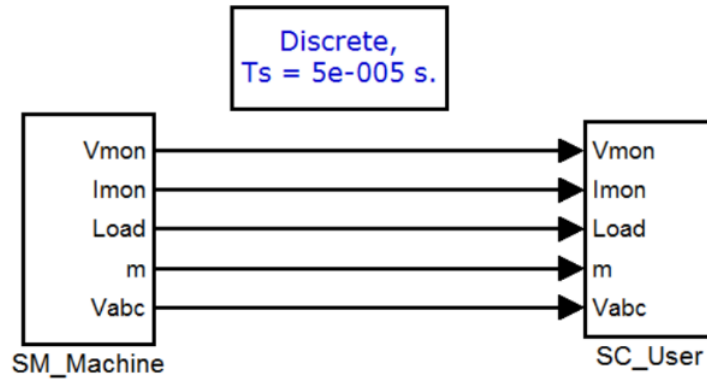


Figure 65. Deployed Model on Opal-RT HIL system.

Figure 66 displays the schematic components internal to the SM\_Machine block. In the lower portion of the figure, the engine-generator model is shown. The input block, where feedback from the voltage and current monitors is processed is located in the upper left side of the figure. In the upper right side of the figure, the sub-block that handles the analog output signals is shown. It is within that block that the stators' output voltages are scaled and sent to the Opal-RT's analog output card. It is within the block labeled 'Power Calculation from External Signals' that the power supplied by the AC/DC power supply is rescaled such that it properly loads the generator model. The benefit of this being in a simulation is that the external measurements can be easily manipulated to draw any desired amount of power out of the generator simulated.

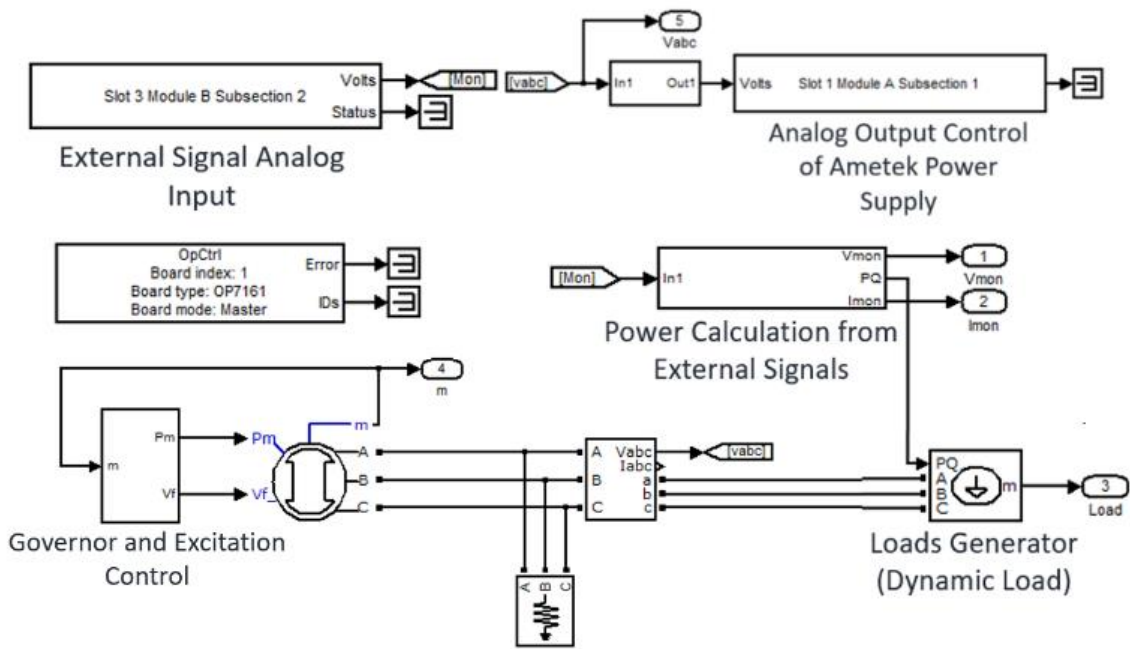


Figure 66. SM\_Machine Simulink model.

The sub-blocks within the SC\_User block are shown in Figure 67. There is nothing too noteworthy happening here other than this is where the each of the input and output signals are displayed for user awareness.

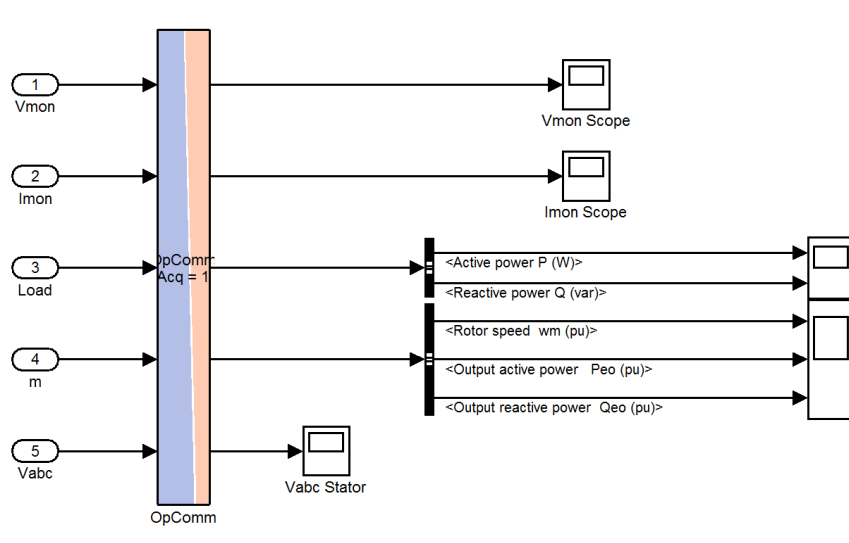


Figure 67. SM\_User monitors the external measurement signals, dynamic load, machine parameters, and stator voltages.

## B. Diesel Engine / Synchronous Generator Emulated Source Experimental Procedure

In this experiment, a diesel engine/synchronous generator was emulated as the AC source will be presented. The rotor speed, power sourced, and Fourier transform of the PHIL generator's stator voltages are compared between two different experiments. In the first, the PHIL generator is the sole provider of power for the transient load. In the second, the PHIL generator is buffered with the HESM during the off period of the transient load. Each experiment starts with a 5 second off period, followed by a 5 second load period, and then one final 5 second off period before it is halted. When the load is off, it acts as a constant 1 k $\Omega$  resistive load to the inverter's AC output bus, drawing roughly 20 W. When it is on, it is set to act as a constant 10  $\Omega$  resistive load on the bus drawing roughly 1.5 kW.

## C. No Buffering of the Diesel Engine / Synchronous Generator Source

In this experiment, only the emulated generator is used to supply the transient load. The HESM is present but the battery is inhibited from sourcing/sinking any power while the EDLC is floating on the bus. At approximately 50 seconds into Figure 68 and Figure 69, the PHIL generator is connected to the DC bus and it begins to charge up the passive EDLC module. This is seen most clearly in Figure 69.

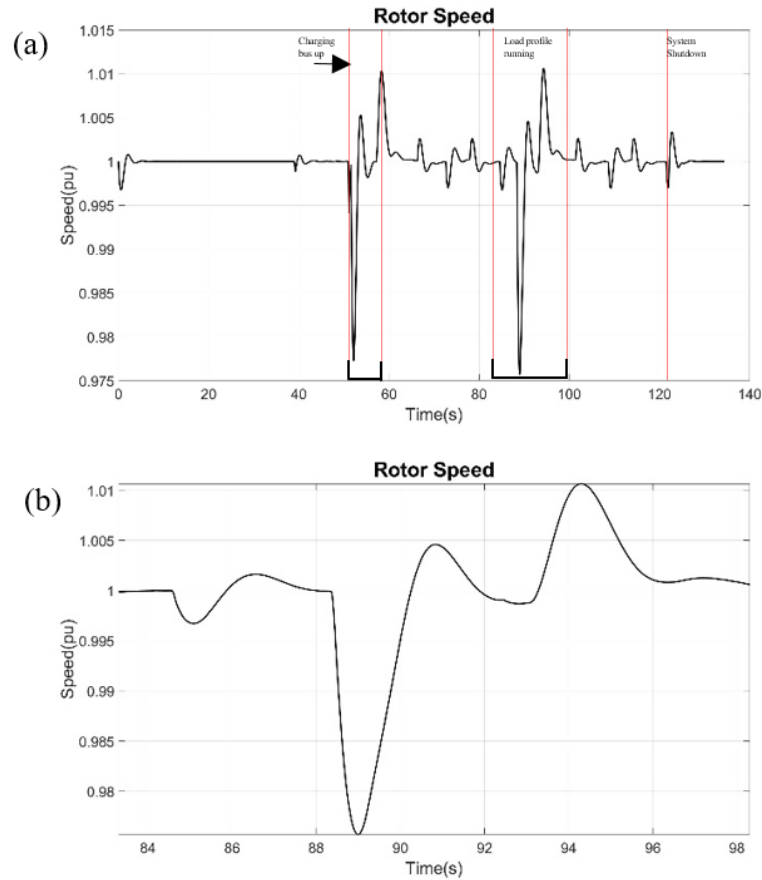


Figure 68. (a) Rotor speed during HIL generator deployed during experiment. (b) Rotor speed during the load profile.

Once the 24V bus is charged up, at approximately 60 seconds, the HIL generator stops supplying power until the bus voltage falls too low. Remember that the bus is always being loaded with roughly 25 W and this is done assuming some sort of controls hardware will always be drawing power. When this happens, the emulated generator recharges the bus back up to its nominal voltage. The oscillation between charging and resting can be seen between 60 and 85 seconds. When the load turns on, the change in the generator's rotor speed is clearly visible in Figure 68, where it appears to constantly be trying to recover. Fluctuations in the rotor speed are seen in the Fourier transform of the stator

voltages plotted in Figure 70. When the PHIL generator is loaded by a transient event, the frequency of the stator voltages varies from the nominal 60 Hz ranging between 58 Hz and 61 Hz. This is considered poor power quality and falls well outside the range of the specified  $\pm 0.750$  Hz which is considered worst case for transient events [4]. This is most easily seen in Figure 70. Though the EDLC is on the bus, without the energy dense energy storage present to maintain the DC bus voltage, it sags significantly and therefore the generator must source the brunt of the power and power quality suffers considerably.

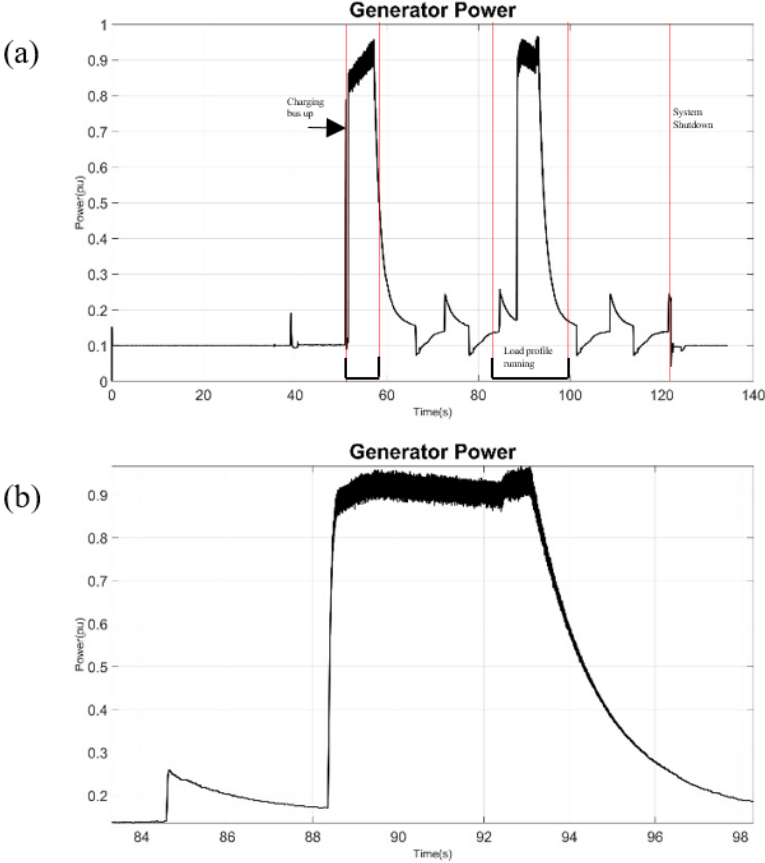


Figure 69. (a) Power sourced during HIL generator deployed during experiment. (b) Power sourced during the load profile

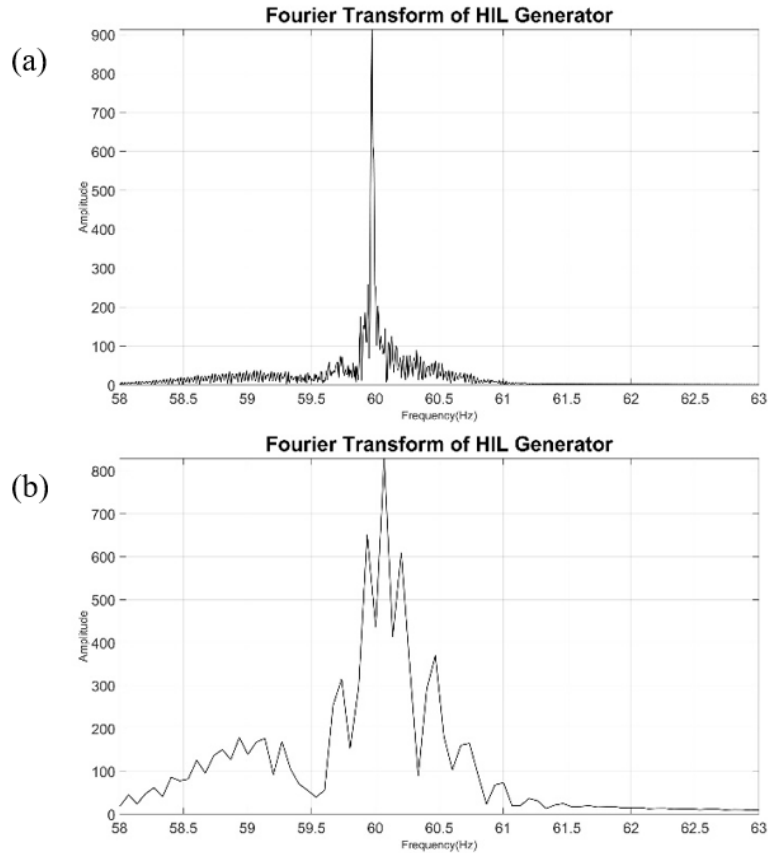


Figure 70. (a) Fourier transform of Stator voltages during HIL generator deployed during experiment. (b) Fourier transform of stator voltage during load profile.

With the PHIL model evaluated with a short transient event, the intelligently controlled HESM will be brought online to buffer the generation source during the transient event. This should significantly narrow the frequency spread during the transient event. Ideally, the frequency deviation should fall within  $\pm 0.100$  Hz to be within the normal operational range [4].

#### D. Diesel Engine / Synchronous Generator with Energy Storage Buffer

In the next experiment, the previously presented experimental conditions were repeated but this time the energy storage is actively controlled to maintain the DC voltage. The rotor speed, generator power, and Fourier transform results obtained when the second

test scenario was implemented are presented in Figure 71, Figure 72, and Figure 73. Approximately 30 seconds into the plots, the PHIL generator is connected onto the 24 V bus and it begins to charge up the passive EDLC module. This is seen most clearly in Figure 72. At approximately 55 seconds, the local controller is enabled and begins to sink power from the generator, establishing a base load. At approximately 80 seconds, the transient profile is initiated. The profile is hard to even make out in Figure 71 because the generator's rotor speed hardly fluctuates once the controller is enabled and it is consistently base loaded. The base load of the generator is shown most clearly in Figure 72, supplying the HESM during periods of load inactivity. The Fourier transform of the stator voltages shown in Figure 73 displays a much sharper spike centered at 60 Hz. While the load profile is executed, the PHIL generator frequency only shifts from 59.9 Hz to 60.1 Hz. This improves the power quality of the system to within the acceptable ranges of  $\pm 0.100$  Hz during the transient events [4]. These results clearly demonstrate the ability of a HESM to improve the power quality of a PHIL deployed fossil fuel powered generation source when transient events occur.



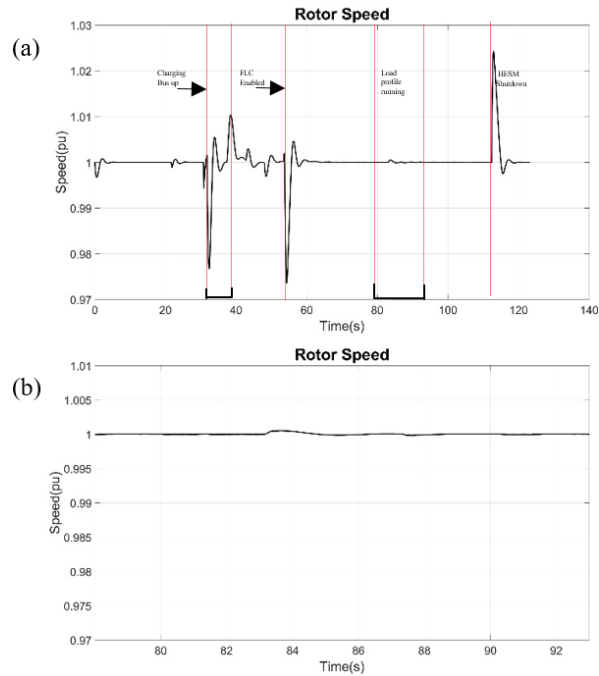


Figure 71. (a) Rotor speed during HIL generator deployed during experiment. (b) Rotor speed during the load profile.

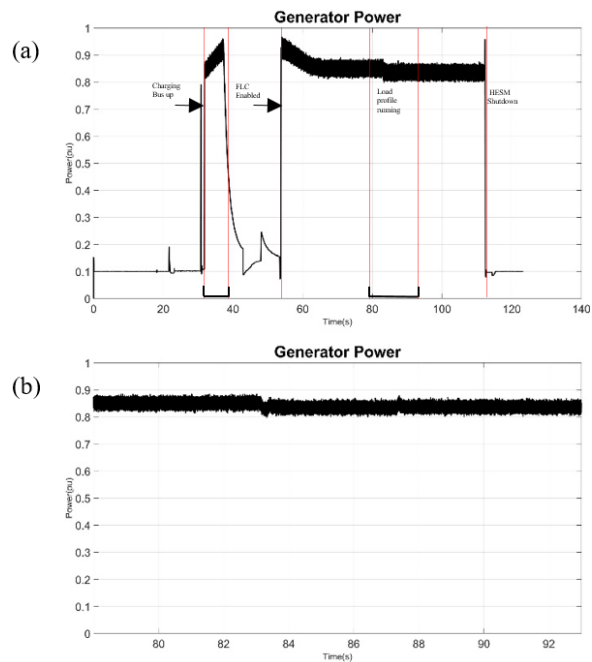


Figure 72. (a) Power sourced during HIL generator deployed during experiment. (b) Power sourced during load profile.

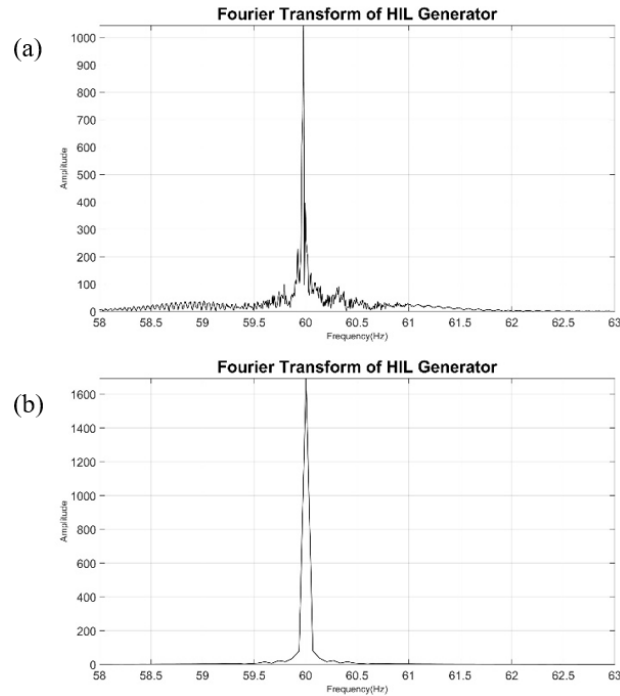


Figure 73. (a) Fourier transform of Stator voltages during HIL generator deployed during experiment. (b) Fourier transform of stator voltages during load profile.

With the previous experiments evaluating the capabilities of generation sources being deployed as a PHIL model for transient analysis and power quality study, this experiment shows that PHIL deployed generation sources can be implemented into an existing testbed as a valid replacement for the physical generation source.

#### E. PHIL Diesel Engine / Synchronous Generator System Integration Conclusion

In this set of experiments, a fuel-based generation source not physically owned was modeled and deployed as a PHIL model within a built actively controlled HESM to demonstrate power quality improvements. This was demonstrated by applying a short transient event to the PHIL model with and without active buffering from the actively controlled HESM. As expected, improvements to the power quality of the AC generation source when actively buffered by a HESM were seen. This improvement was an initial

deviation of  $\pm 3.00\text{Hz}$  to a  $\pm 0.100\text{ Hz}$  which brings the system within the acceptable deviation during normal operation [4]. This demonstrates that PHIL deployed models of generation sources not physically owned are capable of power quality study during short transient events. The capability of emulating a fuel-based generation source within a known test bed, that was used for power quality improvement study, is a viable alternative if the physical source is impractical to implement into a hardware test bed for transient and power quality.

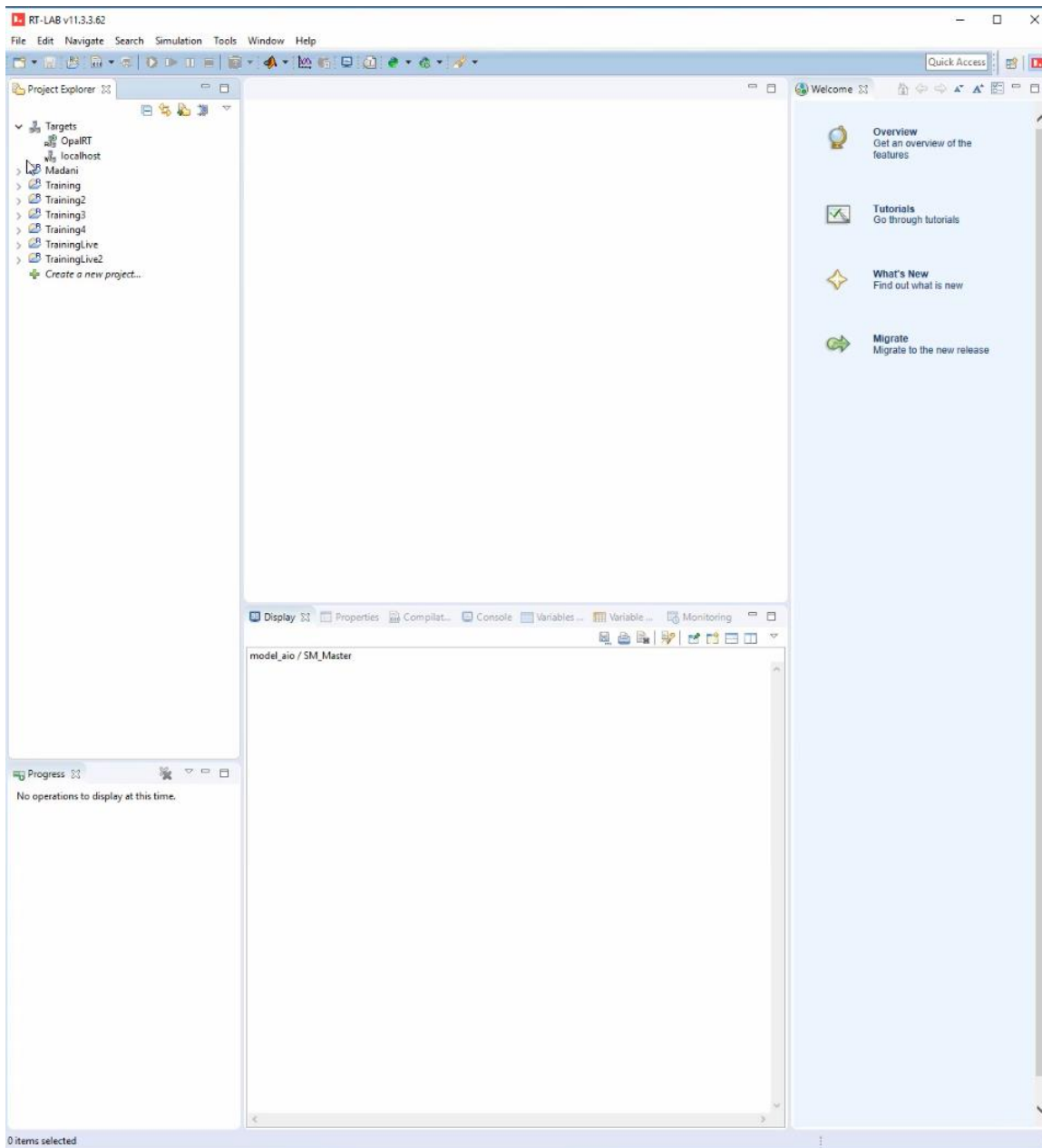
## CHAPTER 9: CONCLUSION

Experimentally evaluating power quality using PHIL deployed models have been shown to be a viable method, if the physical generator is not present for experimentation and power quality study. The work shown here shows the process of PHIL modeling and validation of an acquired motor-generator set for power quality study with an actively controlled HESM to improve the power quality of the AC generation source. Implementing these PHIL models into test beds capable of evaluating AC generator sources for power quality improvements have been shown. There are limitations that need to be overcome when deploying an AC PHIL motor-generator model due to the multiple feedbacks needed into the PHIL model. With these multiple feedbacks, the high transient nature of the feedback could possibly collapse one of the phases causing the system to become unstable with each further step of the PHIL model. This limitation was improved when the feedback into the PHIL model was simplified to a DC current and this showed higher correlated results to the physical system. This limitation was not seen within the fuel-based PHIL model due to the lower response time of a fuel-based generation source. The improvement seen in the fuel-based PHIL deployed model of  $\pm 3.00$  Hz to  $\pm 0.100$  Hz during the transient event shows great promise in the ability of PHIL deployed models to be implemented into physical test beds for validation. This work lays the foundation for future improvements of feedback, filtering of the external signal, implementation into higher voltage test bed, and hardware validation of generation sources not physically owned into hardware test beds.

## APPENDIX A

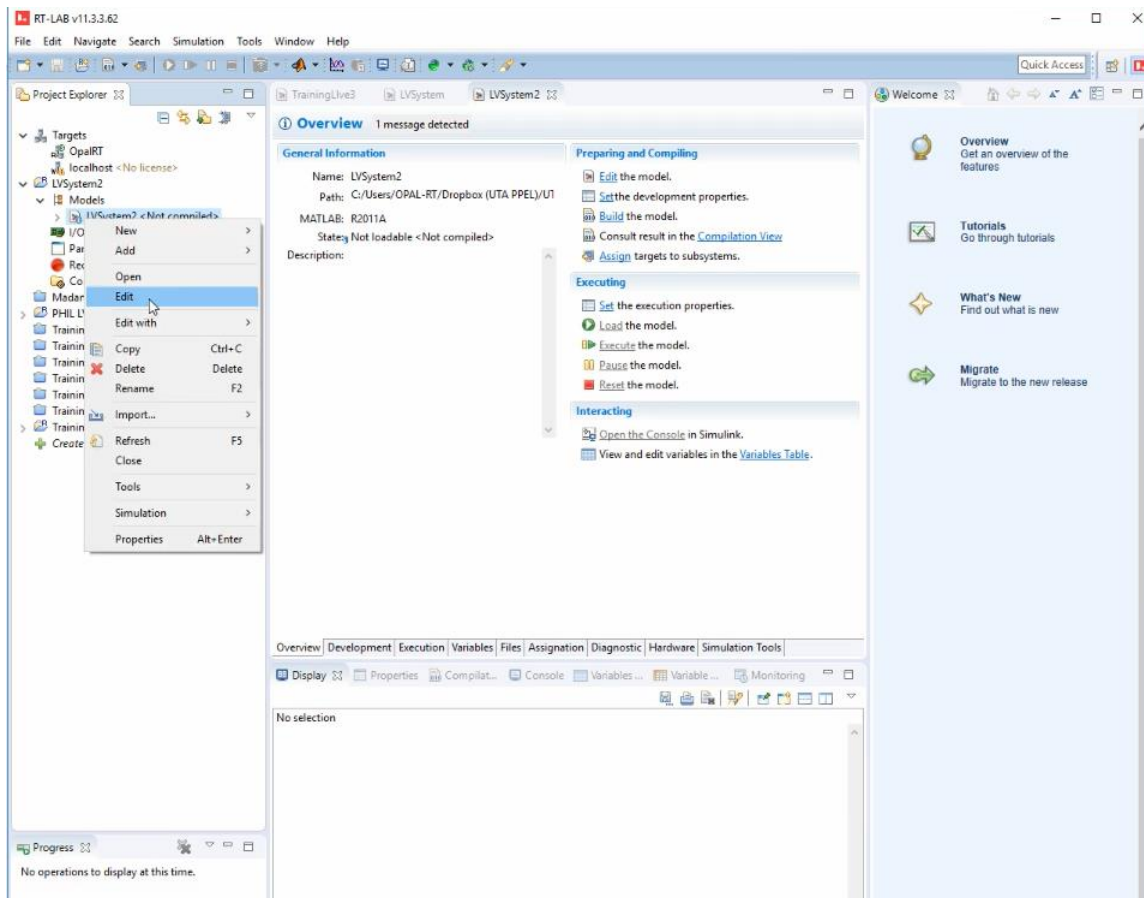
### Basics of OPAL-RT

1. Start RT-Lab
2. Create or choose an existing workspace.
3. Screen shown below will pop up containing either an empty project explorer or the projects created previously.

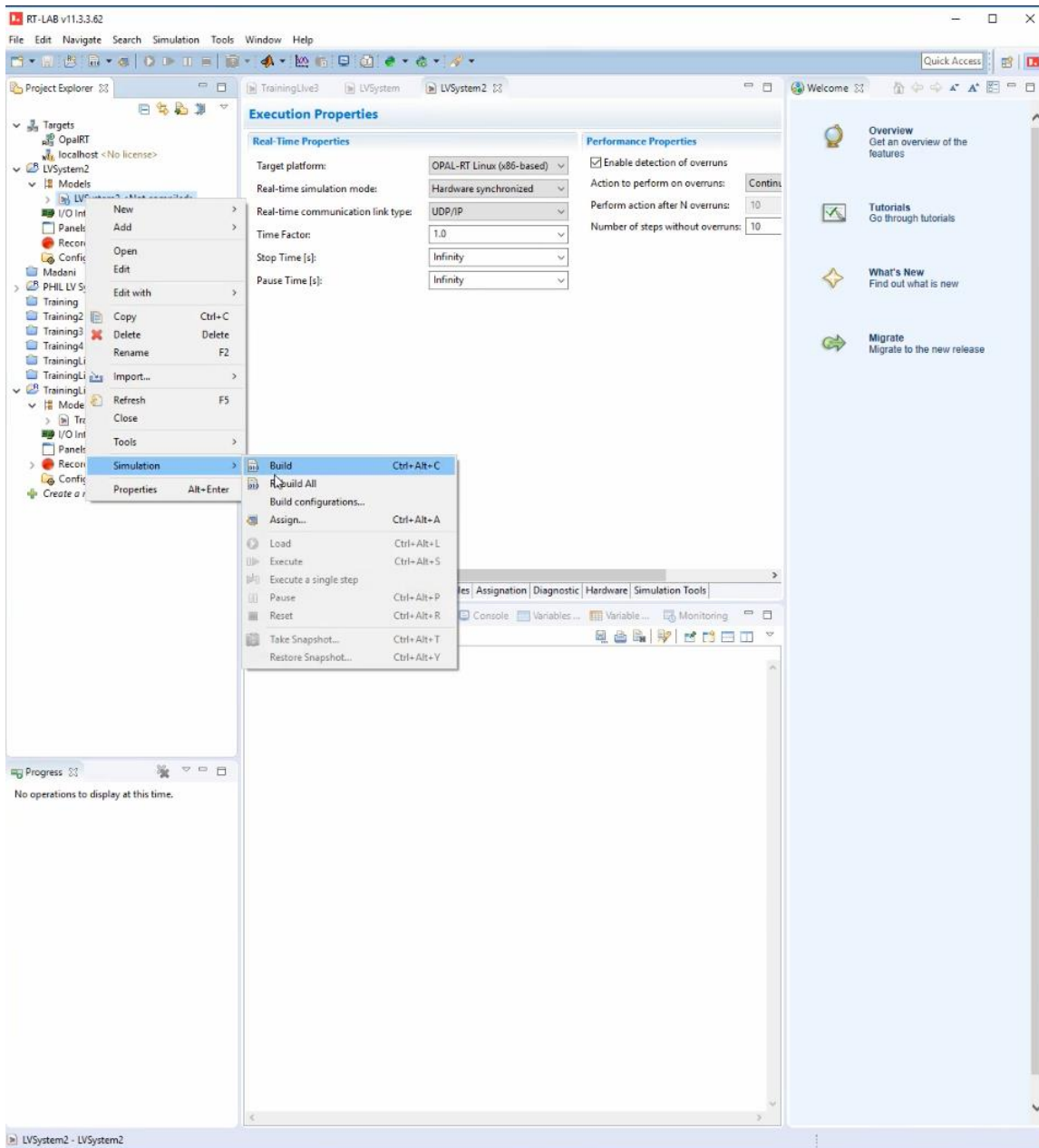


4. Contained in this project folder shown above are training simulations to understand how to use HIL

5. To edit a model in RT-Lab, expand the project folder to the model folder, right click the model and choose which MATLAB edition to edit it with



6. To deploy the model, right click on the model and choose to rebuild all to build the model for deploying onto the real time operating system. Within the execution tab shown below, the real time simulation mode should be set to hardware synchronized in order to run the real time simulation. The default of this is software synchronized



7. After the model has rebuilt, go to the assignment tab and for each subsystem, enable XHP to on in order to assign a node to each subsystem. All warnings should be ignored.

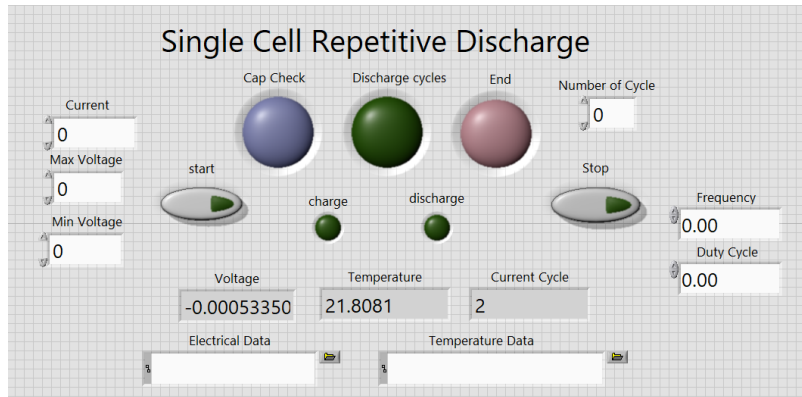




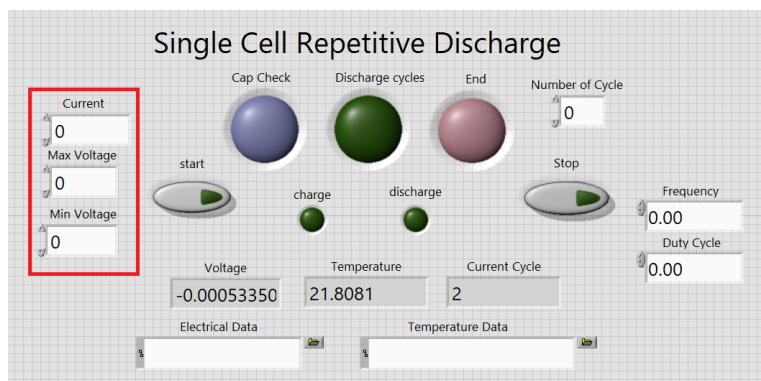
## APPENDIX B

### Repetitive High Rate Discharge LabVIEW VI

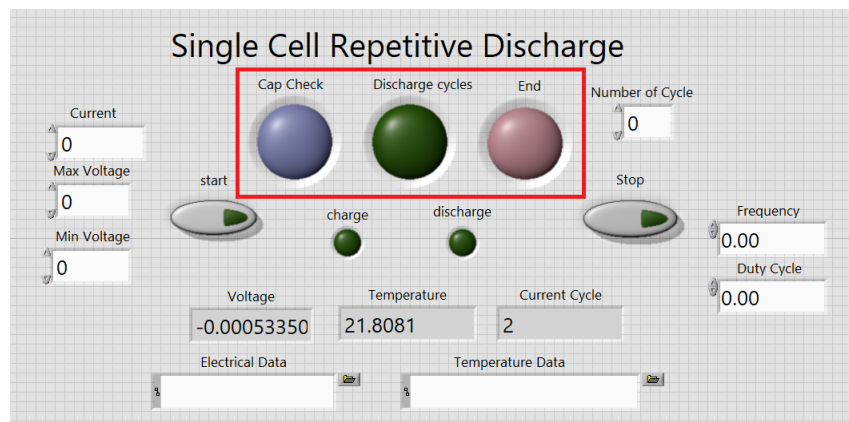
1. VI is located at Dropbox (UTA PPEL) \UTA PPEL Team Folder\Resources\LabVIEW Programs\Repetitive Discharge
2. Open the VI and the front panel is as shown below



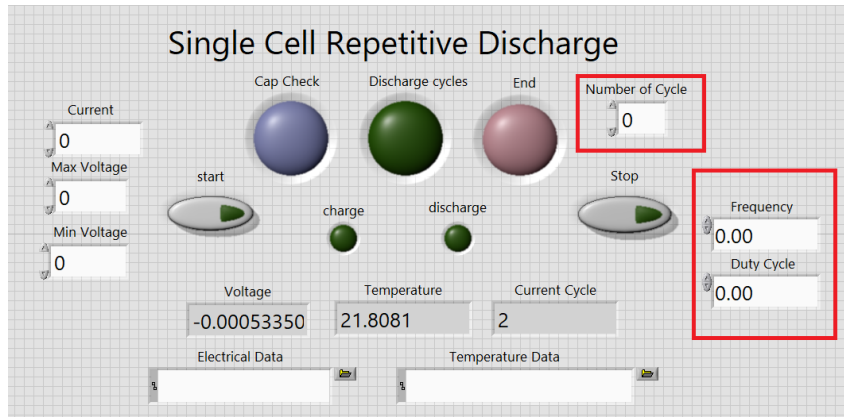
3. On the left, the Current, Max and min voltage.
  - a. Current corresponds to the current drawn from the device under test during each discharge
  - b. Max Voltage corresponds to the voltage that needs to be achieved in order to start the repetitive discharge
  - c. Min voltage corresponds to the voltage that initiate a charge after the repetitive discharge.



4. The three indications on top (blue, green, and red) show which state the VI is in.
  - a. Blue indicates a capacity check at desired rate. This is performed at the beginning and end of the repetitive cycle.
  - b. Discharge Cycles indicates that it is currently in the charge/repetitive discharge portion of the experiment.
  - c. End indicates that the experiment is over. Note: The VI leaves the cell in a discharged state.



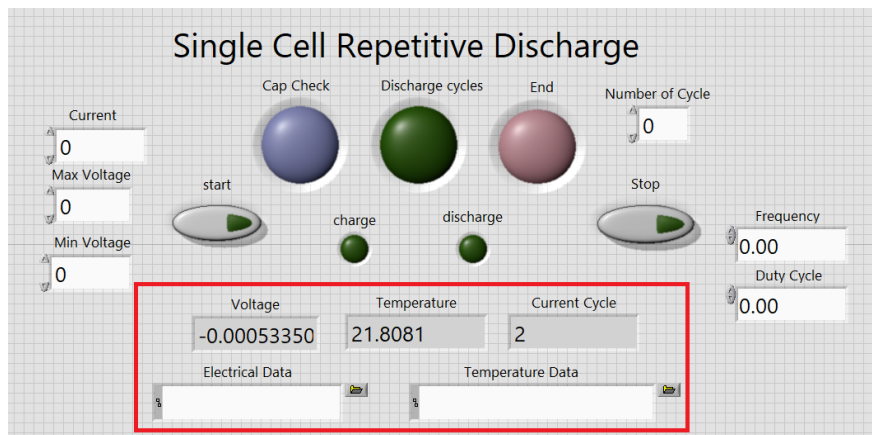
5. On the far right, Number of Cycles, Frequency, and Duty cycle control how the discharge will proceed
  - a. Number of Cycles controls the number of cycles performed during the experiment. Note: the number of cycles should not exceed 200 to keep parsing the acquired data possible.
  - b. Frequency corresponds to the amount of discharges per second until the user desired min voltage is reached.
  - c. Duty cycle controls the percentage of the period a discharge will be in effect.



6. On bottom is the current voltage, temperature, cycle number, Electrical data path, and Temperature data path.

a. Electrical and temperature data and stored in separate files due to the different sampling rates.

b. The electrical data is stored in separate files for each discharge. To parse this data, the MATLAB code is located at Dropbox (UTA PPEL) \UTA PPEL Team Folder\Resources\LabVIEW Programs\Repetitive Discharge



## REFERENCES

- [1] "U.S. Energy Information Administration - EIA - Independent Statistics and Analysis." *Factors Affecting Gasoline Prices - Energy Explained, Your Guide To Understanding Energy - Energy Information Administration*, [www.eia.gov/tools/faqs/faq.php?id=65&t=2](http://www.eia.gov/tools/faqs/faq.php?id=65&t=2).
- [2] "U.S.: Number of Households 1960-2017." *Statista*, Statista,
- [3] *Morris, Lindsay. "Black Start: Preparedness for Any Situation." Black Start: Preparedness for Any Situation, 1 July 2011*
- [4] "IC.2.1-Voltage Level and Range." *Engineering Handbook*, vol. 1-General;Part C-Power Quality, Pasific Power, 2013
- [5] Toolbox, E. (2019). *Generator Set Sizing | MacAllister Power Systems*.
- [6] Arevalo, E. (2016). Diesel generator power quality, Powercity
- [7] "LM2500." Marine Gas Turbine, GE.com/Marine, Feb. 2017.
- [8] h M. Dargahi, A. Ghosh and G. Ledwich, "Stability synthesis of power hardware-in-the-loop (PHIL) simulation," *2014 IEEE PES General Meeting | Conference & Exposition*, National Harbor, MD, 2014
- [9] Brandl, R. (2015). *Multi-Terminal Power Hardware-in-the-Loop Test-Bench for Power System Stability Analyses Focused on Distributed Generation*.
- [10] Nasrallah, D., Lemaire, M., Belanger, J. and Boulon, L. (2016). FPGA-Based PHIL/RCP Simulation of an Electric Vehicle. Montreal: OPAL-RT Technologies.
- [11] Steurer, M. (2014). *Progress on Power Hardware in the Loop based Anti-Islanding Testing of PV Converters* PV Converters.
- [12] Power HIL (P-HIL): A Revolution in the Industry. (2015). .

[13] Krause, Paul C., et al. *Analysis of Electric Machinery and Drive Systems*. IEEE Press, 2013

[14] Panov, Vili. (2009). GasTurboLib: Simulink Library for Gas Turbine Engine Modelling. 10.1115/GT2009-59389.